HSP70 as a Target for Correction of Wilson Disease Causing ATP7B Mutants

Thesis

HSP70 as a target for correction of Wilson Disease causing ATP7B mutants

Mafalda Concilli

Discipline: Life and Biomolecular Sciences

Affiliated Research Center: Telethon Institute of Genetics and Medicine

Thesis submitted in accordance with the requirements of the Open University for the degree of "Doctor of Philosophy"

April 12th 2017

Table of Contents

CHAPTER 1. INTRODUCTION……...8

1.1. Copper distribution in tissues……10

1.2. Cellular Cu homeostasis……....12

1.3. Functions of Cu-transporting ATPases……....13

1.4. Wilson disease……...17

1.5. Impact of WD-causing mutations on ATP7B function……18

1.5.1. ATP7B mutants with impaired Cu-dependent trafficking……..19

1.5.2. Endocytic ATP7B mutants……..21

1.5.3. ATP7B mutants with compromised apical/canalicular targeting……22

1.5.4. ER retention of ATP7B mutants……22

1.6. Correction of ATP7B mutants as a potential therapeutic approach for WD……23

1.7. Proteomic as an effective approach in discovery of targets for pathogenic mutant correction……26

1.8. Project rationale and summary……..27

CHAPTER 2. MATERIALS AND METHODS……..29

2.1. Cell culture……29

2.2. Generation of Recombinant Adenoviruses……...29

2.3. RNA interference ……..30

2.4. RNA Preparation and Q-PCR……...30

2.5. Immunoprecipitation and Traditional Mass Spectrometry Analysis……31

2.6. SILAC Proteomics Analysis……33

2.7. Western Blotting……...34

2.8. Gene ontology enrichment and STRING analysis……...36

2.9. Proximity ligation assay (PLA)……36

2.10. Immunofluorescence……..37

2.11. Statistical Analyses…….37

2.12. Cu-dependent trafficking of ATP7B …….38

2.13. Cell surface biotinylation……38

2.14. Immunoprecipitation……...39

2.15. Treatments with drugs …….……...40

2.16. Chemical Similarity Search…….41

2.17. Bioinformatics search for FDA-approved drugs reducing *HSP70* expression...42

2.18. DSEA Analysis……...43

2.19. MTT assay……...44

CHAPTER 3. RESULTS AND DISCUSSION……45

3.1. HSP70 as new molecular target for the correction of Wilson disease mutants…45

3.1.1. Traditional proteomics analysis reveals specific binding partners for ATP7B-WT and ATP7B-H1069Q……45

3.1.2. SILAC proteomics analysis confirmed the differences between ATP7B-WT and ATP7B-H1069Q interactomes……48

3.2. Inhibition of HSP70 rescues trafficking of the ATP7B-H1069Q……52

3.2.1. Selection of HSP70 as a target for ATP7B-H1069Q mutant correction….52

3.2.2. *HSP70* silencing corrects ATP7B-H1069Q localization……...54

3.2.3. H1069Q mutation increases ATP7B interaction with HSP70……..57

3.2.4. Chemical HSP70 inhibitor rescues ATP7B-H1069Q localization and stability…….60

3.2.5. HSP70 inhibitor facilitates ATP7B-H1069Q trafficking to the appropriate cell- surface domain in hepatic cells…….64

3.2.6. HSP70 inhibitor promotes delivery of ATP7B-H1069Q to plasma membrane……..66

3.3. Search for FDA-approved correctors of ATP7B-H1069Q……...68

3.3.1. Identification of FDA-approved drugs with structure similar to HSP70 inhibitor…….68

3.3.2. Domperidone treatment improves the trafficking of ATP7B-H1069Q and prevents its degradation……..70

3.3.3. Bioinformatics search for FDA-approved drugs that rescue ATP7B mutant……73

3.3.4. FDA-approved glucocorticoid receptor agonists correct localization of ATP7B-H1069Q and reduce its degradation……75

3.3.5. Impact of GCR agonists on ATP7B-H1069Q interaction with HSP70…..77

3.3.6. Drug-set enrichment Analysis (DSEA) suggests a possible molecular pathway of GCR agonist-mediated correction of ATP7B-H1069Q……..……..79

3.3.7. Correctors of ATP7B-H1069Q mutant protect ATP7B-deficient cells from Cu toxicity……81

CONCLUDING REMARKS……..…84

REFERENCES……...87

ABSTRACT

Copper (Cu) is an essential micronutrient, which operates as a cofactor of enzymes regulating a wide range of critical physiological processes. However, Cu overload compromises the redox balance in cells and tissues causing serious toxicity. Removal of excess Cu from the body is driven be Cu-transporting ATPase ATP7B, which sequesters the potentially toxic metal and mediates its excretion into the bile.

Mutations in the *ATP7B* result in Wilson disease (WD) that is caused by the toxic accumulation of Cu in the liver due to the loss of ATP7B function. The most frequent ATP7B mutant, H1069Q, still preserves a significant Cu-transporting activity, but undergoes retention and degradation in the endoplasmic reticulum (ER). Thus, rescue of ATP7B-H1069Q from the ER is expected to recover mutant function and, hence, would be beneficial for a large group of WD patients. Unfortunately, specific targets as well as safe drugs for correction of ATP7B-H1069Q mutant remain to be uncovered.

Comparing interactomes of WT and H1069Q variants of ATP7B, I found HSP70 as a specific mutant interactor that regulates ER retention and degradation of ATP7B-H1069Q. *HSP70* suppression (with either RNAi or allosteric inhibitor) improved stability of the mutant and facilitated its export from the ER to the Golgi and post-Golgi copper excretion sites. These findings prompted me to look for a safe way to inhibit HSP70 and rescue the ATP7B mutant. To this end several bioinformatics tools were employed to search for FDA-approved drugs that modulate HSP70 expression or exhibit structural similarity to HSP70 inhibitors. As a result, Domperidone and glucocorticoid receptor agonists were identified and validated as effective correctors of ATP7B mutant.

In summary, my findings suggest a key role for HSP70 in proteostasis of ATP7B-H1069Q and revealed FDA-approved compounds as safe drugs for ATP7B mutant correction and, thus, for the normalization of Cu homeostasis in Wilson disease patients.

Abbreviations

BCS bathocuproine disulfonate

CFTR cystic fibrosis transmembrane conductance regulator

ER endoplasmic reticulum

ERAD ER-associated protein degradation

GFP green fluorescent protein

GO gene ontology

ICP-MS inductively coupled plasma mass spectrometry

MAPK mitogen-activated protein kinase

MS mass spectrometry

PM plasma membrane

ROS reactive oxygen species

TGN trans-Golgi network

WD Wilson disease

Doxo Doxorubicin

CHAPTER 1. INTRODUCTION

Maintaining homeostasis of trace elements (e.g. biometals and minerals) is pivotal for normal physiology; imbalance in any of them may lead to pathological outcomes in humans (Rayman, 2012; Xu and Zhou, 2013). Trace elements play a wide number of important physiological roles. Therefore their imbalance leads to different diseases varying in degree of severity.

Copper (Cu) is an essential trace element that is indispensable for activity of several vitally important enzymes (Ala et al., 2007). The redox properties of Cu allow it to be used as a cofactor by enzymes operating in several cellular processes, including respiration, iron metabolism, pigmentation, decomposition of superoxides and synthesis of collagens (Camakaris et al., 1999; Kim et al., 2008; Puig and Thiele, 2002; Tapiero and Tew, 2003; Wessling-Resnick, 2002). The main human Cu-dependent enzymes are listed in Table 1.

However, in amounts that exceed cellular needs, Cu is highly toxic, owing its potential to facilitate the production of reactive oxygen species (ROS)(Stohs and Bagchi, 1995). ROS bind most biological structures (like lipids, and nucleic acids), causing direct cellular injury by inducing lipid and protein peroxidation and damaging nucleic acids. Indeed, excess Cu–derived oxidants cause hepatotoxicity in Wilson disease (Nagasaka et al., 2006).

Enzymes	Function	Consequences of deficiency
Ceruloplasmin	Iron and Cu transport	Decreased circulating Cu levels, iron deficiency
Hephaestin	Iron transport	Anemia
Cytochrome C oxidase	Mitochondrial respiration	Hypothermia, muscle weakness
Dopamine β-hydroxylase	Catecholamine production	Hypothermia,neurological defects
Lysyl oxidase	Connective tissue formation	Laxity of skin and joints
Peptidylglycine α-amidating monooxygenase	Peptide amidation	Neuroendocrine defects
Superoxide dismutase	Antioxidant defence	Diminished protection against oxidative stress
Tyrosinase	Pigment formation	Hypopigmentation of hair and skin
Sulfhydryl oxidase	Cross-linking of keratin	Abnormal hair, Dry skin

Table 1. Function of Cu-dependent enzymes.

Adapted from P. de Bie et al. 2007

Organisms have evolved homeostatic mechanisms to regulate uptake, distribution, use, storage, detoxification and efflux of Cu. The failure of these regulatory

mechanisms manifests as severe and debilitating diseases. These disorders can be divided into two major classes:

1. Diseases associated with Cu deficiency, such as Menkes disease (OMIM #309400; Menkes et al., 1962) occipital horn syndrome (OMIM #304150) and distal motor neuropathy, also called as distal spinal muscular atrophy-3 or SMAX3 (OMIM #300489; Kaler, 2013).
2. Diseases associated with Cu excess, such as Wilson disease (OMIM #277900), Indian childhood cirrhosis (OMIM #215600; Tanner, 1998) and idiopathic Cu toxicosis (OMIM #215600; Muller et al., 1998).

To introduce this thesis, I would like to describe the molecular mechanisms behind the pathogenesis of Wilson disease, and how Cu homeostasis is impaired in this disease.

1.1 Cu distribution in tissues

The average daily intake of Cu varies between 1 and 3 mg and is sufficient for human body needs. Dietary Cu is primarily absorbed through the intestinal epithelium. Cu is exported from the enterocytes into the blood by Cu-ATPase ATP7A (Monty et al., 2005; see Fig. 1). In Menkes disease, ATP7A is inactivated and Cu export from enterocytes is greatly impaired. As a result, Cu accumulates in intestinal cells and less Cu is delivered to the blood, resulting in restricted Cu supply to other tissues (Kodama et al., 1993). The majority of Cu that absorbed by the intestinal epithelium arrives to the liver through the portal vein. The liver plays a central role in Cu homeostasis. Hepatocytes load adsorbed Cu onto newly-synthesized serum protein ceruloplasmin. In this way liver distributes Cu to the systemic circulation to provide tissues with the required amount of the metal (Linder et al., 1998). Hepatocytes also

excrete excess Cu to the biliary flow and in this way facilitate removal of the metal from the body.

Cu uptake into the liver does not appear to be highly regulated. In contrast, the export of Cu from the liver represents a tightly regulated Cu-dependent process, which is driven by Cu-transporting ATPase ATP7B (Fig. 1). Failure of biliary Cu excretion leads to toxic accumulation of metal in the liver of patients with Wilson disease, Indian childhood cirrhosis or idiopathic Cu toxicosis (Fig. 1).

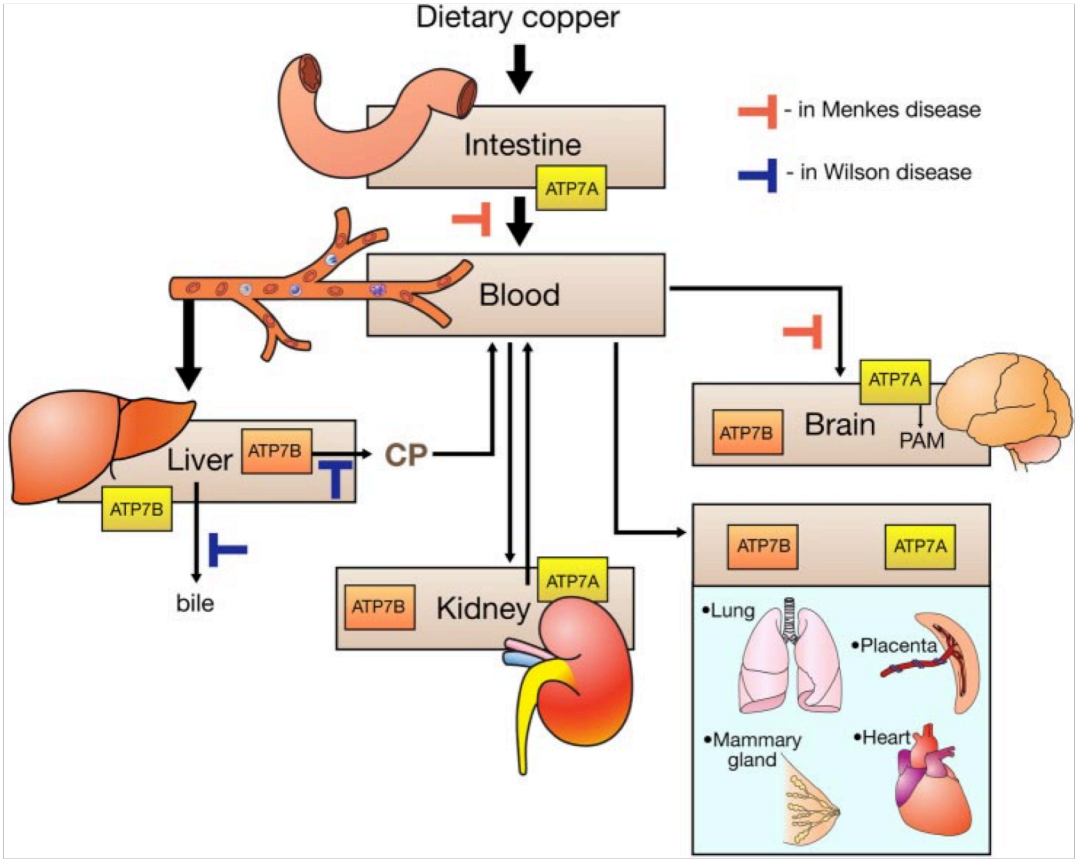

Adapted from Lutsenko, et al. 2007

Fig. 1. Schematic representation of the physiology of Cu homeostasis. Cu is exported from the enterocytes into the blood by Cu-ATPase ATP7A in a process that involves trafficking of the transporter towards the basolateral membrane. In Menkes disease, ATP7A is inactivated and Cu export from the enterocytes is greatly impaired. The majority of Cu that emerges from the intestinal epithelium into the blood is delivered to the liver, and less to kidney and other tissues. The liver is the central organ of Cu homeostasis and is primarily responsible for the export of excess Cu out of the body. The export of Cu from the liver is a regulated Cu-dependent process, which is mediated by a Cu-transporting ATPase ATP7B.

1.2 Cellular Cu homeostasis

Refined mechanisms have evolved to regulate Cu homeostasis at the cellular level. Cu import into the cells mainly takes place via high affinity Cu transporters 1 and 2 (CTR1, CTR2) (Moller et al., 2000; van den Berghe et al., 2007; Zhou and Gitschier, 1997). After entry into the cell Cu immediately binds to specific proteins, Cu chaperones, which distribute metal towards various intracellular destinations (Fig. 2). In the cytosol, Cu is utilized by a radical-detoxifying enzyme Cu, zinc-dependent superoxide dismutase (SOD1), which acquires Cu with the help of a Cu-specific metallochaperone CCS (Cu chaperone of superoxide dismutase) (Culotta et al., 1997; Culotta et al., 2006). Cu also enters mitochondria, where COX17 chaperone facilitates metal incorporation into cytochrome-*c* oxidase (COX). The third important destination of Cu in the cell is the secretory pathway (Polishchuk and Lutsenko, 2013).

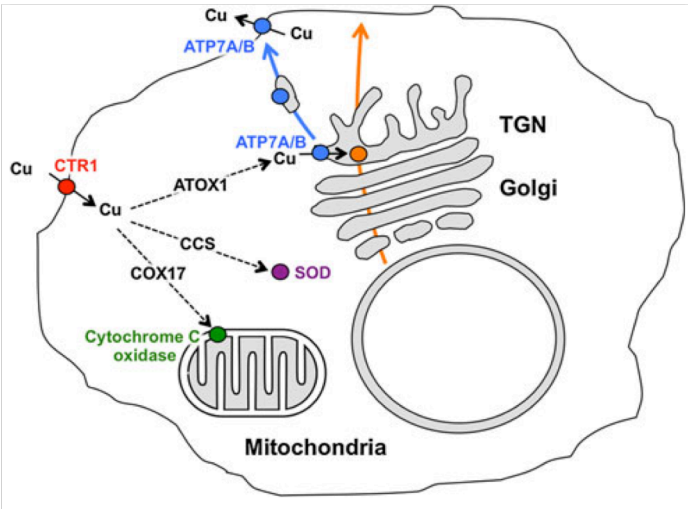

Fig. 2. Schematic depiction of Cu distribution in a mammalian cell.

Cu, taken up via CTR1 (red), is transferred to chaperones ATOX1, CCS and COX17, which ferry it (black dash arrows) to ATP7A/B (blue) in the Golgi, to Cu–Zn superoxide dismutase (magenta) in the cytosol and to cytochrome c oxidase (green) in the mitochondria, respectively. In the Golgi, ATP7A/B load Cu on newly synthesized cuproenzymes (orange ball), which traffic along the biosynthetic pathway (orange arrow). Significant increase in intra-cellular Cu induces export of ATP7A/B (blue arrow) toward post- Golgi compartments and plasma membrane where ATP7A/B drive the efflux of excessive Cu from the cell.

Adapted from Polishchuk and Lutsenko, 2013

Within the secretory pathway, the *trans*-Golgi network (TGN) compartment harbors Cu-ATPase(s) (ATP7A and/or ATP7B), which receive(s) Cu from the cytosolic Cu chaperone *Atox1* (Klomp et al., 1997; Lin et al., 1997). ATP7A and ATP7B transport

Cu from the cytoplasm to the TGN lumen where the metal atom is loaded onto newly synthesized cuproenzymes moving through the secretory pathway (Fig. 2).

1.3 Functions of Cu-transporting ATPases

The Cu-transporting ATPase, ATP7A and ATP7B, move Cu away from the cytosol across the membrane using the energy of ATP hydrolysis. Experimental evidence for the Cu-transporting function of ATP7B/ATP7A emerged in 1978. Cell culture studies showed that the loss of *ATP7A* in fibroblasts from patients with Menkes disease resulted in cellular Cu accumulation and Cu retention phenotype was rescued by overexpression of either *ATP7A* or *ATP7B* (Voskoboinik et al., 1998). The direct involvement of ATP7A/ATP7B in Cu translocation across the membrane was further demonstrated in 1998.This study showed that overexpression of *ATP7A* or *ATP7B* resulted in increased transport of [^{64}Cu] into isolated membrane vesicles. Similar results were also obtained using purified ATP7A, which was reconstituted in soybean asolectin liposomes (Hung et al., 2007; Voskoboinik et al., 1998; Voskoboinik et al., 2001). Taken together, these data suggest that both ATP7A and ATP7B work as ATP-dependent Cu-export pumps.

Cu ATPases have a dual function: the homeostatic function is involved in the regulation of cellular Cu export, while the biosynthetic function is required for the correct biosynthesis of Cu-dependent enzymes. The homeostatic function of ATP7A/ATP7B heavily relies on their ability to traffic from the TGN to the peripheral vesicular compartments and cell membrane where ATP7A/B facilitate rapid excretion of the metal from the cells.

At the organismal level, the post-Golgi trafficking of Cu ATPases to distinct apical/basolateral membranes in polarized cells and the differential expression of Cu ATPases in tissues and organs allow higher vertebrates to deal with systemic changes in Cu levels (Lutsenko, 2010; Nevitt et al., 2012). *ATP7A* is expressed in most tissues (except adult hepatocytes), but its most important function is in the small intestine. In enterocytes, ATP7A receives adsorbed dietary Cu and moves from the Golgi to the basolateral surface of the cells to release Cu toward the portal circulation (Fig. 3). Mutations, which result in a loss of the ATP7A protein, its transport activity or a failure to traffic out of the Golgi, do not allow Cu to move beyond the intestinal barrier. As a result, severe Cu deficiency is observed in most tissues of Menkes disease patients (de Bie et al., 2007; Lutsenko, 2010; Lutsenko et al., 2007). In contrast to ATP7A, ATP7B is highly expressed in the liver and present at lower levels in a few other organs (brain, eye, heart, kidney, bone and placenta (Bull et al., 1993; Kuo et al., 1997; Michalczyk et al., 2000). In the liver, ATP7B receives Cu from the portal circulation and utilizes it in the Golgi for metallation of ceruloplasmin, which carries the metal through the blood flow and uses Cu for regulation of iron balance. Cu elevation beyond a certain threshold activates ATP7B export from the Golgi to the endo-lysosomal structures. These endo-lysosomal structures use ATP7B to sequester excess Cu and then undergo tightly regulated exocytosis at the canalicular surface of hepatocytes to release metal into the bile and hence to eliminate it from the body (Polishchuk et al., 2014) (Fig. 3). In Wilson disease, the lack of ATP7B activity and/or trafficking induces a marked accumulation of Cu in hepatocytes, development of morphologic and metabolic abnormalities, culminating in liver failure (de Bie et al., 2007; Lutsenko, 2010; Lutsenko et al., 2007). When Cu levels in the cells decrease both ATP7A and ATP7B use endocytic pathway(s) to return from the

peripheral Cu excretion compartments back to the TGN (Polishchuk and Lutsenko, 2013) .

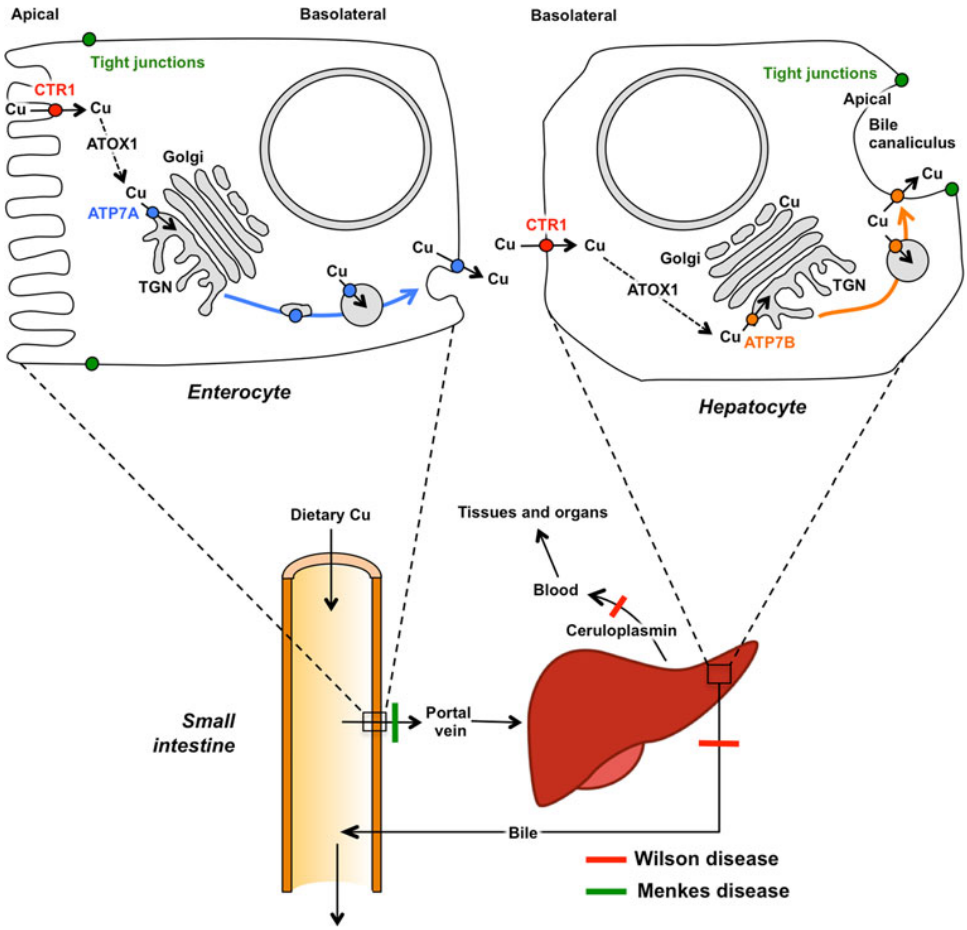

Adapted from Polishchuk and Lutsenko, 2013

Fig. 3. Schematic representation of Cu homeostasis in the body.
Cu is absorbed through the apical CTR1 channel by the enterocytes in the small intestine and effluxed across the basolateral surface of these cells by ATP7A into the portal circulation. The latter process requires ATP7A trafficking from the Golgi to the basolateral surface of the cells (blue arrow). Lack of ATP7B function in Menkes disease patients (green bar) results in accumulation of Cu in the enterocytes and overall Cu deficiency in the body. Most of the newly absorbed Cu is normally taken up by the hepatocytes in the liver, where Cu is loaded in the TGN by ATP7B on newly synthesized ceruloplasmin, the principal Cu carrier in the blood. In cases of Cu overload, ATP7B traffics to Cu excretion sites (orange arrow), i.e. apical (canalicular) membrane and associated vesicular structures. Mutations in the *ATP7B* gene that affect activity and trafficking of the corresponding protein block Cu delivery to ceruloplasmin and its efflux into the bile (red bars). As a result, Cu accumulates in the liver and causes its toxicosis in Wilson disease patients.

Studies of Menkes and Wilson diseases also provided a growing body of evidences regarding biosynthetic roles of ATP7A/B. Loss of function of several cuproenzymes represents a characteristic feature of both Menkes and Wilson disease. Using

fibroblast isolated from patients with Menkes disease, it has been shown that *ATP7A* deficiency results in reduced activities of the Cu-dependent enzymes such as lysyl oxidase and tyrosinase (Petris et al., 2000; Royce et al., 1980). In its turn ATP7B dysfunction causes dramatic reduction in serum caeruloplasmin levels as a result of rapid degradation of the Cu-free form of caeruloplasmin secreted from hepatocytes of patients with Wilson disease (Riordan and Williams, 2001; Scheinberg and Gitlin, 1952) .

The first evidence for ATPase-mediated Cu transport into the secretory pathway was obtained in 1995 in the yeast *Saccharomyces cerevisiae*, which express an *ATP7B/ATP7A* orthologue, known as *Ccc2p* (Yuan et al., 1995). Ccc2p is localized in the late Golgi apparatus, where it provides Cu for Fet3p (a Cu-dependent metallo-oxidase that is involved in iron uptake). Genetic deletion of *Ccc2p* suppresses Cu incorporation into Fet3p and impairs iron uptake, as illustrated by the inability of ΔCcc2 to grow under iron-limiting conditions (Yuan et al., 1995). Overexpression of either *ATP7B* or *ATP7A* can rescue Fet3p activity, and therefore the growth of the Ccc2 knockout yeast on iron-deficient media, making this a good model to study Cu-transporting ATPase-dependent cuproenzyme biosynthesis (Yuan et al., 1995).

Using this Ccc2 knockout complementation assay, the effects of Wilson disease and Menkes disease mutations on translocation of Cu into TGN lumen and subsequent incorporation of Cu in cuproenzymes have been determined. Indeed, it was demonstrated that several Menkes and Wilson disease mutations decrease or even completely abrogate the ability of ATP7A or ATP7B to rescue Fet3p biosynthesis or the Ccc2 knockout growth phenotype (Yuan et al., 1995).

Taken together, these studies suggest that ATP7A and ATP7B play a critical role in both delivery of Cu to the TGN and subsequent cuproenzyme biosynthesis. Moreover,

these results indicate that mutations in *ATP7A* and *ATP7B* that perturb this process account for many of the clinical symptoms of Menkes and Wilson disease.

1.4 Wilson disease

Wilson disease (WD) is an autosomal recessive disorder with an estimated incidence between 1:7000 and 1:30000 (Bandmann et al., 2015). As mentioned above WD is caused by mutations in *ATP7B*, which drives excretion of Cu at the biliary domain of hepatocytes. Indeed, the clinical features of WD result from the toxic accumulation of Cu, primarily in the liver and the brain, and include: hepatic abnormalities (cirrhosis and chronic hepatitis, culminating in progressive liver failure) (Fig. 4), neurological defects (Parkinsonian features, seizures), and psychiatric symptoms (personality changes, depression, psychosis) (Ala et al., 2007; Gitlin, 2003).

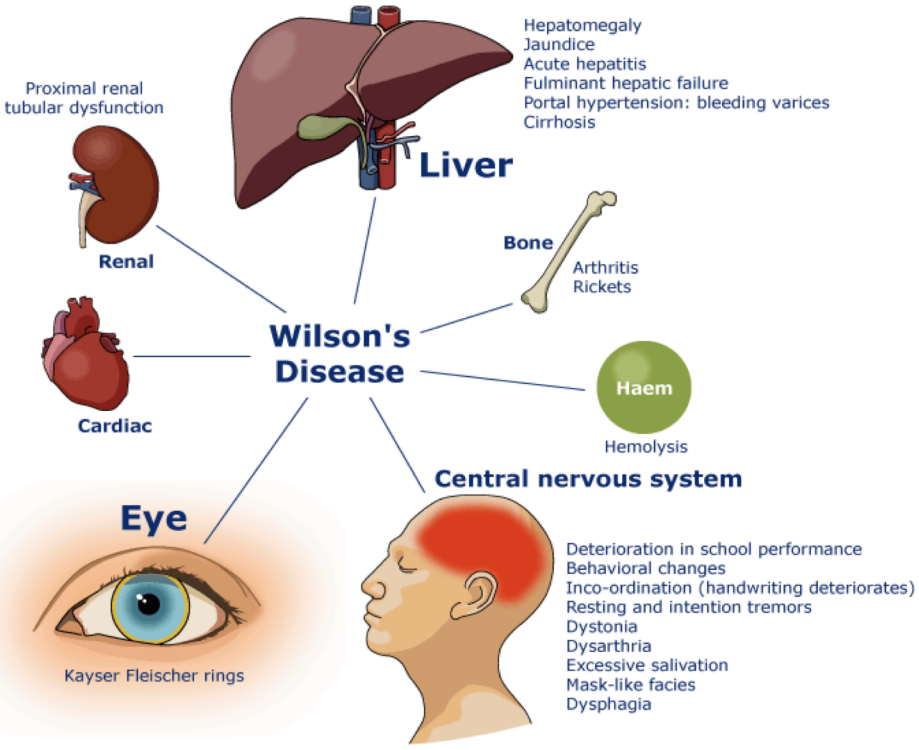

Fig. 4: Organs involved in Wilson Disease. In Wilson Disease patients Cu accumulates in several organs: Liver, Central nervous system, Eyes, Heart, Bone, Placenta, Blood and Kidney.

Adapted from eurowilson site (http://www.eurowilson.org/en/professional/clinical-presentation/index.phtml)

WD may present symptomatically at any age, although the majority presents between ages 5 and 35. The diagnosis of Wilson disease is determined by the presence of the signs and symptoms noted previously, in conjunction with laboratory tests that indicate impaired hepatic Cu metabolism. The clinical hallmark of Wilson disease is the Kayser–Fleischer ring, which is present in 95% of patients with neurologic symptoms and somewhat over half of those without neurologic symptoms. Neurologic signs are variable, most often tremor, ataxia, and dystonia.

A peculiarity of WD is that it exhibits highly heterogeneous phenotypes, even between patients who have the same mutations. Differences have been found in age at presentation, severity of the disease and the predominance of hepatic versus neurological symptoms (Riordan and Williams, 2001).

1.5. Impact of WD-causing mutations on ATP7B function.

ATP7B is a complex multispan membrane protein (Fig. 5A) that belongs to a P1B-type ATPase family. The N-terminal portion of ATP7B contains six metal binding domains (MBDs) followed by eight transmembrane domains that form a Cu translocation pathway to move Cu from the cytosol across the membrane at the expense of ATP hydrolysis. Autophosphatase, nucleotide binding and phosphorylation domains in 2nd and 3rd cytosolic loops coordinate the catalytic activity of ATP7B.

A number of mutations that affect *ATP7B* results in lower catalytic activity and/or several trafficking defects, namely: (i) retention of the mutant within the ER due to mis-folding, (ii) failure to exit the Golgi in response to increasing Cu, (iii) constant

targeting to post-Golgi sites even at low Cu levels and (iv) loss of apical polarized targeting (fig. 5B) (de Bie et al., 2007). The localization of these mutations along the protein backbone frequently helped to reveal the role of several domains in the ATP7B function and trafficking.

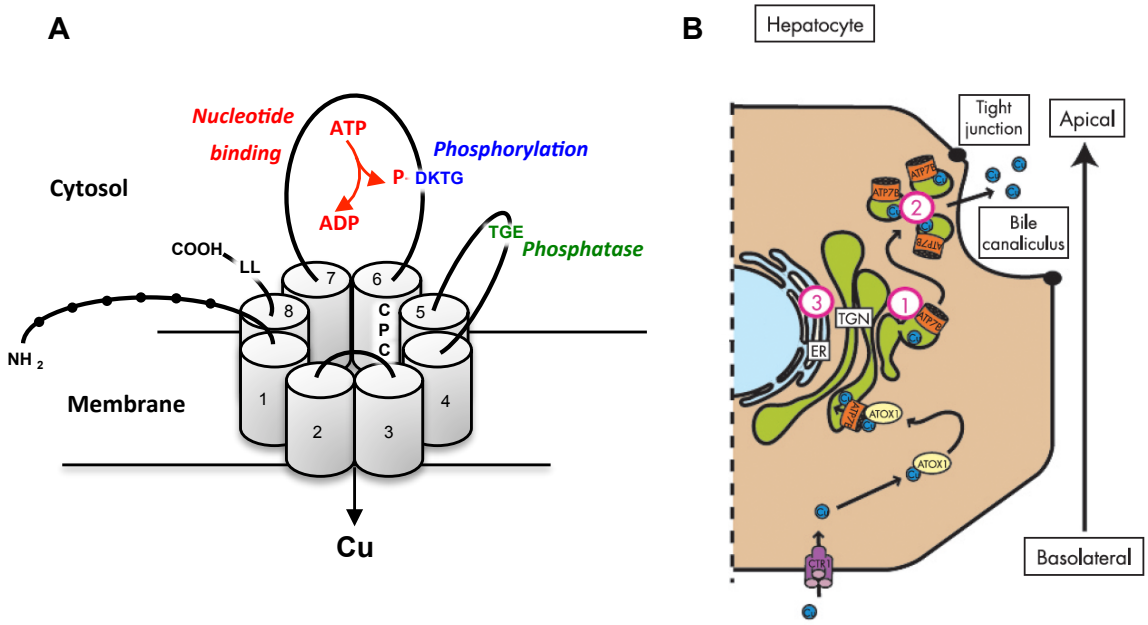

(A) Adapted from Polishchuk and Lutsenko, 2013 (B) Adapted from De Bie and Klomp, 2007

Fig. 5: **(A) Structure of Cu-translocating ATPase.** Three-dimensional representation of the Wilson (ATP7B) Cu-ATPase. Protein is predicted to have eight transmembrane (TM) domains, with most of the protein on the cytoplasmic side. ATP7B protein contains ATP-binding (red), phosphatase (green), and phosphorylation (blue domain), which regulate catalytic activity. N-terminal region comprises six Cu binding motifs that interact with Cu chaperonins and presumably deliver Cu to the channel. In addition, CPC motif in the 6th transmembrane domain plays a key role in Cu translocation along the channel, while LL signal in the C-tail is required for ATP7A/B endocytosis. **(B) Schematic representation of Cu-induced relocalisation of ATP7B**. The figure represents the hepatocyte. Cu enters through the Cu transporter 1 (CTR1), and is then distributed via the Cu chaperone ATOX1 to ATP7B residing in the TGN. After a rise in Cu concentrations, ATP7B relocalise from the TGN to the cell periphery, and also the plasma membrane, to facilitate excretion of Cu. In the hepatocyte Cu is excreted at the apical side into the bile. The numbers indicate localisation defects of ATP7B due to WD-causing mutations: (1) lack of Cu responsiveness, resulting in constitutive localisation at the TGN, (2) constitutive localisation at the cell periphery, and (3) mislocalisation at the ER, presumably due to misfolding.

1.5.1. **ATP7B** *mutants with impaired Cu-dependent trafficking*

The ability to traffic in response to Cu was acquired by ATP7B during the course of evolution. Yeast control their intracellular Cu balance predominantly through the transcription of genes functioning in Cu uptake, efflux and storage rather than through repositioning of the proteins between different compartments (Nevitt et al., 2012). In contrast to ATP7B, yeast homolog Ccc2 does not traffic in response to increasing Cu and remains in the Golgi compartment where Ccc2 operates, almost exclusively, in biosynthetic processes (Yuan et al., 1997). In comparison to mammalian orthologues, Ccc2 has only 2 MBDs in its N-terminal part (instead of 6 in ATP7A/B). Thus, it turns out that domains, missing in yeast Ccc2, enable ATP7B to traffic in response to altering Cu levels. Indeed, MBD 5 or 6 seems to be indispensable for Cu-dependent export of ATP7B from the TGN (Cater et al., 2004; Strausak et al., 1999). Several Wilson disease missense mutations of ATP7B have also been mapped to this region (Guo et al., 2005).

Catalytic phosphorylation is also required for post-Golgi trafficking of Cu pumps. As part of their catalytic cycle the Cu P-type ATPases undergo transient auto-phosphorylation at the invariant aspartate residue in DKTG motif to form an acyl-phosphate intermediate (Inesi et al., 2014; Tsivkovskii et al., 2002). For both ATP7A and ATP7B, formation of this intermediate depends on Cu (Petris et al., 2002) and appears to be essential for the Cu-dependent relocalization of the proteins (Bartee and Lutsenko, 2007). Several *ATP7A/B* variants with mutations in the regions which coordinate ATP binding and hydrolysis, fail to relocate from the TGN to Cu excretion sites (Petris et al., 2002). As an example, the WD-causing E1064A mutation in the nucleotide binding domain disrupts the catalytic activity of ATP7B and strongly inhibits its export from the TGN in response to Cu overload (Morgan et al., 2004).

Interestingly, the neighbouring H1069Q mutation results in completely different ATP7B localization within the ER (see below) indicating that even mutations within the same domain may have a diverse impact on trafficking/activity of Cu ATPases.

On the other hand, dephosphorylation of the aspartate in DKTG stretch supports retrograde trafficking of Cu ATPases to the Golgi. Inhibition of the auto-phosphatase activity through mutation in the phosphatase domain strongly impairs retrieval of both ATP7A and ATP7B to the Golgi when Cu levels decrease (Petris et al., 2002).

1.5.2 Endocytic ATP7B *mutants*

Another key determinant for retrieval of ATP7B to the Golgi is a tri-leucine signal in the C-tail. Such leucine-based signal undergoes recognition by adaptor proteins that drive clathrin-mediated endocytosis of membrane proteins (Traub and Bonifacino, 2013). Substitution of these leucines with alanines results in ATP7B arrest in peripheral endocytic compartment and reduced retrieval of ATP7B to the Golgi even in the case of decrease in intracellular Cu levels (Cater et al., 2006). No WD-causing mutations were detected within LLL motif of ATP7B. However, several mutations may affect recognition of LLL signal in C-tail region of ATP7B. ATP7B$^{L1373P/R}$ mutants reside in the peripheral endocytic structures and do not return to the Golgi even when Cu is deprived. These mutations may destabilize C-tail of ATP7B and, hence, prevent recognition of leucine-based sorting signals. As a result, these mutants instead of being sorted to the Golgi are directed towards lysosomes, where undergo rapid degradation (Braiterman et al., 2011). A similar mechanism is likely to cause trafficking aberrations in WD-causing ATP7B mutants with C-terminal truncations at the positions Q1399, W1410 and P1438 (Braiterman et al., 2011). Although these

mutants seem to be catalytically active, their faster degradation and reduced amount in the TGN (where ceruloplasmin is metallated) can contribute to WD symptoms.

1.5.3. **ATP7B** *mutants with compromised apical/canalicular targeting*

To provide efficient excretion of excess Cu into the bile, ATP7B trafficking has to be directed to the apical/canalicular domain in hepatocytes (Nyasae et al., 2014). The N-terminal portion of ATP7B plays a crucial role in apical delivery of the protein as it contains ^{37}FAFDNVGYE^{45} apical targeting signal (Nyasae et al., 2014). In addition the N-terminal part participates in ATP7B interaction with the p62/DNCT4 subunit of dynactin/dynein motor complex (Lim et al., 2006; Polishchuk et al., 2014), which move ATP7B endo-lysosomal organelles (frequently called "vesicles") to the canalicular surface in response to Cu overload (Polishchuk et al., 2014). WD-associated N41S mutation resides within apical sorting signal and causes basolateral mistargeting of ATP7B in hepatocytes (Braiterman et al., 2009). A number of other mutations in the N-terminal part of ATP7B were detected in WD patients. A few of them cause ER retention of ATP7B, while it remains to be determined whether others compromise apical delivery of the protein.

1.5.4. ER retention of **ATP7B** *mutants*

The most frequent *ATP7B* mutations, H1069Q (40%-75% in the white population) and R778L (10%-40% of the Asian patients), result in ATP7B proteins with significant residual activities (Forbes and Cox, 1998; Iida et al., 1998; van den Berghe et al., 2009), which, however, are strongly retained in the endoplasmic reticulum (ER)

(Payne et al., 1998). Notably, many other WD-causing ATP7B mutants with substantial Cu-translocating activity undergo complete or partial arrest in the ER (Efremov et al., 2004; Harada et al., 2005; Harada et al., 2000; Huster et al., 2012; Lutsenko and Petris, 2003; Morgan et al., 2004; Petris et al., 2002; Vanderwerf and Lutsenko, 2002; Voskoboinik et al., 2001). Thus, although potentially able to transport Cu, these mutants cannot reach the Cu excretion sites to remove excess Cu from hepatocytes. ER retention of such ATP7B mutants occurs due to their mis-folding (Huster et al., 2012; Payne et al., 1998) and increased aggregation (D'Agostino et al., 2013), and hence is due to their failure to fulfil the requirements of the ER quality control machinery. As a result, the cellular proteostatic network may recognize ATP7B mutants as defective and direct them towards the ERAD pathway, as in the case of the most frequent ΔF508-CFTR mutant in cystic fibrosis (van den Berghe et al., 2009). Therefore, identifying molecular targets for recovery of partially- or fully-active ATP7B mutants from the ER to appropriate functional compartment(s) would be beneficial for WD patients with such mutations.

1.6 Correction of ATP7B mutants as a potential therapeutic approach for WD

Existing treatment of Wilson disease mainly relies on two strategies: increasing Cu excretion from the body, and reducing Cu absorption from the diet (Ala et al., 2007). The first strategy is mainly represented by Cu chelation therapy, using penicillamine, trientine (Walshe, 1956a, b) or ammonium tetrathiomolybdate (Brewer et al., 1991). Cu chelators act by ligating Cu and promoting its urinary excretion. These chelators have been shown to effectively ameliorate hepatic and neuropsychiatric signs in large

cohort of patients and to prevent the onset of disease in asymptomatic individuals (Brewer et al., 1994). The second therapeutic strategy requires treatment with zinc salts, which results in decreased intestinal absorption of Cu. Zinc acts by inducing the expression of metallothionein, which capture dietary Cu in enterocytes and inhibits its entry into the portal circulation. In circumstances of advanced liver failure, due to delayed diagnosis, poor compliance with treatment, or rapid, fulminant hepatitis, mortality is almost certain without hepatic transplantation. Currently, about 5% of patients with Wilson disease require liver transplantation for their survival (Schilsky et al., 1994).

Although clearly effective, existing treatments have serious toxicities, including hypersensitivity reactions, bone marrow suppression, and the development of autoimmune disease. In addition recent study suggests that about 33% of patients with Wilson disease do not respond to either Zn or Cu chelators (Roberts et al., 2008). Moreover, the morbidity and mortality of liver transplantation remains substantial, and this should be considered as a viable treatment option only in life-threatening circumstances (Schilsky et al., 1994). Taken together, there is a clear demand for novel treatment strategies for patients with Wilson disease.

Importantly, most *ATP7B* mutations belong to missense (58%) or small deletion/insertion (27%) categories (Hsi et al., 2004) and frequently result in aberrant protein products, which still exhibit residual Cu-transporting activity, but due to misfolding undergo strong retention and degradation in the ER (Forbes and Cox, 1998; Iida et al., 1998; van den Berghe et al., 2009). This is the case for the most frequent ATP7B mutants H1069Q (40-50% in European and North American patients) and R778L (40% in East Asian patients) (Gomes and Dedoussis, 2016).

Therefore correction of such mutants to appropriate intracellular localization in the Golgi complex is expected to recover Cu homeostasis and, hence, to alleviate WD symptoms in large cohort of patients.

In recent years, several attempts have been made in this direction, with the use of pharmachochaperones such as curcumin and phenylbutyrate (van den Berghe et al., 2009). These drugs were shown to reduce the degradation of several ER-retained mutants of ATP7B (van den Berghe et al., 2009), while their potential for correction of mutant localization remains to be demonstrated. Several ATP7B interactors have also been reported to modulate the degradation of the ATP7B mutants and/or their retention in the ER. These include COMMD1 (de Bie et al., 2007), clusterin (Materia et al., 2011) and CRYAB (D'Agostino et al., 2013). So their potential as therapeutic targets could be explored.

Our recent study indicates that the expression of ER-retained ATP7B mutants triggers the activation of the p38 and JNK stress kinase pathways (Chesi et al., 2016). p38 and JNK accelerate arrest and further degradation of the ATP7B mutants in the ER through the cluster of downstream effectors regulating ER quality control processes (Concilli et al., 2016). Thus, suppression of p38 and JNK signaling renders ER quality control machinery less stringent towards aberrant *ATP7B* variants and allows mutants to escape towards the Golgi and post-Golgi compartments. As a result, the delivery of the ATP7B mutant to the Cu excretion sites strongly attenuates the toxic accumulation of the metal (Chesi et al., 2016). Therefore, targeting the ER quality control system emerges as a promising approach for the correction of the ATP7B mutant and cure of Wilson disease.

1.7 Proteomic as an effective approach in discovery of targets for pathogenic mutant correction.

Unfortunately, in contrast to the similar Δ508F mutant of the CFTR, the regulation of the proteostatic network dealing with ATP7B mutants remains poorly understood and requires new approaches to detect targets for safe mutant correction (Klomp et al., 1997). For this reason, changes in the interactome of ATP7B that are caused by WD-associated mutation(s) deserve a detailed analysis, which is likely to reveal potential candidates to rescue localization and function of aberrant ATP7B variants. A similar approach has already been used to find key novel interactors, whose loss promotes ΔF508 CFTR channel function in cystic fibrosis epithelia (Pankow et al., 2015). In general, mass spectrometry (MS)-based quantitative proteomic strategies are used to study protein alterations in different biological states (Trinkle-Mulcahy et al., 2008). Among these strategies, stable isotope labeling by amino acids in cell culture (SILAC) is most widely used for comparative proteomics. In SILAC, proteins in cell populations are metabolically encoded with 'heavy' isotopes of lysine and arginine and are used as internal standards for relative quantification of differentially altered proteins. Characterizing protein–protein interactions (PPIs) helped to discover new pathways of disease progression, thereby aiding diagnostic and preventative strategies. Hosp et al. (Hosp et al., 2015) took this approach, using quantitative interaction proteomics to develop interactome maps for a number of neurodegenerative diseases (NDDs) as Alzheimer's disease (AD), Parkinson's disease, Huntington's disease and spinocerebellar ataxia type 1. Hosp et al. (Hosp et al., 2015) examined interactomes associated with both wild type and disease-associated variants. Thus, comparing interactomes of wild type with disease-specific

ATP7B isoforms, I hoped to gain insight in functional proteostatic changes that contribute to WD pathogenesis as well as to find key binding partners that could be utilized for ATP7B mutant correction.

1.8 Project rationale and summary

It is known that a residual Cu-translocating activity (5-10%) is sufficient for the rescue of Cu homeostasis if an ATPase mutant can be targeted to where the Cu transport is required (Iida et al., 1998; Kaler, 2013; Rodriguez-Granillo et al., 2008; Tsivkovskii et al., 2003). Therefore, correction of the trafficking and localization of the ATP7B mutants should (at least partially) allow the recovery of the normal Cu metabolism that is affected in Wilson disease, and this would be beneficial for the large cohort of patients with this pathology.

Here, I used traditional and SILAC proteomic analyses to find specific ATP7B-H1069Q interactors that can be targeted for correction of this mutant. Using this approach I identified HSP70 as the most evident mutant specific binding partner, which when suppressed (by either RNAi or allosteric inhibitor) allows the mutant to circumvent ER retention and degradation. Considering the importance of HSP70 for several key homeostatic processes such as protein folding and quality control, prevention of aggregation, transport and regulation of proteins, signal transduction and apoptosis (Bukau et al., 2006; Frydman, 2001; Hartl et al., 2011; Kettern et al., 2010; Mayer and Bukau, 2005; Pratt and Toft, 2003; Tyedmers et al., 2010), I attempted to find safe drugs that would inhibit HSP70 activity/expression without significant impact on cell/organism health. To this end the TIGEM Bioinformatics Core searched in available databases for FDA-approved drugs that reduce *HSP70* expression or exhibit structural similarity to HSP70 inhibitors. Among couple of hundreds of potential candidates resulting from this analysis, we found that

Mometasone (MF), Dexamethasone (Dexa), Beclomethasone (Beclo) and Domperidone (Domp.) reduce ATP7B mutant degradation and improve delivery of ATP7B-H1069Q to the Golgi membranes, where wild type ATP7B (ATP7B-WT) normally operates.

In summary, I found 4 FDA-approved drugs for *ATP7B*-H1069Q correction using combination of proteomics and bioinformatics approaches. Moreover my study revealed HSP70 as an attractive target for the correction of Wilson disease mutants, and for the development of new therapeutic strategies for the treatment of patients with Wilson disease.

CHAPTER 2. MATERIALS AND METHODS

2.1 Cell culture

All cell lines were maintained in a humidified 5% CO_2 atmosphere at 37 ºC, and passaged upon reaching ~80% confluency. To passage cells, the growth medium was aspirated off the adherent cell population, and the cells were rinsed with PBS and then harvested by incubation in Trypsin/EDTA (Invitrogen), according to the appropriate cell line. HeLa and $HepG_2$ cells were grown in Dulbecco's modified Eagle's medium (DMEM) supplemented with 10% (v/v) fetal calf serum (decomplemented at 56 °C for 30 min for HepG2 cells), 2 mM L-glutamine, penicillin and streptomycin. HepG2 cells with knock out of ATP7B gene (HepG2-KO) and stable ATP7B mutant hepatic cell lines (Chandhok et al., 2016; Chandhok et al., 2014) were grown in RPMI 1640 Medium supplemented with 10% (v/v) fetal calf serum, 2 mM L-glutamine, penicillin and streptomycin.

2.2 Generation of Recombinant Adenoviruses

Generation of recombinant first generation human type 5 adenovirus containing DNAs encoding either ATP7B-WT-GFP or ATP7B-H1069Q-GFP was performed by Vector biolabs (Philadelphia, PA, USA). To sub-clone the entire expression cassette, the following oligonucleotides were used:

SV40revAscI (5'- AATGGCGCGCCTAAGATACATTGATGAGTTTGGA -3') and CMVfwAscI (5'- TCCGGCGCGCCTGTTATTAATAGTAATCAATTACGG -3').

Cells were infected with adenovirus carrying ATP7B-WT-GFP or ATP7B-H1069Q-GFP respectively with a different Multiplicity Of Infection (MOI) depending on the

cell type. Generation of control helper-dependent adenovirus containing GFP (HDAd-GFP) was performed by the adenoviral core at Tigem. HDAd-GFP was produced in 116 cells with the helper virus AdNG163 as described previously (Palmer and Ng, 2003; Suzuki et al., 2010) .

2.3 RNA interference

Small interfering RNA (siRNA) oligonucleotides targeting the *HSPA1A/B*, were purchased from Sigma-Aldrich (St. Louis, USA). Following siRNA were utilized:

si *HSPA1A/B -1* SASI_Hs01_00051449 CUUUCCAGGUGAUCAACGA

si *HSPA1A/B -2* SASI_Hs01_00051450 AGGACGAGUUUGAGCACAA

Scrambled siRNAs were used as a control. $HepG_2$ or HeLa cells were transfected with siRNA using Darmafect4 (Dharmacon, Pittsburgh, USA) or Oligofectamine TM Reagent (Invitrogen, Carlsbad, USA) respectively according to manufacturer's instructions. SiRNA-treated cells were prepared for Q-PCR, Western Blot and confocal microscopy (see below) to analyze the efficiency of silencing and the intracellular distribution of ATP7B-WT-GFP or ATP7B-H1069Q-GFP.

2.4 RNA Preparation and Q-PCR

The efficiency of silencing was checked using QRT-PCR. For this, the total RNAs from control cells and silenced HeLa cells infected with Adenoviruses carrying ATP7B-WT-GFP and ATP7B-H1069Q-GFP were purified using the QIA shredder and extracted using the RNeasy Protect Mini Kit. The total RNA was converted into cDNA using the QuantiTect Reverse Transcription Kit. Q-PCR experiments were performed using the LightCycler 480 SYBR Green MasterMix for cDNA

amplification and the LightCycler 480 II for signal detection. The Q-PCR results were analyzed using the comparative Ct method normalized against the housekeeping gene β-actin. SiRNA-treated cells were prepared for confocal microscopy to analyze the intracellular distribution of *ATP7B*WT and mutant.

ATP7B forward (5'- TCTCTGGTCATCCTGGTGGTT-3')

ATP7B reverse (5'- GGGCTTCTGAGGTTTTGCTCT-3')

2.5 Immunoprecipitation and Traditional Mass Spectrometry Analysis

To identify the interactors of ATP7B-WT and ATP7B-H1069Q in liver cell line regular proteomics analysis was performed in collaboration with the Proteomics facility at CEINGE (Naples, Italy).

To immunoprecipitate ATP7B-H1069Q-GFP or ATP7B-WT-GFP $HepG_2$ cells were transduced with corresponding adenoviruses. Then cell lysates were incubated for overnight at 4°C with the anti-GFP Antibody A-11120 (Thermo Fisher Scientific, MA, USA) and protein A Sepharose P9424 (Sigma, St Louis, MO, USA) for 5 hours. The beads were resuspended in sample loading buffer and loaded onto 12% SDS-PAGE.

The gel was stained with Coomassie colloidal blue (Pierce). Protein bands were excised from the gel and destained by repeated washings with 50 mM NH_4HCO_3 pH 8.0, and acetonitrile. Samples were reduced and carboxyamidomethylated with 10 mM DTT and 55 mM iodoacetamide in 50 mM NH_4HCO_3 buffer, pH 8.0. Tryptic

digestion of the alkylated samples was performed at 37 °C overnight, using 100 ng trypsin.

MALDI mass spectra were recorded on an Applied Biosystems Voyager DE-PRO mass spectrometer equipped with a reflectron TOF analyser and used in delayed extraction mode. One µl of peptide mixture was mixed with an equal volume of α-cyano-4-hydroxycynnamic acid as matrix (in acetonitrile/50 mM citric acid [70:30, v/v]), applied to the metallic sample plate and air dried. Mass calibration was performed using the standard mixture provided by the manufacturer. Raw data, reported as monoisotopic masses, were then introduced into the MASCOT peptide mass fingerprinting search programme (Matrix Science, Boston, USA) and used for protein identification.

LC-MS/MS analyses were performed on a CHIP MS Ion Trap XCT Ultra equipped with a 1100 HPLC system and a chip cube (Agilent Technologies, Palo Alto, CA, USA). After loading, the peptide mixture (10 µl in 0.2% formic acid) was first concentrated and washed at 4 µl/min in a 40 nL enrichment column (Agilent Technologies chip), with 0.1% formic acid as eluent. The sample was then fractionated on a C_{18} reverse-phase capillary column (75 µm x 43 mm) onto the CHIP (Agilent Technologies chip) at a flow rate of 200 nl/min, with a linear gradient of eluent B (0.2% formic acid in 95% acetonitrile) in A (0.2% formic acid in 2% acetonitrile) from 7% to 60% in 50 min. Peptide analysis was performed using data-dependent acquisition of one MS scan (mass range from 400 to 2000 m/z) followed by MS/MS scans of the three most abundant ions in each MS scan. Raw data from nanoLC-MS/MS analyses were introduced into the MASCOT software (Matrix Science, Boston, USA) to search a non-redundant protein database. The specific interactors for ATP7B-WT and ATP7B-H1069Q are listed in fig. 8.

2.6 SILAC Proteomics Analysis

To evaluate quantitative differences in ATP7B-H1069Q and ATP7B-WT interactomes I performed Stable isotope labeling by amino acids in cell culture (SILAC) (Ong et al., 2002) proteomics analysis in collaboration with Oxford University Proteomics Facility (Oxford, UK).

HepG2 cells transduced with ATP7B-WT-GFP, ATP7B-H1069Q-GFP or GFP (control) adenoviruses were grown in cell culture medium supplemented with different arginine and lysine isotopes. DMEM containing medium *R6K4,* heavy *R10K8* or light *R0K0* isotopes (Dundee cell products, Dundee, United Kingdom) and supplemented with 10% SILAC dialysed FCS was supplied to ATP7B-H1069Q-GFP, ATP7B-WT-GFP or GFP expressing cells respectively for six passages.

Lysates from HepG2 cells expressing ATP7B-H1069Q-GFP, ATP7B-WT-GFP or GFP alone were mixed at 1:1:1 ratio. An immunoprecipitation of GFP-tagged protein from lysate mixture and further gel preparation for proteomics analysis was performed as described in the previous section.

Protein bands were excised from the gel and send to Proteomics Oxford Facility to proceed with digestion Nano-LC/MSMS and analysis of relative expression level of proteins.

Peptides were resuspended in 10% formic acid. They were separated on an Ultimate 3000 UHPLC system (Thermo Fischer Scientific) and electrosprayed directly into a QExactive mass spectrometer (Thermo Fischer Scientific) through an EASY-Spray nano-electrospray ion source (Thermo Fischer Scientific). The peptides were trapped

on a C18 PepMap100 pre-column (300µm x 5mm,100Å, Thermo Fisher Scientific) using solvent A (0.1% Formic Acid in water) at a pressure of 500 bar. The peptides were separated on a PepMapRSLC C18 column (2um, 100Å, 75umx50cm, Thermo Fisher Scientific) using a linear gradient (length: 120 minutes, 7% to 28% solvent B (0.1% formic acid in acetonitrile), flow rate: 200 nL/min). The raw data was acquired on the mass spectrometer in a data-dependent mode (DDA). Full scan MS spectra were acquired in the Orbitrap (scan range 350-2000 m/z, resolution 70000, AGC target 3e6, maximum injection time 50 ms). After the MS scans, the 20 most intense peaks were selected for HCD fragmentation at 30% of normalised collision energy. HCD spectra were also acquired in the Orbitrap (resolution 17500, AGC target 5e4, maximum injection time 120 ms) with first fixed mass at 180 m/z. On the basis of Mass Spectrometry Analysis several parameters like score, coverage and number of peptides were considered, most importantly the ratio between Heavy/Light, Medium/Light and Medium/Heavy was calculated.

2.7 Western Blotting

Cells grown in 6-well plates were placed on ice and washed twice with ice-cold Tris-buffered saline (TBS), incubated with lysis buffer (0.5 % Triton X-100, 20 mM Tris/HCl (pH 7.4), 150 mM NaCl, 1mM EDTA (pH: 8), 0.5% NP-40, 10% glycerol, supplemented with 1× protease inhibitor cocktail (Sigma), scraped and transferred into a pre-cooled microcentrifuge tube. Samples were spun down at 13,200 rpm for 15 min and the supernatants were transferred to fresh tubes, while the pellets were discarded. A small volume of each lysate was removed to determine protein concentration using Bradford reagent (Biorad, California, United States). 80 µg of

each sample were taken and added to SDS sample buffer. Each cell lysate was boiled in sample buffer at 95°C for 5 min and centrifuged at 13,200 rpm for 1 min.

Equal amounts of protein (80 μg) were loaded into the wells of a S600 Hoefer Apparatus SDS-PAGE gel, along with molecular weight markers. The gel was run for 45 min at 35 mA and then the strength of an electric current was increased to 40 mA to finish the run in about 3 h 30 min. A 10% gradient gel was used to separate proteins that have to be detected.

The membrane was stained with Ponceau solution to check the transfer quality and then washed with 5% glacial acetic acid. The blot was rinsed 3 times for 5 min with TBST and then blocked in 1% BSA in PBS or 5% milk in TBST at RT for 1 hr. The membrane was incubated with primary antibody of interest for 1 hour at RT, rinsed with TBST and incubated with secondary antibodies for 45 min at RT. Finally the blot was rinsed with TBST and TBS for further analysis.

Antibodies used are : anti-GFP (kindly provided from De Matteis's lab), Anti-α 1 Sodium Potassium ATPase antibody [464.6] - Plasma Membrane Marker (ab7671), anti-HSP90 4874S Cell Signaling, anti-GAPDH (6C5) sc32233 from Santa Cruz, anti-α Tubulin T5168 from Sigma, anti-actin (A2066) from Sigma, HRP-conjugated secondary antibody Goat Anti-Mouse IgG, H and L Chain Specific Peroxidase Conjugate (401215; Calbiochem) to reveal: GAPDH, α-Tubulin, α 1 Sodium Potassium ATPase proteins and HRP-conjugated secondary antibody Goat Anti-Rabbit IgG, H and L Chain Specific Peroxidase Conjugate (401315; Calbiochem) to reveal: GFP, Actin and HSP90 proteins.

The blot was incubated with chemiluminescent substrate Pierce ECL Western Blotting Substrate (32106, Thermo Scientific) according to the manufacturer's

instruction. Chemiluminescent signals were captured using Chemidoc Amersham Imager 600 and the loading control protein levels: GAPDH or α-tubulin or actin protein were used to normalize the target protein levels.

2.8 Gene ontology enrichment and STRING analysis

To evaluate gene ontology enrichments in ATP7B-WT or ATP7B-H1069Q interactomes the specific binding partners of the WT protein or of the mutant were entered into the Gene Functional Annotation Tool that is available at the Database for Annotation Visualisation and Integrated Discovery (DAVID) website (http://david.abcc.ncifcrf.gov) by using their official gene symbols. The gene ontology (GO) options GOTERM_BP_ALL, GOTERM_MF_ALL, GOTERM_CC_ALL were selected for enrichment analyses and a functional annotation chart was generated. A maximum p -value of 0.01 was chosen to select only the significant categories. In addition, to analyze connections between specific interactors of ATP7B mutant the STRING 9.1 database was used (Franceschini et al., 2013).

2.9 Proximity ligation assay (PLA)

In-situ ATP7B-GFP and HSPA1A/B interaction, revealed as red fluorescent dots, was detected using the Duolink II PLAkit (Olink Bioscience, Uppsala, Sweden), according to the manufacturer's instructions. As a positive control, cells were infected with ATP7B-H1069Q-GFP and labelled with an anti-p62 antibody (Dynactin p62 Antibody (H-4): sc-55603) from Santa Cruz in combination with an anti-GFP antibody (Polishchuk et al., 2014). As a negative control, cells were infected with ATP7B-H1069Q-GFP and labeled with an anti-GFP antibody in combination with the

antibody against the luminal domain of transferrin receptor (TfR) (Invitrogen) to demonstrate no interaction between ATP7B-GFP and TfR (D'Agostino et al., 2013).

In the case of HSPA1A/B was used Anti-HSP70 antibody [C92F3A-5] (ab47455) by Abcam. Coverslips were stained with Hoechst, mounted in Mowiol and analyzed by confocal immunofluorescence microscopy.

2.10 Immunofluorescence

Cells were fixed for 10 min with 4% paraformaldehyde (PFA) in 0.2 M HEPES followed by incubation with blocking/permeabilizing solution (0.5% bovine serum albumin (BSA), 0.1% saponin, 50 mM NH_4Cl in PBS) for 20-30 min. Primary and secondary antibodies were diluted in blocking/permeabilizing solution and added to the cells for 1h or 45 min respectively. Samples were examined with a ZEISS LSM 700 or LSM 710 confocal microscopes equipped with a 63X 1.4 NA oil objective. Images were processed using Photoshop CS3.

The antibodies used in immunofluorescence experiments are the following: anti-MRP2 (Enzo Life Sciences, Lausanne, Switzerland), anti-TGN46 (AbD Serotec, Oxford, UK) anti-human LAMP1 (H4A30) from Developmental Studies Hybridoma Bank, Iowa City, USA) and secondary Alexa Fluor 568-conjugated antibodies (Invitrogen-Life Technologies, Grand Island, NY, USA).

Morphometric analysis shows the percentage of cells (average ± SD, n=10 fields) with ATP7B mutant in the ER.

2.11 Statistical Analyses

Data are expressed as mean values ± SD. Statistical significance was computed using the Student's two-tail t test. A p value < 0.05 was considered statistically significant. In all figures, $^{*}p < 0.05$, $^{**}p < 0.01$, and $^{***}p < 0.001$. Experiment was done in triplicate. Mean ± SD.

2.12 Cu-dependent trafficking of ATP7B

To compare trafficking of ATP7B-WT and ATP7B-H1069Q in high and low Cu conditions, cells were treated with 200 μM of $CuSO_4$ for 2 or 8 hours in HeLa and HepG2 cells. After Cu treatment the cells were prepared for either surface biotinylation (in the case of HeLa) or Immunofluorescence (both HeLa and HepG2).

2.13 Cell surface biotinylation

HeLa cells were used to evaluate delivery of either ATP7B-WT-GFP or ATP7B-H1069Q-GFP to the plasma membrane using cell surface biotinylation. To this end the cells were infected with adenovirus carrying either ATP7B-WT-GFP or ATP7B-H1069Q-GFP. The day after infection cells were rinsed twice with PBS containing 0.1 mM $CaCl_2$ and 1 mM $MgCl_2$ followed by two successive 20 min incubations with 0.5 mg/ml EZ-Link Sulfo-NHS-Biotin (Pierce) diluted in PBS. The biotinylation reaction was stopped by washing the cells with PBS/NH_4Cl quenching solution for 10 min. Cells were then solubilized in a lysis buffer containing 0.5 % Triton X-100, 20 mM Tris/HCl (pH 7.4), 150 mM NaCl, 1mM EDTA (pH: 8), 0.5% NP-40, 10% glycerol, supplemented with 1× protease inhibitor cocktail (Sigma). The mixture was placed into a microfuge tube, kept on ice for 10 min, and then spun at 14 000 rpm for 15 min at 4°C.

The lysate was incubated with streptavidin beads (Pierce) at 4°C overnight. After incubation, beads were pelleted by centrifugation at 4000 rpm for 1min. The beads were then washed in lysis buffer (20 mM HEPES pH 7.4, 150 mM NaCl, 10% glycerol, 0.1% Triton X-100), supplemented with 1× protease inhibitor cocktail.

Biotinylated proteins were eluted with SDS sample buffer, containing 100 mM β-mercaptoethanol and analyzed by immunoblot analysis.

The primary antibodies used are: anti-GFP (kindly provided from De Matteis's lab), Anti-α 1 Sodium Potassium ATPase antibody [464.6] - Plasma Membrane Marker (ab7671), anti-HSP90 (4874S) Cell Signaling, anti-GAPDH (6C5) sc32233, anti-α Tubulin T5168 from Sigma, anti-actin (A2066) from Sigma.

The secondary antibodies used were: HRP-conjugated secondary antibody Goat Anti-Mouse IgG, H and L Chain Specific Peroxidase Conjugate (401215; Calbiochem) to reveal: GAPDH, α-tubulin, α 1 Sodium Potassium ATPase proteins and HRP-conjugated secondary antibody Goat Anti-Rabbit IgG, H and L Chain Specific Peroxidase Conjugate (401315; Calbiochem) to reveal: GFP, Actin and HSP90 proteins.

2.14 Immunoprecipitation

Immunoprecipitation to test specific interactions between ATP7B-H1069Q-GFP and HSPA1A/B was as follows. Cell lysates from HeLa cells (1 mg) were incubated with 1.5 µg anti-GFP antibody (GFP Tag Antibody (*A-11120*) Thermo Fisher) overnight at 4°C. Then, protein A Sepharose beads (Sigma) were added to each specimen for 4 hours at 4°C and immune complexes were collected by centrifugation. The beads

were then washed and immunoprecipitated proteins were eluted, separated by SDS-PAGE and analyzed by Western blot.

2.15 Treatments with drugs

To investigate localization of ATP7B-H1069Q-GFP in HeLa, HepG2 and HepG2 KO cells were treated with the HS-72 inhibitor, cells were treated with 10μM, 50μM and 100 μM respectively for 24 hours at 37°C. Then cells were processed for immunofluorescence experiment to see whether ATP7B-H1069Q-GFP protein was delivered to the Golgi and vesicles in treated cells. To inhibit HSPA1A/B, specific inhibitor called HS-72 was added to the HeLa and HepG2 cells for 24 hours at the final concentrations of 10μM or 20μM, respectively. HeLa or HepG2 or HepG2 KO cells were infected with first generation adenovirus containing ATP7B-WT-GFP or ATP7B-H1069Q-GFP, respectively, with different multiplicity of infection (MOI) based on the physical title of Adenoviruses. To see the stabilization in time of mutant protein with the treatments, cells were incubated with 100 μg/ml cycloheximide at different times: 30 min, 1 hours and half and 5 hours and then were processed for Western Blot.

To explore the effect of FDA-approved drugs on modulation of HSP70 activity HeLa, HepG2 and HepG2 KO cells were treated with concentration of four different compounds: 10-50 μM of Domperidone*, 30 μM of Mometasone*, 30 μM of Dexamethasone* and 1 or 10 μM of Beclomethasone* (* = Glucocorticoid agonists that could modulate the expression of HSP70) for 24 hours. Then, cells were analyzed for RT-PCR, Western blot, immunoprecipitation and immunofluorescence experiments. Morphometric analysis based on percentage of cells that present ATP7B

in the ER for immunofluorescence experiment, quantification of the bands with Image J for WB and immunoprecipitation experiments and fold-change percentage parameter of mutant protein in treated-cells compared to the control cells for RT-PCR were considered to understand whether the treatments made impact on ATP7B mutant localization and stabilization.

2.16 Chemical Similarity Search

The software FLAP v. 2.0 (Baroni et al., 2007) was used to compute and performe a comparison of HS-72-like FDA-approved drugs by 3D Molecular Interaction Fields (MIFs) (fig. 20). The program FLAP is an algorithm designed primarily for virtual screening, 3D QSAR, as well as pocket comparison via three-dimensional superposition (Sirci et al., 2012a; Sirci et al., 2012b). FLAP allows 3D molecular superimposition of two molecules and computes a pairwise similarity scores based on Molecular Interaction Fields (MIFs), in order to evaluate type, strength and direction of the interactions a molecule can have. The GRID tool, (Carosati et al., 2004; Goodford, 1985) part of the FLAP software was used to compute the Molecular Interaction Fields of 3D chemical structures based on three interaction probes: H, DRY and OH2. The hydrogen probe H is used to compute the shape of a small molecule. The hydrophobic probe DRY finds places at which hydrophobic atoms on the surface of a target molecule will make favourable interactions with hydrophobic ligand atoms. The probe OH2 represents polar and hydrophilic interactions mainly generated by hydrogen bond donor and acceptor functional groups and charges interactions.

Firstly, all molecules of interest are described by the GRID force-field, and the resulting MIFs are reduced in complexity by extracting an adequate amount of

hotspots (pharmacophores) which is proportional to the strength of interaction of the MIF considered (Baroni et al., 2007). Susequently, four-point pharmacophores derived from the MIFs were iteratively extracted and used to align their 3D chemical structures, as performed in previuos 3D-QSAR and Virtual Screening works (Carosati et al., 2004; Goodford, 1985). Finally, the evaluation of MIF volume superpositions is reported as similarity between the different structures, ranging from 0 to 1 for each of the three probes. A global score (GLOB-S) is then obtained as the sum of the three scores of the individual probes. Higher GLOB-S values correspond to more similar structures.

2.17 Bioinformatics search for FDA-approved drugs reducing *HSP70* expression

"Connectivity Map" collection (or CMap), a catalog of gene-expression data collected from human cells treated with chemical compounds and genetic reagents, was utilized to find drugs that probably could modulate the expression of HSP70 protein and with the help of F. Napolitano (TIGEM Bioinformatics Core), I selected the most significant drugs based on their p-value.

The database of gene expression data is made of 6,100 differential expression publicly available as the "Connectivity Map" collection (Lamb et al., 2006). Each gene expression profile was sorted so that most up-regulated genes appear at its top and most down-regulated genes appear at its bottom. The 6,100 sorted profiles were then reduced to 1,309 (one per treatment) by merging together those obtained after treatment with the same small molecule, as described in (Iorio et al., 2010).

HSPA1A and *HSPA1B* genes were defined as the molecular targets to screen for HSP70 drugs that reduce expression of these genes. Among the hits we then

considered only compounds that increase expression of *HSP90A1* and *HSP90A2* (see Results). For the analysis the gene expression profile for each drug from the CMap was searched for dysregulation of each of the 4 genes. In particular, the mean rank of the two *HSP70* targets (say r1) and the mean rank of two *HSP90* targets (say r2) were recorded for each CMap drug. Finally, all CMap drugs were ranked according to the score: r1 + 1310 - r2. Top drugs in this ranking are expected to down-regulate *HSPA1A* and *HSPA1B* and up-regulate *HSP90AA1* and *HSP90AB1*.

2.18 Drug-set Enrichment Analysis (DSEA)

In order to find which are the common pathways that are affected by FDA-approved drug, with the help of F. Napolitano, DSEA Analysis was performed on three different compound: Dexametasone, Mometasone and Beclometasone.

(DSEA), aims at identifying the mechanism(s) of action shared by a set of compounds in terms of the molecular pathways consistently targeted by most of them. The main hypothesis underlying DSEA is that if pharmacologically different drugs induce the same phenotype of interest, then some of the molecular pathways they target must be shared by most of them. DSEA takes advantage of a large database of pathways by merging 9 different publicly available collections, including generic gene sets (co-localised genes, coregulated genes, protein complex subunits, etc.) and disease-related gene sets. In order to define the list of pathways targeted by a drug, DSEA analyses were performed according to the Connectivity Map dataset (Lamb et al., 2006), which consists of about 7000 microarray assays following treatment of four different cell lines with 1309 drugs. Relevant pathways for the drugs of interest are thus selected against the background of all the other drugs in the CMap. In this way,

pathways that are relevant for the phenotype of interest tend to emerge, while drug-specific pathways, which are unrelated to the phenotype of interest, tend to cancel out.

2.19 MTT assay

Knockout cells harboring wild type *ATP7B* (WT ATP7B KO cells) or mutagenized *ATP7B* clones (H1069Q and R778L cells) (Chandhok et al., 2016) were maintained in RPMI media (Euroclone) containing 10% fetal bovine serum (FBS) with 100 U/ml penicillin/streptomycin and supplemented with 6 μg/ml blasticidin (Sigma). $15x10^3$ cells were seeded in 96 well plates in 100 μl of complete medium. After 48h, cells were incubated with 10 μM Mometasone, Dexamethasone or Beclomethasone, 1 μM of Domperidone or 100 nM of HS-72 inhibitor, respectively. 24h later, cells were exposed to 1mM $CuCl_2$ (Sigma) overnight. For the MTT (3-(4,5-dimethylthiazol-2-yl)-2,5-diphenyltetrazolium bromide) assay, cells were washed twice in PBS (Euroclone), resuspended in 12mM MTT (Invitrogen) dissolved in 100 μl of DMEM media lacking phenol red (Invitrogen) and supplemented with 10% FBS and 100 U/ml penicillin/streptomycin and incubated for 2.5h in 5% CO_2 at 37 °C. Incubation was stopped using 100 μl of a solution of 25% aqueous ammonia (Sigma) in DMSO (Sigma) for 10min in 5% CO_2 at 37 °C. Absorbance was recorded at 540 nm on a multi-well plate reader (Synergy/neo, Biotek) and results analyzed as percentage of treated compared to untreated cells (no $CuCl_2$ considered as 100% viability). Differences in viability between 1mM $CuCl_2$ treated cells and cells treated with drugs and 1mM $CuCl_2$ were analysed using an T-test. A value of $P<0.05$ was considered significant. All data are presented as a mean ± SEM.

CHAPTER 3. RESULTS AND DISCUSSION

3.1. HSP70 as new molecular target for the correction of Wilson disease mutants

3.1.1. Traditional proteomics analysis reveals specific binding partners for ATP7B-WT and ATP7B-H1069Q

To understand which molecular target(s) could be explored for the correction of WD-causing mutants, I used proteomics approach. As outlined in the previous chapter disease-causing mutations frequently induce significant remodelling of protein's interactome. Therefore, my first objective was to compare interactomes of wild type ATP7B (ATP7B-WT) and of its most frequent H1069Q mutant (ATP7B-H1069Q). Considering that a large number of ATP7B interactions require Cu to occur (Lim et al., 2006), cell expressing ATP7B or its mutant were enrolled into proteomics study after exposure to Cu. I also took in account that ATP7B is expressed mainly in the liver (Bull et al., 1993; Kuo et al., 1997; Michalczyk et al., 2000) and thus used hepatic HepG2 cell line to detect ATP7B binding partners.

To characterize ATP7B-WT and ATP7B-H1069Q interactomes I used an immunoprecipitation approach combined with mass spectrometry analysis, which was carried out in collaboration with the proteomics facility in CEINGE (Naples). Unfortunately, a hepatic cell line with endogenous expression of ATP7B-H1069Q mutant has yet to be developed. Therefore, I used GFP-tagged variant of ATP7B-H1069Q in HepG2 cells and WT version of ATP7B with the same tag as a control. To this end HepG2 cells were transduced with adenoviruses carrying either ATP7B-WT

(Ad-ATP7B-WT) or ATP7B-H1069Q (Ad-ATP7B-H1069Q). Protein complexes in transduced cells were allowed to form and the proteins of interest were immunoprecipitated from cell extracts with anti-GFP antibody. The immunoprecipitated material containing the ATP7B bait and its binding partners were then fractionated by SDS-PAGE and the individual protein components were identified by mass spectrometry. Analysis of the interactome revealed that WT protein and mutant have a large cohort of 52 common binding partners (Fig. 6A). The presence of the known ATP7B interactor glutaredoxin (Lim et al., 2006) among the pulled-down proteins confirmed the specificity of the IP approach. However, both ATP7B variants exhibited specific interactions (31 for WT protein and 51 for the mutant), indicating that H1069Q mutation remodels ATP7B interactome (Fig. 6A; see supplementary data).

Gene Ontology (GO) analysis indicated that the group of mutant-specific interactors exhibited significant enrichments in such categories as “unfolded protein binding”, “protein folding” and “protein stabilization” (Fig. 6C). In contrast WT protein interactome exhibited enrichments in proteins that belong to membrane trafficking and cell adhesion groups (Fig. 6B). Apparently, differences in the interactomes of ATP7B-WT and ATP7B-H1069Q indicated the consequences of the mislocalisation of the mutant ATP7B-H1069Q to the ER, such as enhanced interactions with the components of the ER-associated quality control and degradation (ERAD) machineries. So, it is possible that ATP7B-H1069Q expression modulates ER quality control mechanisms and accelerates the degradation of the protein, as reported previously (Chesi et al., 2016; de Bie et al., 2007).

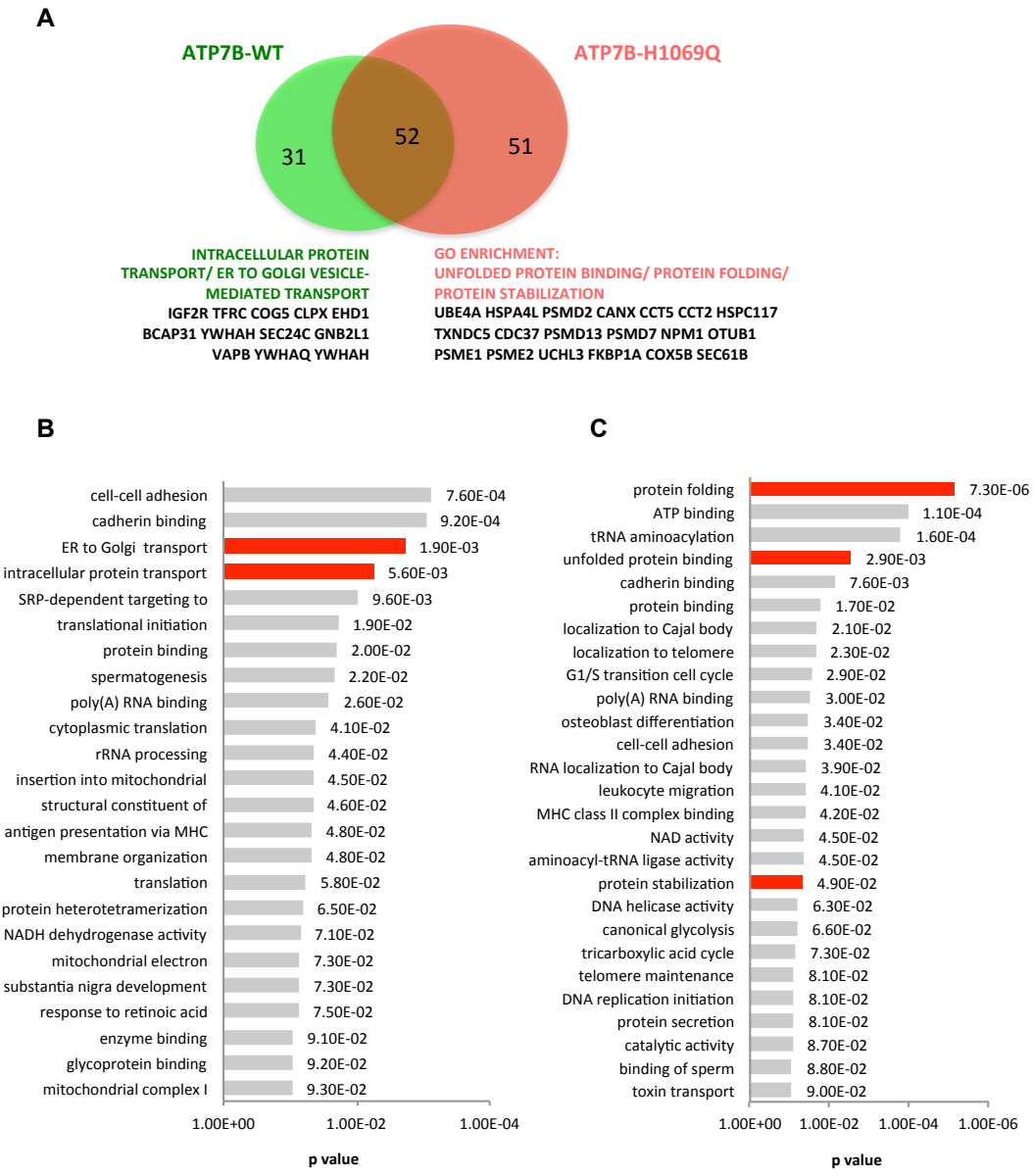

Fig. 6: Proteomics reveals strong differences in ATP7B-WT and ATP7B-H1069Q interactomes.

Putative interactors of ATP7B-WT and ATP7B-H1069Q were identified using a standard proteomics approach (see Methods). The diagram in panel A shows the number of interactors that were specific for ATP7B-WT or for ATP7B-H1069Q as well as the number of common interactors. GO analysis revealed ATP7B-WT interactors to be enriched in proteins belonging to membrane trafficking categories, while mutant-specific interactors were enriched in proteins involved in ER-associated protein quality control and degradation. Panel **B** shows the enriched GO Biological Process Categories for ATP7B-WT interactors based on their p value. Red bars indicate membrane trafficking categories. Panel **C** shows the enriched GO Biological Process Categories for mutant interactors. In contrast to ATP7B-WT interactors, GO reveals that mutant interactome is enriched in protein folding, unfolding protein binding and protein stabilization classes (red bars).

Interestingly, the well-known ΔF508 mutant of CFTR exhibits the similar trend in interactome remodelling towards increase of ER quality control component binding

(Young, 2014) indicating that disease-causing mutations significantly affect the binding landscape of these complex transmembrane proteins.

3.1.2 SILAC proteomics analysis confirmed the differences between ATP7B-WT and ATP7B-H1069Q interactomes

Apart from the specific binding partners WT and H1069Q forms of ATP7B exhibited common component in their interactomes. Several proteins from this common group (DNAJB1, ERLIN1, PSMA1 to name few) belong to ER proteostatic machinery and thus could be involved in quality control of WT ATP7B and of its mutant. Unfortunately, traditional proteomics approach does not allow evaluation of quantitative difference in these common proteins binding to ATP7B-WT or ATP7B-H1069Q. Thus, to detect these differences I decided to use a very sensitive proteomics approach, SILAC analysis (Fig. 7). SILAC is a straightforward metabolic labelling technique used for mass spectrometric (MS)-based quantitative proteomics. It allows the identification and quantitation of thousands of proteins in a single experiment (Ong et al., 2002). In this approach, samples under comparison are differentially labelled and then mixed prior to analysis by nano-LC-MSMS. To detect the molecules that may interact with ATP7B, I used in my experiments cells expressing GFP as a negative control, and compared interactomes of ATP7B-WT and ATP7B-H1069Q in HepG2 cells (Fig. 8; see also Supplementary data).

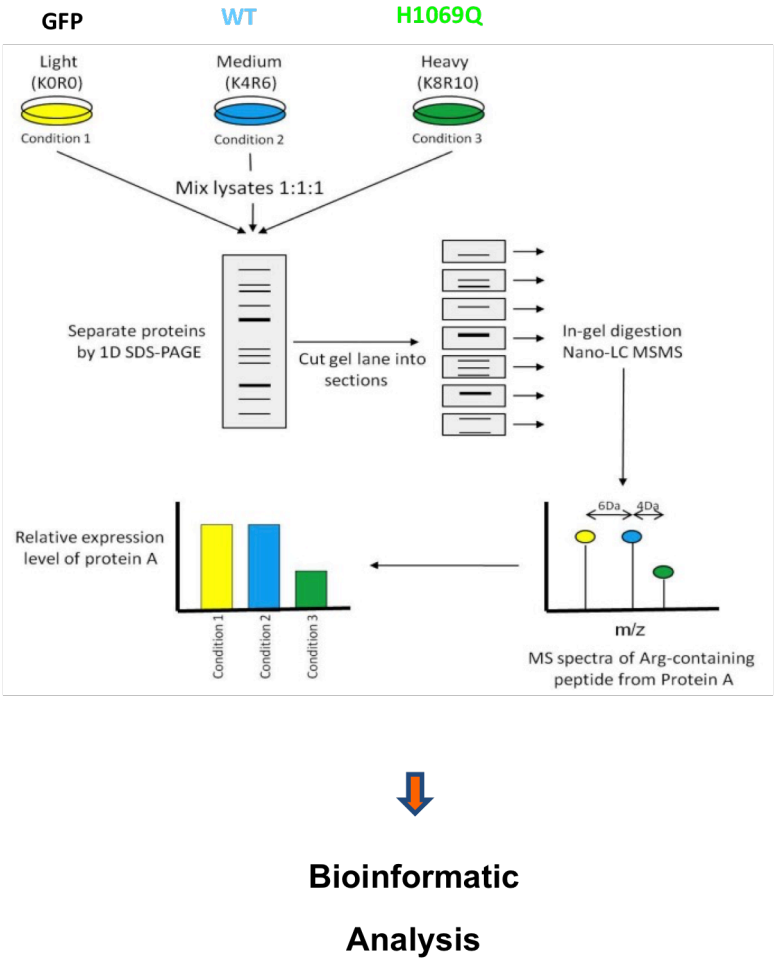

Fig. 7: SILAC analysis. HepG2 cells were preloaded with light (K0R0), medium (K4R6) and heavy (K8R10) isotopes if lysine and arginine. Then light, medium and heavy cells were infected with adenovirus carrying GFP alone, ATP7B-WT-GFP or ATP7B-H1069Q-GFP respectively and treated treated with $CuSO_4$ 200 µM. Anti-GFP antibody was utilized to immunoprecipitate GFP-tagged ATP7B and control GFP from total cell lysates. Interactors were identified using spectrometry and bioinformatics analysis.

The cells were loaded with amino acid isotopes of different weight. Then the protein complexes were allowed to form and the cell extracts immunoprecipitated with α-GFP antibody. The immunoprecipitated material containing the ATP7B bait and its binding partners was then fractionated by SDS-PAGE and the individual protein components were identified by mass spectrometry (See the supplementary table with SILAC results in supplemental data).

This approach allowed me to identify interactions of ATP7B that are affected by the H1069Q mutation in the *ATP7B* gene, and potentially cause retention of the mutant

within the ER. I evaluated the strength of interaction in SILAC experiments and found that although some interactors bind both WT and mutant proteins proteins exhibit preference for one of the ATP7B variants (determined from herein as "WT-specific" and "mutant-specific" as well). As in the case of traditional proteomics GO analysis revealed strong enrichment of mutant interactome in categories that were associated to protein unfolding, such as "chaperone binding", "unfolded protein binding", and "response to unfolded protein". (Fig. 8). In particular we noted "HSP70 protein binding" and "regulation of cell response to heat" enrichments that suggest preferential interaction of the mutant with a subset of HSP70-associated chaperones/proteins. Interactome of ATP7B-WT also contained several components of proteostatic machinery (mainly associated to proteasome regulation) but did not exhibit specific enrichments in unfolded protein terms. This indicates that the mutant is retained in the ER with specific subset of quality control proteins, which could be targeted to circumvent ER accumulation and degradation of ATP7B-H1069Q.

To prioritize interactors that could be targeted for mutant correction I considered the interaction score of each binding partner. This parameter reflects the strength of the interaction and takes in account peptides detected with SILAC and the percentage of protein sequence coverage by these peptides. The interactors with higher score in both categories were considered as the straightforward candidates for validation in further ATP7B trafficking experiments. In addition to above approaches, each putative interactor of either ATP7B, or ATP7B-H1069Q or both were evaluated for its relevance for membrane trafficking and ER quality control.

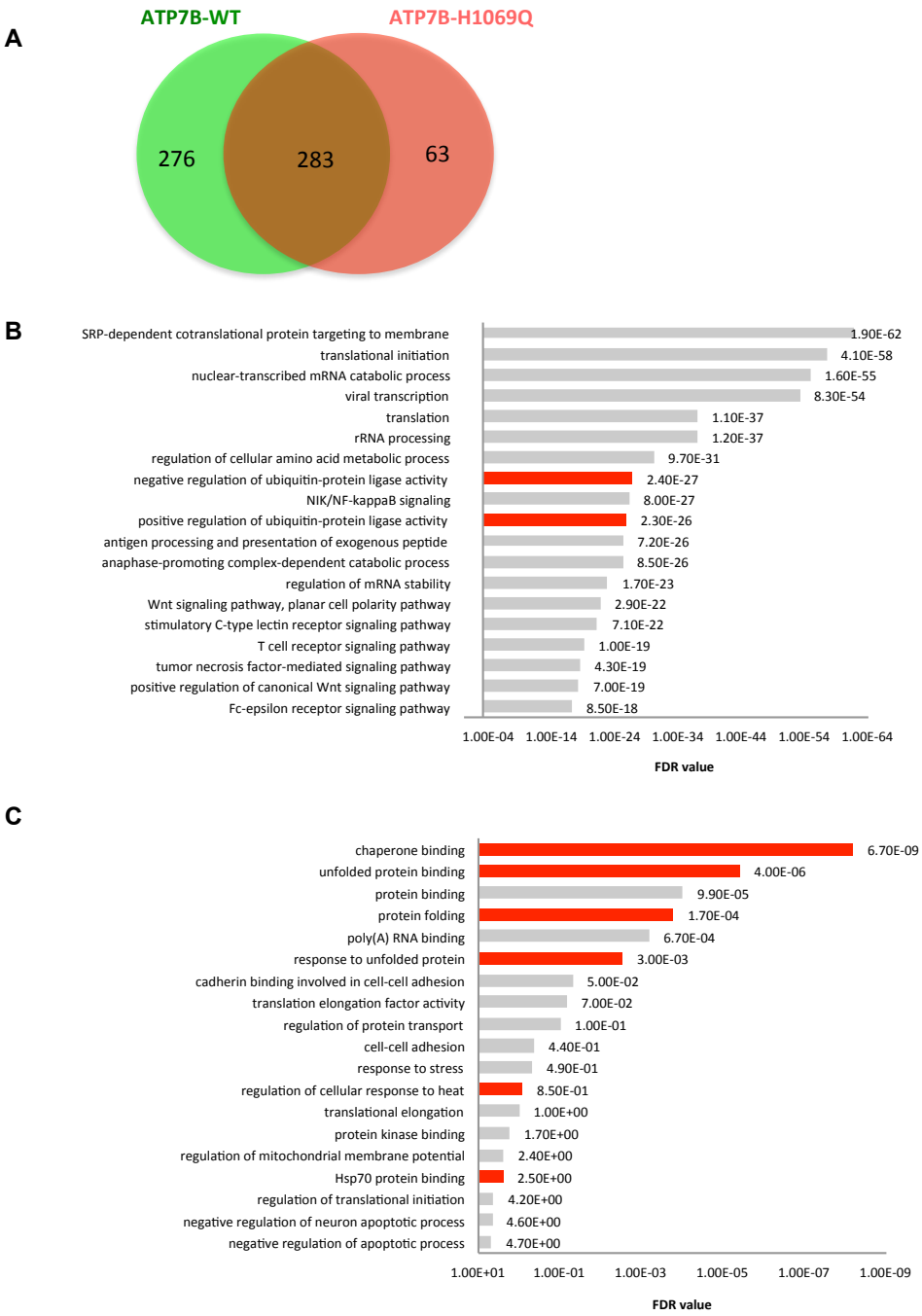

Fig. 8: SILAC Analysis reveals differences in ATP7B-WT and ATP7B-H1069Q interactomes. (A) Putative interactors of ATP7B-WT and ATP7B-H1069Q were identified using SILAC proteomics approach. The diagram shows the number of interactors that were specific for ATP7B-WT or for ATP7B-H1069Q as well as the number of common interactors. **(B-C)** . Panel **B** and **C** show the GO biological process categories enriched in ATP7B-WT and ATP7B-H1069Q interactomes respectively. Protein quality control categories are indicated in red. In contrast to ATP7B-WT interactors, GO analysis revealed enrichment of ATP7B-H1069Q interactome in chaperone binding, unfolded protein binding protein folding, response to unfolded protein, regulation of cellular response to heat, HSP70 protein binding classes as revealed by red bars.

3.2. Inhibition of HSP70 rescues trafficking of the ATP7B-H1069Q

3.2.1. Selection of HSP70 as a target for ATP7B-H1069Q mutant correction

Among different specific interactors of the ATP7B mutant, HSP70, looked particularly interesting for three different reasons. HSP70 exhibited particularly high score as 27 peptides that cover 43% of its sequence were detected in ATP7B pulldowns. SILAC proteomics indicated almost 2.5 fold increase in HSP70 binding to mutant compared ATP7B-WT. GO analysis of mutant interactome revealed specific enrichment in HSP70 binding proteins. Finally, a recent study from our lab suggests that p38 and JNK stress kinases upregulate HSP70 to accelerate ER degradation of ATP7B-H1069Q mutant (Concilli et al., 2016).

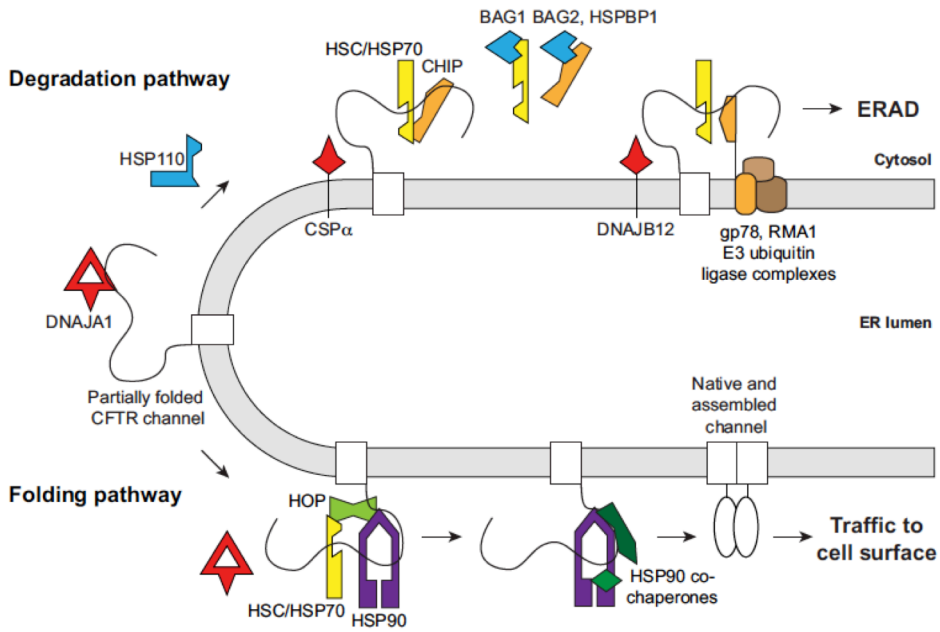

Fig. 9. Mechanisms of HSP70-mediated folding/degradation pathways. CFTR follows chaperone-mediated pathways for degradation (top) as well as folding (bottom). In the folding pathway, starting from the left, DNAJA1 (red) activates the binding of HSC/HSP70 (yellow) to CFTR to initiate folding; co-chaperone HOP (light green) transfers CFTR from HSC/HSP70 to HSP90 (purple) and its co-chaperones (dark green) to complete folding and allow trafficking to the cell surface. In the degradation pathway, the HSC/HSP70 co-chaperone CHIP (orange) is an E3 ubiquitin ligase that promotes degradation of misfolded CFTR. CHIP functions in parallel to membrane-anchored E3 ubiquitin ligases gp78 and RMA1 and associated components (brown), which do not depend on HSC/HSP70. The DNAJ co-chaperones (red) CSPα and DNAJB12 promote CFTR degradation by CHIP, and by gp78 and RMA1, respectively. The NEFs (blue) BAG2, BAG1 and HSPBP1 interfere with CHIP activity, BAG1 by causing HSC/HSP70 to release substrate, BAG2 and HSPBP1 by binding directly to CHIP. The NEF HSP110 also promotes CFTR degradation. HSP110 is homologous to HSC/HSP70 in the ATP-bound state.

Adapted from Young et al., 2014

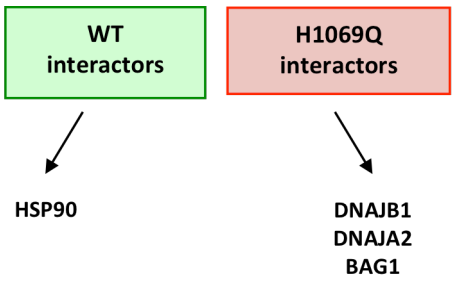

Fig. 10. ATP7B-H1069Q interactome contains the components of HSP70-mediated degradation pathway.

HSP70 is a chaperone that plays a key role in proteostasis of wide range of proteins via regulating their folding/degradation (Bukau et al., 2006; Frydman, 2001; Hartl et al., 2011; Mayer and Bukau, 2005). Excessive association of HSP70 with ATP7B mutant could reflect a so called "chaperone trap" of misfolded membrane protein in the ER that usually activates degradation of the aberrant protein product. Such a chaperone trap and its involvement in ΔF508 mutant of CFTR has been well documented (Coppinger et al., 2012; Young, 2014) (Fig. 9). Thus I reasoned that HSP70 could be explored as a target for ATP7B mutant correction. Hsp70 plays a key role in ER-associated quality control of the transmembrane proteins. The available literature indicates that it may target misfolded proteins to ERAD or facilitate their folding and sorting into the secretory pathway. This depends on the degree of protein misfolding and other chaperons that cooperate with Hsp70 (Young, 2014). The scheme in Fig. 9 illustrates how HSP70 drives either folding or degradation of CFTR. So it is tempting to speculate that HSP70 could deal in the same way with ATP7B mutant.

Interestingly, SILAC proteomics data suggest that ATP7B-H1069Q exhibits stronger interaction with HSP70 partners such DNAJs and BAG1 (Fig. 10) that promote degradation of misfolded proteins (Young, 2014). This suggests that HSP70 is likely to direct the mutant to degradation rather than to folding pathway. Indeed, SILAC

experiments indicate reduced ATP7B-H1069Q binding to HSP90, which cooperates with HSP70 in the process of protein folding.

3.2.2. *HSP70* silencing corrects ATP7B-H1069Q localization

As outlined in the introduction, ATP7B-WT resided within the TGN (labelled by TGN46) at low Cu conditions and moved to the post-Golgi endo-lysosomal vesicles and cell surface upon exposure to Cu (Fig. 11A). In contrast, significant amounts of ATP7B-H1069Q remained in the ER independently of the Cu concentrations (Fig. 11B). To determine whether inactivation of HSP70 facilitates ATP7B-H1069Q export from the ER, I decided to suppress *HSP70* using RNAi in HeLa and HepG2 cells. HepG2 cells were used as WD-relevant type, while HeLa cells were added because usually siRNA-mediated silencing works very efficiently in this cell type. The cells were incubated with HSP70-specific siRNAs and subsequently transduced with Ad-ATP7B-H1069Q to express the mutant. Then the cells were fixed and the intracellular distribution of ATP7B-H1069Q in *HSP70*-silenced cells was compared to cells incubated with control siRNAs (siControl). Given that ATP7B-H1069Q exhibited similar ER distribution at both low and high Cu levels, we did not modulate Cu levels and analysed pattern of ATP7B mutant in both control and silenced cells at steady state conditions.

Ablation of HSP70 caused a remarkable impact on the ATP7B-H1069Q localisation, as its amounts within the ER were strongly reduced (Fig. 12A). Instead of the ER, ATP7B mutant was observed in the perinuclear Golgi area and to some extent within post-Golgi LE/lysosome like structures (Fig. 12A, arrows) in HSP70-deficient cells. Western blot revealed efficient silencing of *HSP70* in both HeLa and HepG2 cells,

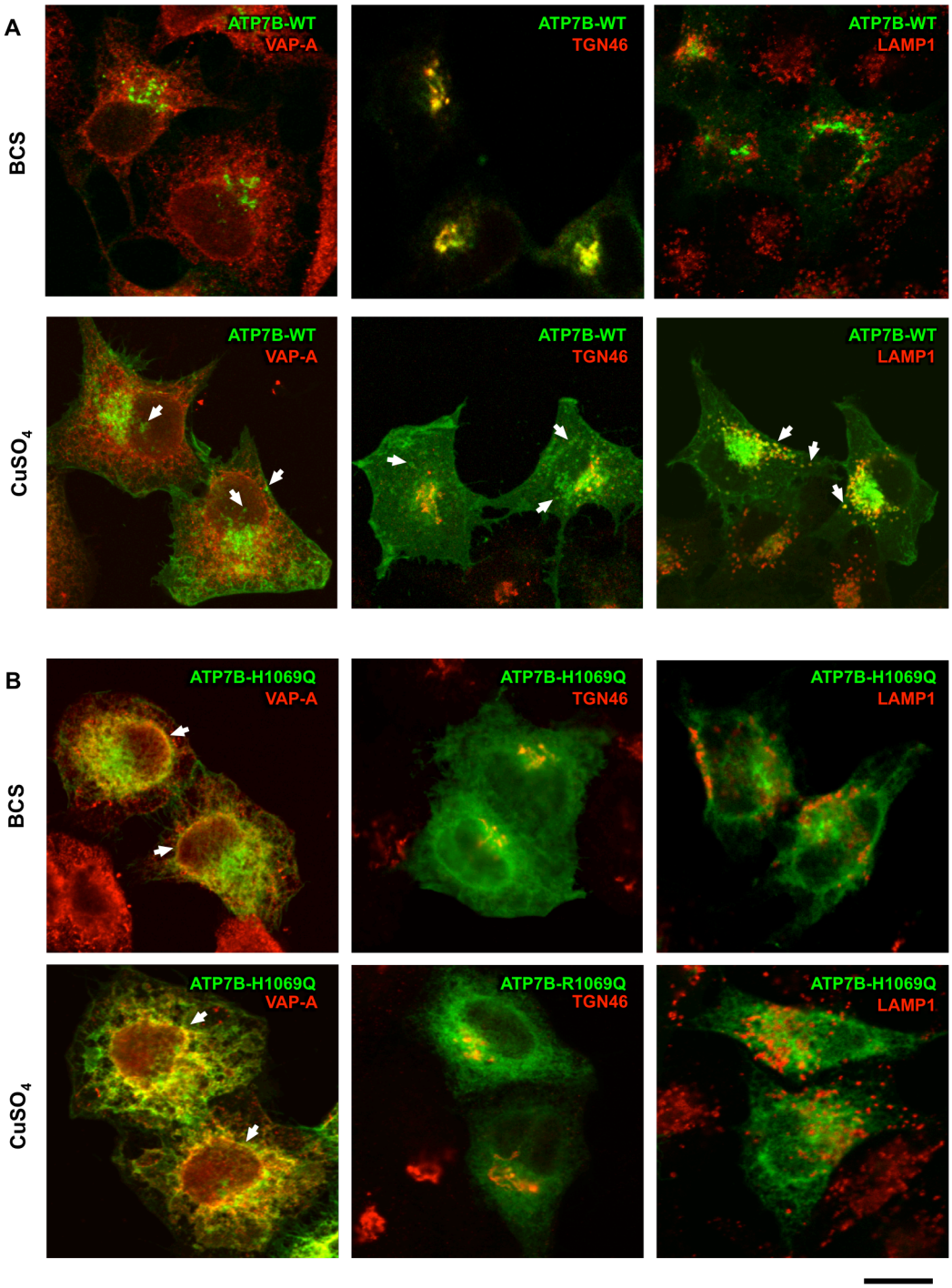

Fig. 11. Trafficking of ATP7B-WT and ATP7B-H1069Q under low and high copper condition. HepG2 cells expressing GFP-tagged version of ATP7B-WT **(A)** or ATP7B-H1069Q **(B)** were treated with Cu chelator BCS (200 µM overnight) or CuSO4 (200 µM for 2h) fixed and stained with ER marker VAP-A, Golgi marker TGN46 and late endosome (LE)/lysosome marker LAMP1. Confocal microscopy revealed that ATP7B-WT moved from the Golgi (A, top row) to the cell surface (A, bottom row) and LE/lysosome structures (arrows in A). Most of ATP7B-H1069Q remained within the ER independently from Cu depletion (B, top row) or Cu supply (B, bottom row). Arrows in panel B indicate overlap of ATP7B-H1069Q with VAP-A in the ER. Scale bar for panels A and B = 4.5 µm. Experiment was done in triplicate. Mean ±SD.

although in contrast to my expectation siRNA better suppressed HSP70 expression in HepG2 cells than in HeLa cells (Fig. 12B). This could explain why in HepG2 line the

percentage of cells with ATP7B-H1069Q in the ER was stronger impacted upon HSP70 ablation (Fig. 12C).

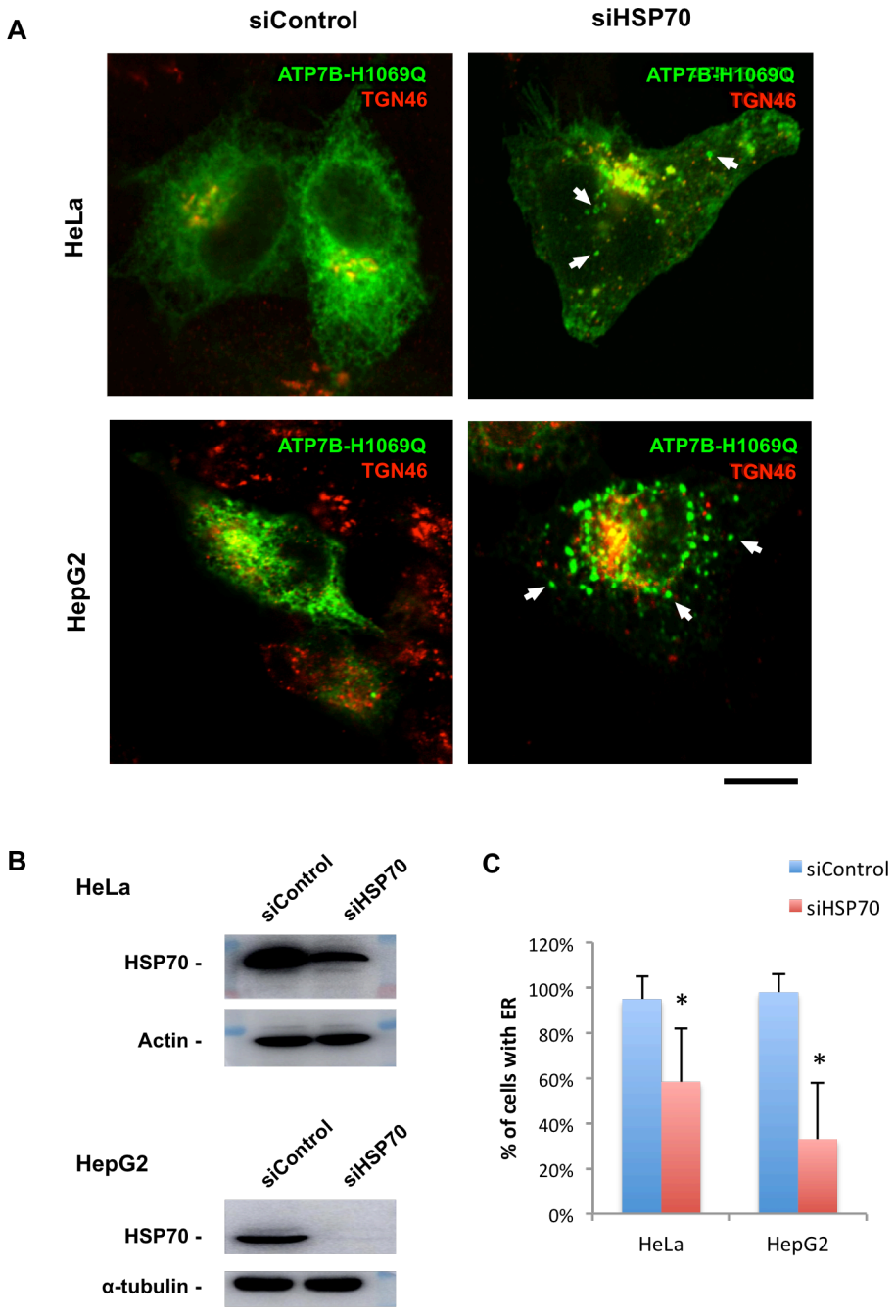

Fig. 12. *HSP70* silencing reduces retention of ATP7B-H1069Q in the ER.

HeLa or HepG2 cells expressing GFP-tagged ATP7B-H1069Q were treated with control (siControl) or HSP70-specific (siHSP70) siRNAs and further processed for confocal microscopy (A, C) or Western blot (B). **(A)** Confocal microscopy revealed that HSP70 silencing reduces amount of ATP7B- H1069Q within the ER and promotes the mutant trafficking to the Golgi and LE/lysosome-like post-Golgi structures (arrows). Scale bar for panel A = 4.7 µm. **(B)** Western blot shows reduction of HSP70 expression in both HeLa and HepG2 cells. **(C)** Morphometric analysis confirms that HSP70 depletion decreases the percentage of the cells exhibiting ATP7B-H1069Q mutant within the ER (n= 10 fields). * - $p<0.05$ (t-test). Experiment was done in triplicate. Mean ±SD.

This indicates that suppression of HSP70 facilitates export of ATP7B mutant from the ER into distal compartments of secretory pathway, where ATP7B normally resides and functions. Thus, HSP70 could be explored as a potential target for correction of the most frequent Wilson disease-causing mutant.

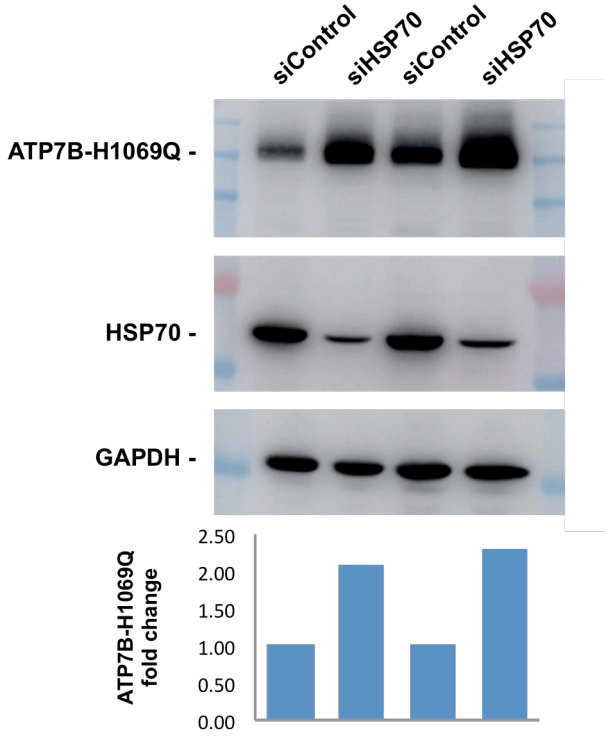

Fig. 13. HSP70 depletion attenuates degradation of ATP7B-H1069Q.

HepG2 cells expressing GFP-tagged ATP7B-H1069Q were treated with control (siControl) or HSP70-specific (siHSP70) siRNAs and further processed for Western blot to reveal ATP7B mutant with anti-GFP antibody. Western blot shows increase in the levels of ATP7B-H1069Q expression in cells treated with HSP70-specific siRNAs indicating reduced degradation of the mutant. The graph shows the changes in ATP7B mutant. Experiment was done in triplicate.

Faster export of ATP7B-H1069Q from the ER in HSP70-depleated cells may reduce exposure of the mutant to the protein quality surveillance and, hence, inhibit the mutant degradation. Thus, I decided to check whether HSP70 suppression also has an impact on H1069Q turnover. To this end I performed WB experiment in which HeLa cells infected with Ad-ATP7B-H1069Q were treated with either control or HSP70-specific siRNAs. I found that the level of ATP7B-H1069Q signal was higher in HSP70-silenced cells compared to the control (Fig. 13). This observation suggests that HSP70 is involved in the degradation of the mutant and that suppression of HSP70 attenuates the degradation process.

3.2.3. H1069Q mutation increases ATP7B interaction with HSP70

HSP70 interacts with wide range of proteins (Young, 2014) and frequently appears as a false positive interactor in proteomics studies. Thus, in order to confirm and characterize in detail the interaction between HSP70 and ATP7B, I performed a CoIP experiment in HepG2 cells expressing WT and H1069Q ATP7B variants. I observed considerably higher amounts of HSP70 in ATP7B-H1069Q pull downs when compared to WT protein (Fig. 14). This indicates stronger interaction of the mutant

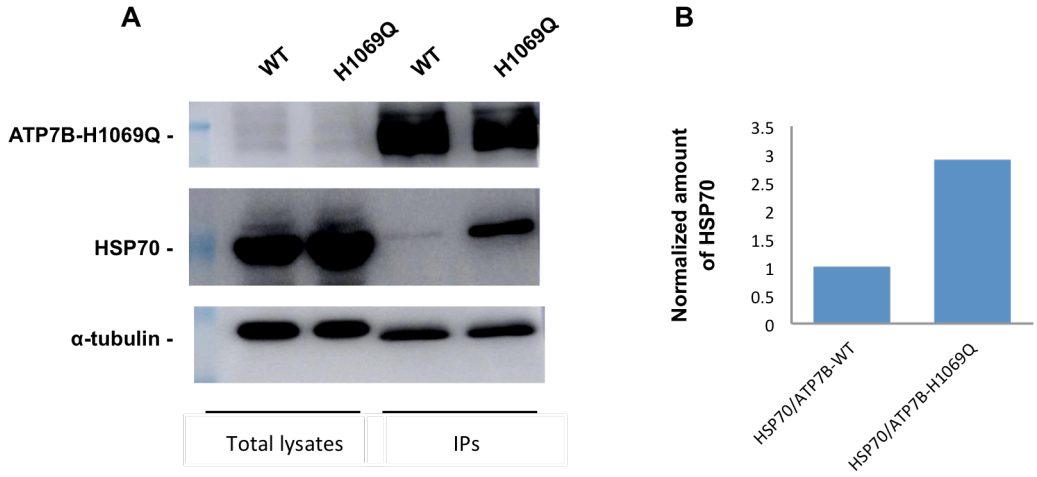

Fig. 14. **ATP7B-H1069Q exhibits stronger interaction with HSP70.**

GFP-tagged ATP7B-WT or ATP7B-H1069Q were expressed in HepG2 cells. Then ATP7B-GFP was immunoprecipated from cell lysate. Western blot (A) shows higher levels of HSP70 in ATP7B-H1069Q pulldowns indicating stronger interaction of the mutant with HSP70. Notably, the level of HSP70 signal was also higher in total lysates from cells expressing ATP7B-H1069Q protein than from cells expressing WT protein. The graph (B) shows normalized level of HSP70 bound either WT protein or H1069Q mutant. Experiment was done in triplicate.

with HSP70. Interestingly, overall levels of HSP70 expression were higher in total lysates of cells expressing ATP7B mutant than in cells expressing WT protein. This can be expected because recent study from our lab suggests that the presence of ATP7B-H1069Q mutant activates p38- and JNK-driven stress response pathways (Chesi et al., 2016), which in turn upregulate a cluster of ER quality control genes comprising *HSP70* (Concilli et al., 2016). However, the magnitude of ATP7B-H1060Q interaction with HSP70 could not be exclusively explained by increased

HSP70 levels in mutant-expressing cells. It seems that HSP70 only moderately rise in total lysates upon mutant expression, while amount of HSP70 in ATP7B-H1069Q pull down exhibit several fold increase.

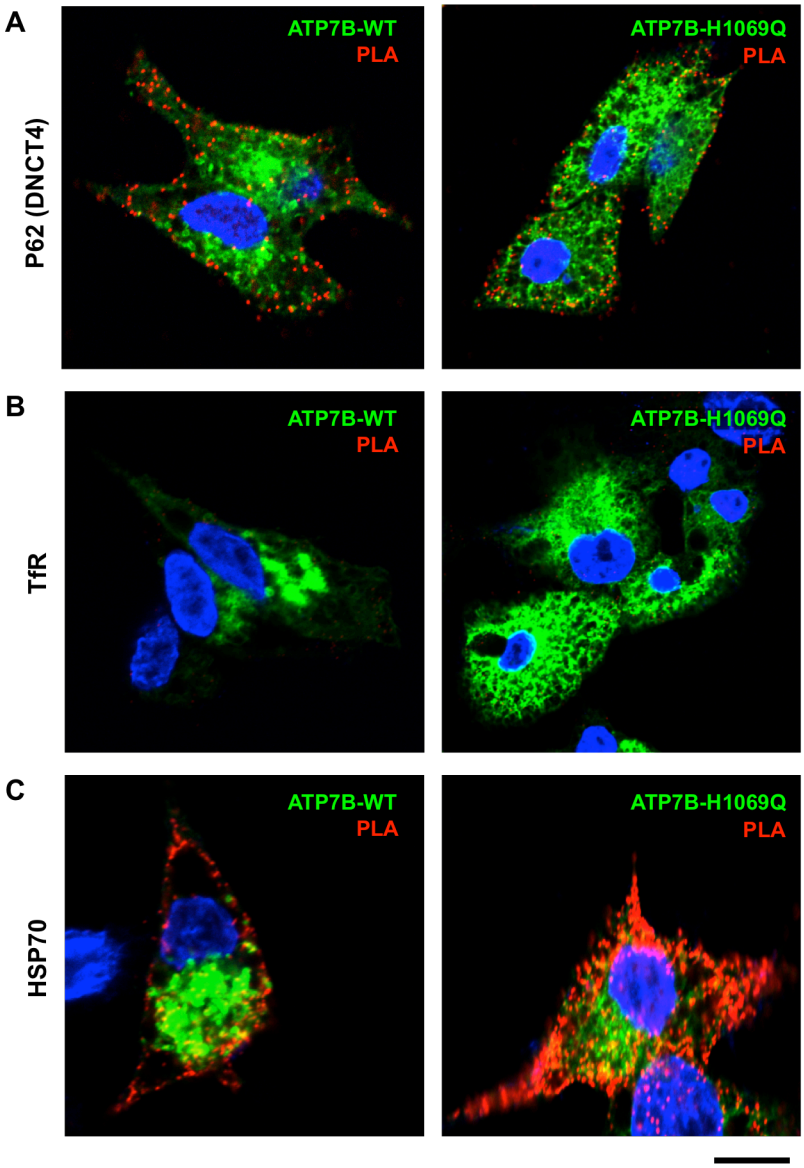

Fig. 15. Proximity ligation assay (PLA) reveals stronger association of HSP70 with ATP7B mutant. HepG2 cells were infected with adenoviruses carrying GFP-tagged ATP7B-WT or ATP7B-H1069Q, treated with Cu and processed for PLA analysis. **(A)** Efficiency of PLA assay was confirmed by presence of the PLA signal (red spots) between ATP7B variants and p62 (DNCT4), a well-known interactor of ATP7B. **(B)** ATP7B proteins did not generate PLA signal with TfR (employed as a negative control). (C) ATP7B-H1069Q induced stronger PLA signal with HSP70 in comparison to WT protein, indicating that HSP70 exhibits higher affinity for the mutant protein. Scale bars = 5µm (A-C) Experiment was done in triplicate.

To confirm the interaction using complementary approach I utilized proximity ligation assay (PLA). In this way protein association within 40nm range from each other can be detected (Soderberg et al., 2006). The strength of such association could be evaluated on the basis of the presence of red fluorescent spots that indicate interaction. The HepG2 cells were infected with Ad-ATP7B-WT or Ad-ATP7B-H1069Q and processed for PLA analysis. First I used positive control and found that

both ATP7B variants generates PLA signal with well-known ATP7B interactor p62 (DNCT4) (Fig. 15A). In contrast I did not obtain (as expected) the PLA signal between ATP7B proteins and Transferrin Receptor (TfR), which was used as a negative control (Fig. 15B). Finally I found that the ATP7B-H1069Q induces stronger PLA staining with HSP70 than WT protein (Fig. 15C), indicating that HSP70 binds preferentially the mutant protein, as in the case of co-IP experiments and SILAC proteomics data.

3.2.4. Chemical inhibitor of HSP70 rescues ATP7B-H1069Q localization and stability

To test further the potential of HSP70 as a target for correction of ATP7B-H1069Q mutant I thought to suppress HSP70 with a different approach. Over the last decade several chemical compounds that inhibit HSP70 were reported (Kim et al., 2014; Prota et al., 2012; Yu et al., 2010). In 2014 Howe et al. published a paper, in which they found a small molecule inhibitor of HSP70 called HS-72 (Fig. 16). This

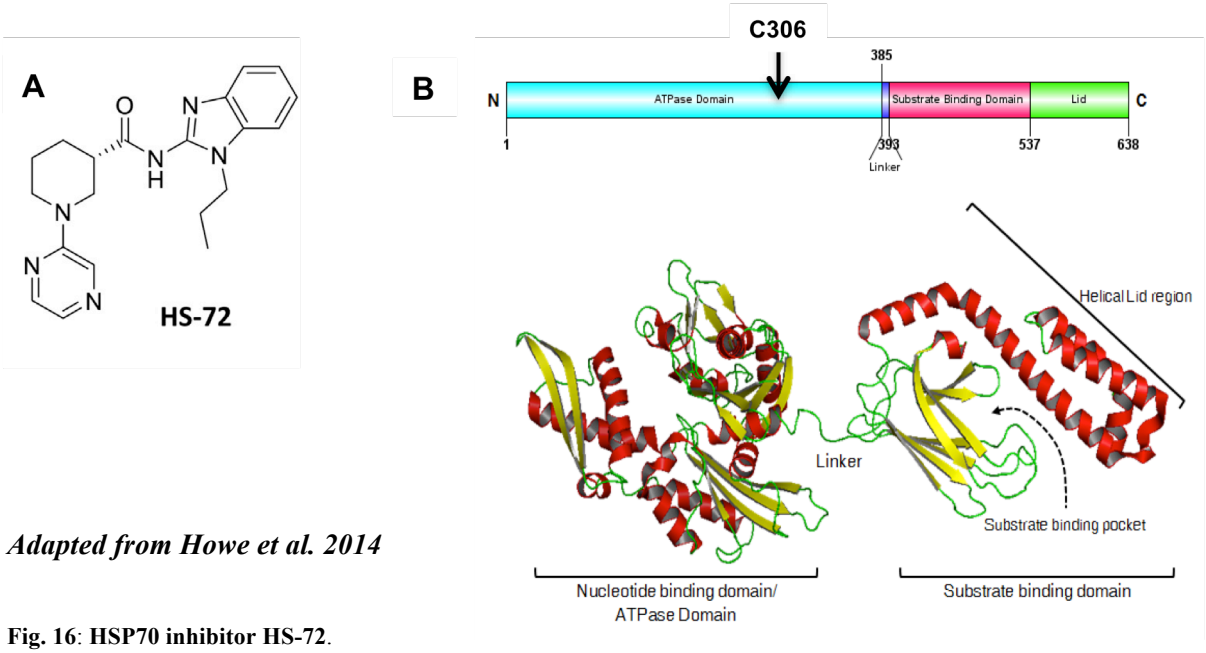

Adapted from Howe et al. 2014

Fig. 16: **HSP70 inhibitor HS-72**.

Panel A depicts chemical structure of HSP70 inhibitor HS-72. Panel B shows 2D and 3D structures of ATP7B. Arrow indicated putative binding site of HS-72 at C306 position.

molecule acts as an allosteric inhibitor reducing ATP binding in the ATPase domain of the HSP70 protein. Moreover, the authors demonstrated very high specificity of the inhibitor for HSP70 and lack of any significant impact on other similar chaperones. Apparently, this inhibitor binds to HSP70 at the C306 residue, which is not shared by other Hsp70 family members such as Hsc70, Grp78, and Grp75, and Hsp90 (Howe et al., 2014).

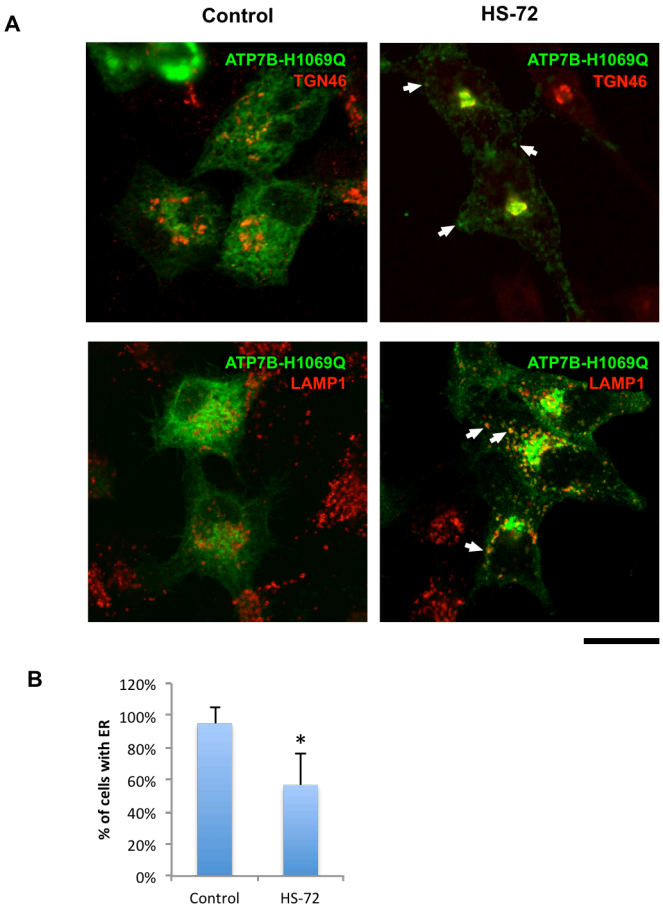

Fig. 17. HSP70 inhibitor reduces retention of ATP7B-H1069Q in the ER.

HepG2 cells expressing GFP-tagged ATP7B-H1069Q were treated with 10 µM HSP70-specific inhibitor HS-72 for 24 hours and further processed for confocal microscopy. **(A)** Confocal microscopy revealed that HS-72 reduces the amount of ATP7B- H1069Q within the ER and promotes the mutant trafficking to the Golgi and LE/lysosome-like post-Golgi structures (arrows). Scale bars for panel A= 4 µm **(B)** Morphometric analysis confirms that HSP70 suppression with HS-72 decreases the percentage of cells exhibiting ATP7B-H1069Q mutant within the ER (n= 10 fields). * - $p<0.05$ (t-test). Experiment was done in triplicate. Mean ±SD.

I took advantage of this inhibitor and treated cells to test whether suppression of HSP70 with specific chemical compound leads to correction of ATP7B-H1069Q in terms of localization and stability of the protein product. First I checked whether the inhibitor rescues ATP7B localization. When I stained HS-72-treated cells with marker

of Golgi (TGN46) or lysosomes (LAMP1) at the steady state conditions, I found the mutant in both Golgi and to some extent in post-Golgi Lamp1-positive structures while in control cells it was mainly distributed over the ER (Fig. 17A). Morphometric analysis confirmed that HS-72 significantly reduced the proportion of cells that contained ATP7B-H1069Q in the ER (Fig. 17B). Thus, this HSP70 inhibitor seems to be quite effective in mutant rescue from the ER to the compartments where ATP7B normally works.

Then, I tested whether HS-72 reduces ATP7B-H1069Q degradation (Fig. 18). Immunoblotting experiment revealed that exposure to different concentrations of HSP70 inhibitor increased expression levels of ATP7B mutant in HeLa cells indicating that suppression of HSP70 reduces degradation of ATP7B-H1069Q. Similar experiments were also performed in WD-relevant hepatic cell line HepG2. As in HeLa cells, HS-72 treatment increased stability of ATP7B mutant although higher concentrations of inhibitor were required to prevent degradation in HepG2 cells (Fig. 18A). This prompted me to investigate the impact of HS-72 on ATP7B-H1069Q stability using complimentary approach.

At the ER level, all newly synthetized proteins undergo folding, to be then delivered to their final destinations through the appropriate membrane-trafficking routes. The failure of a protein to pass the quality-control monitoring directs the mis-folded protein to degradation (Chakrabarti et al., 2011). The kinetics of the degradation process can be easily investigated using cycloheximide, an eukaryote protein synthesis inhibitor. Cycloheximide treatment helps to understand whether a given protein remains stable over time or undergoes rapid turnover (Buchanan et al., 2016). Several studies reported that the half-life of ATP7B-H1069Q protein product is shorter than the half-life of ATP7B-WT and usually ranges between 30 minutes and 1

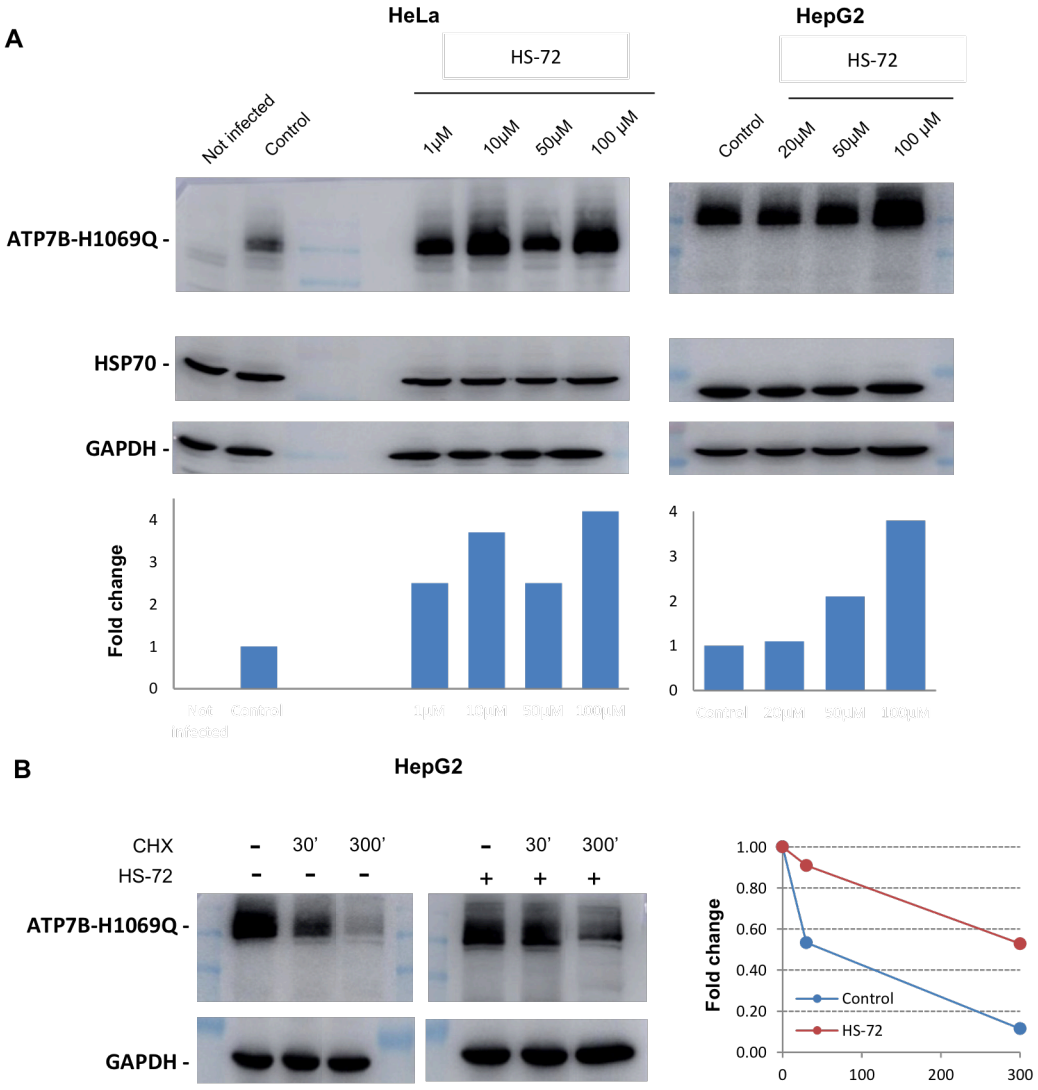

Fig. 18. HSP70 inhibitor attenuates degradation of ATP7B-H1069Q. (A) HeLa and HepG2 cells expressing ATP7B-H1069Q were treated with different concentrations of HS-72 inhibitor for 24 h. Western blots show an increase in ATP7B-H1069Q levels mutant protein in cells treated with HS-72 inhibitor in contrast to control cells. The graph shows the changes in ATP7B mutant.**(B)** HepG2 cells expressing ATP7B-H1069Q were treated with 10 μM HS-72 for 24 h or kept untreated before incubation with cycloheximide (CHX) for either 30 minutes or 5 hours. Western blot indicates that the treatment with HS-72 slowed down dynamics of CHX-induced decay of ATP7B mutant protein. The graph shows the changes of the mutant over the time. Experiment was done in triplicate.

hour and half (Payne et al., 1998). Thus, in order to see if HSP70 inhibitor reduces degradation of ATP7B mutant, I treated HepG2 cells expressing ATP7B-H1069Q with HS-72 and blocked protein biosynthesis with cycloheximide (CHX) for two different time intervals: 30 min and 5 hours. Western blot revealed that HS-72 increased amounts of ATP7B mutant at both 30min and 5h intervals of CHX treatment (Fig. 18B) indicating that HSP70 inhibitor slows down the mutant degradation.

Thus, taken together, these observations suggest that the suppression of HSP70 allows the most frequent Wilson disease ATP7B-H1069Q mutant to overcome ER retention, probably escaping the HSP70-dependent ER quality control mechanisms.

3.2.5. HSP70 inhibitor facilitates ATP7B-H1069Q trafficking to the appropriate cell-surface domain in hepatic cells

Considering that suppression of HSP70 with either RNAi or chemical inhibitor produced almost identical impact on ATP7B-H1069Q stability/localization, I utilized HS-72 as a simpler tool to inhibit HSP70 in further experiments. The first series of such experiments was designed to understand to what extent HSP70 suppression facilitates delivery of ATP7B-H1069Q to the Cu excretion sites.

To support excretion of Cu into the bile, ATP7B has to be delivered towards the canalicular (called also apical or biliary) area of hepatocytes (Nyasae et al., 2014). Biliary flow in turn eliminates excess Cu from the body preventing reabsorption of the metal in the intestine (Linder et al., 1998). The failure of ATP7B to reach this specific domain of the hepatocyte membrane results in Cu accumulation in the liver and the further developments of the main symptoms of Wilson disease. Targeting of ATP7B to the canalicular surface of hepatocyte relies on the N-terminal 9 amino acid ^{37}FAFDNVGYE^{45} stretch (Braiterman et al., 2009). Wilson disease-causing N41S mutation in this region severely impairs ATP7B targeting to the canalicular surface (Braiterman et al., 2009). In contrast, this N-terminal signal of ATP7B should not be affected by H1069Q mutation and should allow the mutant to reach canalicular area once the mutant would be able to leave ER. In this context, I tried to understand

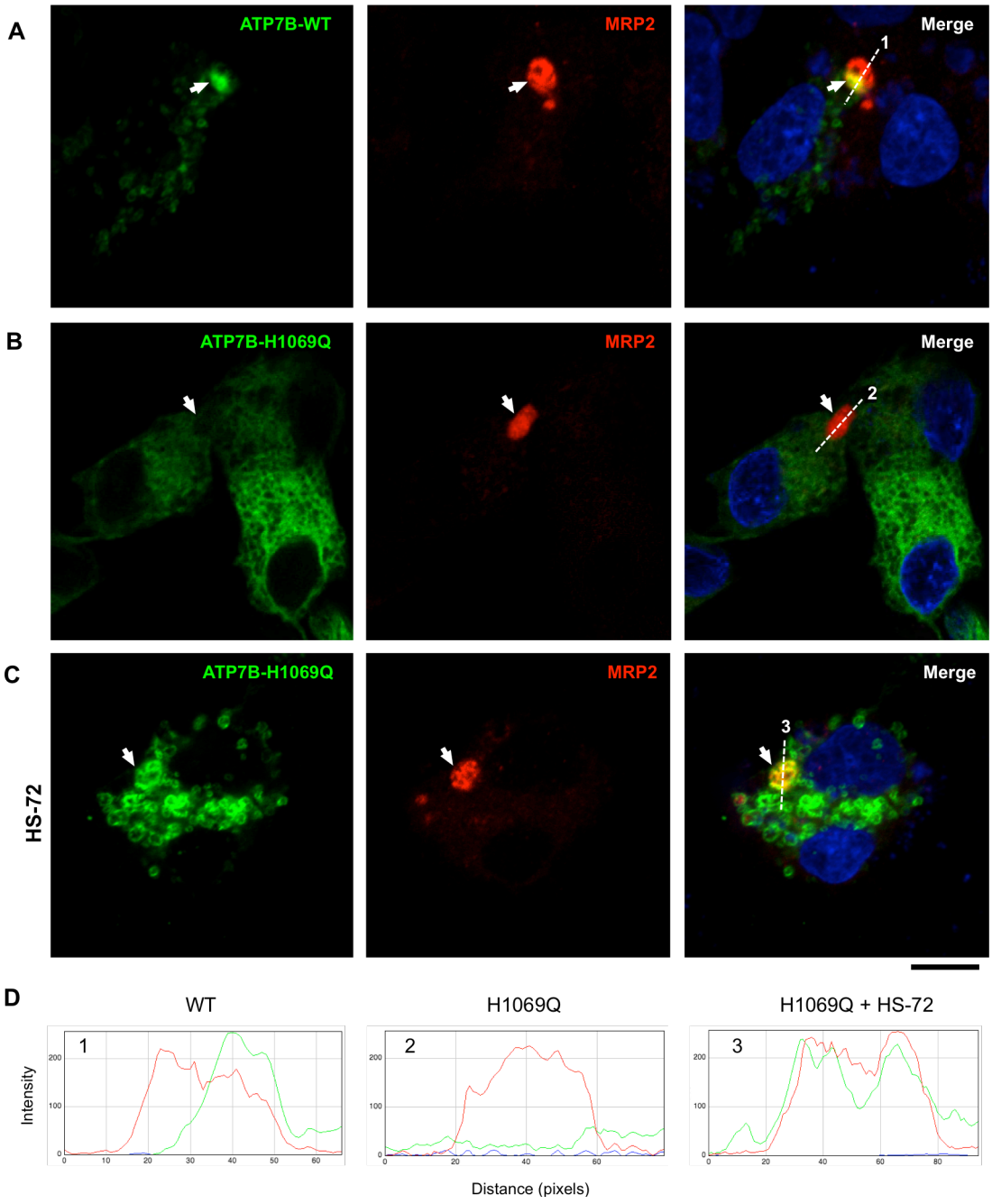

Fig. 19. HSP-70 inhibitor facilitates delivery of ATP7B-H1069Q to canalicular domain of polarized hepatic cells.

Polarized HepG2 expressing either WT (A) or H1069Q (B, C) were exposed to CuSO4 for 4h and stained with canalicular marker MRP2 and nuclear marker DAPI. HS-72 was added to the some wells with ATP7B-H1069Q expressing cells before exposure to Cu. Arrows in all images indicate MRP2-positive canalicular vacuole (cyst), which received ATP7B-WT (A), while mutant failed to reach canalicular area (B). HS-72 treatment induced ATP7B-H1069Q trafficking to canalicular surface (C). Panel D shows intensities of ATP7B (green) and MRP2 (red) signals along the lines 1, 2, and 3 drawn through the canalicular vacuole in panels A, B and C respectively. Peaks of ATP7B and MRP signals coincided in the case of WT (1) and mutant proteins exposed to HS-72 (3), while ATP7B signal did not exhibit any increase in MRP-positive canalicular area of untreated cells expressing H1069Q mutant. Scale bars for panels A-C = 4.8 µm (A-C). Experiment was done in triplicate..

whether the ATP7B-H1069Q recovered from the ER by HSP70 inhibitor arrives at the biliary surface of hepatic cells.

To determine whether this is the case, I grew the HepG2 cells under conditions that allow them to achieve maximal polarisation and to develop the apical canalicular cysts (also known as biliary cysts) (Treyer and Musch, 2013). Thus, these polarised HepG2 cells were exposed to Cu to trigger ATP7B transport, and then stained for MRP2 to reveal the apical (biliary) surface. Fig. 19A shows that exposure to Cu resulted in efficient delivery of ATP7B-WT to the canalicular domain of the cells. In contrast, no ATP7B-H1069Q was detected at the canalicular surface of these HepG2 cells, even when Cu was added to the medium at high concentrations (Fig. 19B). However, exposure of these cells to HS-72 inhibitor resulted in an increase of the amounts of ATP7B-H1069Q in the canalicular region (Fig. 19C). This suggests that HS-72 facilitates mutant delivery of the mutant to the main Cu excretion site at the biliary surface of hepatic cells. Quantification (in Fig. 19D) confirmed this conclusion and revealed coincidence ATP7B and MRP2 fluorescence picks in the case of WT protein and of H1069Q mutant in HS-72-treated cells. In contrast, untreated cells expressing the mutant did not exhibit any increase in the ATP7B signal within MRP2-positive area (Fig. 19D).

Thus, once HS-72 inhibitor promotes the release of ATP7B-H1069Q from the ER, the ATP7B-H1069Q shows correct targeting to the biliary domain of the cell surface, where the Cu excretion occurs.

3.2.6. HSP70 inhibitor promotes delivery of ATP7B-H1069Q to plasma membrane

Ability to drive Cu excretion from the cells constitutes the main homeostatic function of ATP7B (Lutsenko, 2010). A recent study from our lab shows that in response to increasing Cu ATP7B traffics from the TGN to endo-lysosomal organelles, where ATP7B sequesters Cu into lysosome lumen and stimulates exocytosis of such Cu-loaded lysosomes. As a result of this exocytic process cells release excess Cu from internal storage compartments and deliver ATP7B to the cell surface, where ATP7B can directly pump toxic metal away from the cytosol across the plasma membrane (Polishchuk et al., 2014). Cu-dependent delivery of ATP7B to the cell surface was successfully investigated by surface biotinylation in a number of cell types (Polishchuk et al., 2014; van den Berghe et al., 2009). Thus, we employed this method in HeLa cells to test whether HSP70 suppression increases ATP7B-H1069Q mutant trafficking to the plasma membrane.

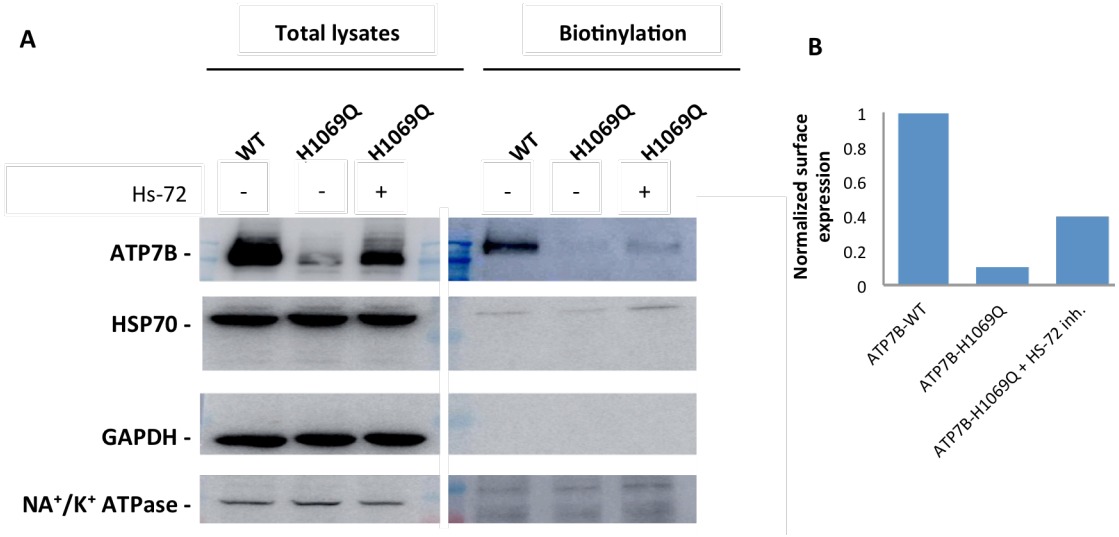

Fig. 20. HSP70 inhibitor stimulates ATP7B-H1069Q delivery to the cell surface.
HeLa cells were infected with adenovirus carrying ATP7B-WT or ATP7B-H1069Q, treated with 10 μM HS-72 inhibitor for 24 h and then with 200μM CuSO4 for 2 hours. Subsequently the cells were processed for cell surface biotinylation. (A) Western Blot shows that the treatment with HS-72 results in appearance of ATP7B-H1069Q in biotinylated fraction indicating partial correction of the mutant to the plasma membrane. (B) The graph shows normalized levels of ATP7B at the cell surface. Experiment was done in triplicate.

I found that ATP7B-WT was abundantly expressed at the cell surface, while ATP7B-H1069Q was missing at the plasma membrane (Fig. 20) likely due to retention and degradation in the ER. Indeed, amount of ATP7B mutant in total cells lysates was significantly lower when compared to WT protein. Incubation with HS-72 significantly increased overall amounts of ATP7B-H1069Q and resulted in increase of the mutant protein in cell surface biotinylated fraction (Fig. 20), demonstrating that the inhibition of HSP70 improves delivery of mutant to the plasma membrane where ATP7B usually operates in Cu excretion.

3. 3. Search for FDA-approved correctors of ATP7B-H1069Q

3.3.1. Identification of FDA-approved drugs with structure similar to HSP-70 inhibitor

Several lines of evidence (see above) suggest that HSP70 represents an attractive target for correction of ATP7B mutant. However, HSP70 is known to be involved in wide range of vitally important processes such as cellular prevention of protein aggregation, protein folding, trasport and regulation of proteins and others (Bukau et al., 2006; Frydman, 2001; Hartl et al., 2011; Kettern et al., 2010; Mayer and Bukau, 2005; Pratt and Toft, 2003; Tyedmers et al., 2010). It also plays a key role in ER-associated quality control of the numerous transmembrane proteins (Young, 2014). For this reason it would be risky to completely suppress HSP70 activity in patients with ATP7B-H1069Q mutation. On the other hand, it would be important to explore the potential of HSP70 inhibition for ATP7B mutant correction. Thus any eventual therapeutic strategy would require modulating the activity of HSP70 in a safe manner.

How might this objective be achieved? I had an idea to look for FDA approved drugs that could modulate HSP70 activity. FDA approved drugs are safe for patients as their toxicity has already been tested in clinical trials. I reasoned that some FDA approved drugs could be similar in terms of chemical structure to HS-72 and hence reduce the activity of HSP70, while other compounds may reduce expression of HSP70 protein product. Therefore, I decided to use two strategies for detection of FDA-approved drugs that could impact on HSP70. Firstly, I tried to find compounds whose structure resembles HSP70 inhibitor. Secondly, I attempted to detect FDA approved drugs that could modulate the expression of HSP70 protein.

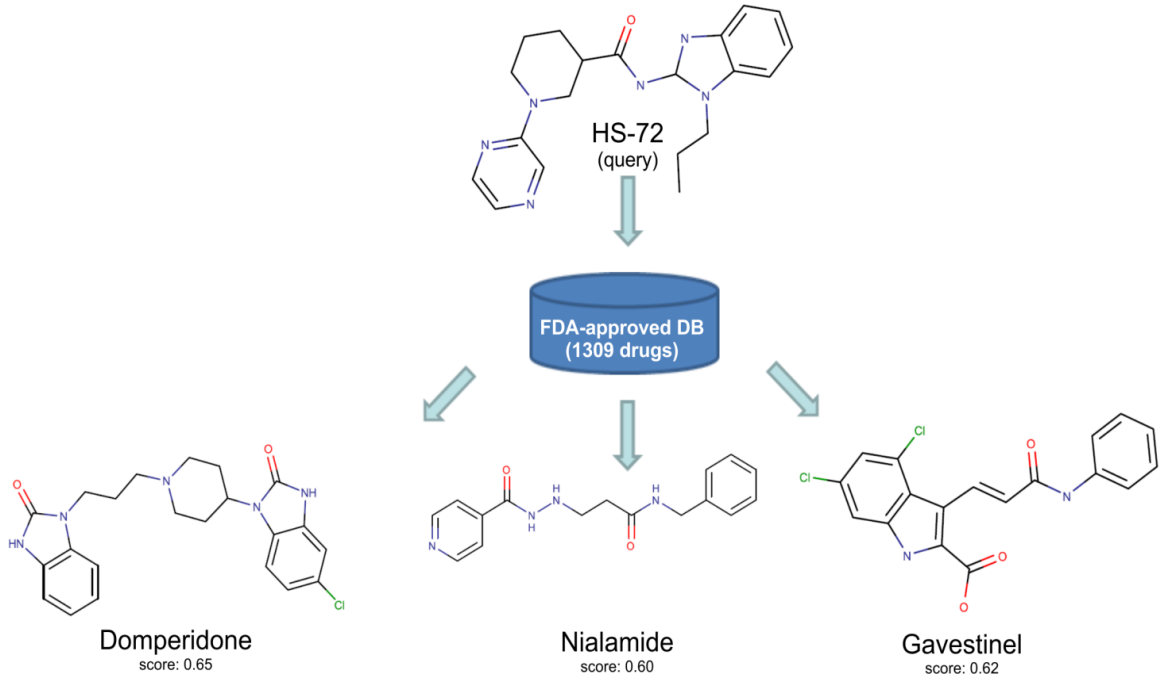

Fig. 21. FDA approved drugs exhibiting structural similarity to allosteric HSP70 inhibitor.
HS-72 was used as query structure for 3D ligand-based screening of a collection of FDA-approved drugs. Structural similarity score was calculated Molecular Interaction Fields (MIFs) overlapping of the query structure with 1309 FDA-approved drugs. Three hits were retrieved with a structural similarity score more than 0.5 to HS-72 inhibitor (Nialamide, Domperidone and Gavestinel).

The TIGEM Bioinformatic Core found three different FDA approved drugs using HS-72 (Howe et al., 2014) as a query structure for 3D ligand-based screening of a

collection of FDA-approved drugs. Structural similarity score of each compound was calculated on the basis of Molecular Interaction Fields (MIFs) overlapping of the query structure with 1309 FDA-approved drugs (Baroni et al., 2007). Three hits with a structural similarity score more than 0.5 (Carosati et al., 2004; Goodford, 1985) were retrieved: Nialamide, Domperidone and Gavestinel (Fig. 21). All 3 drugs were enrolled in further experiments to test their potential for ATP7B-H1069Q mutant correction.

3.3.2. Domperidone treatment improves the trafficking of ATP7B-H1069Q and prevents its degradation

Among 3 tested drugs, only Domperidone had a beneficial impact on ATP7B mutant,

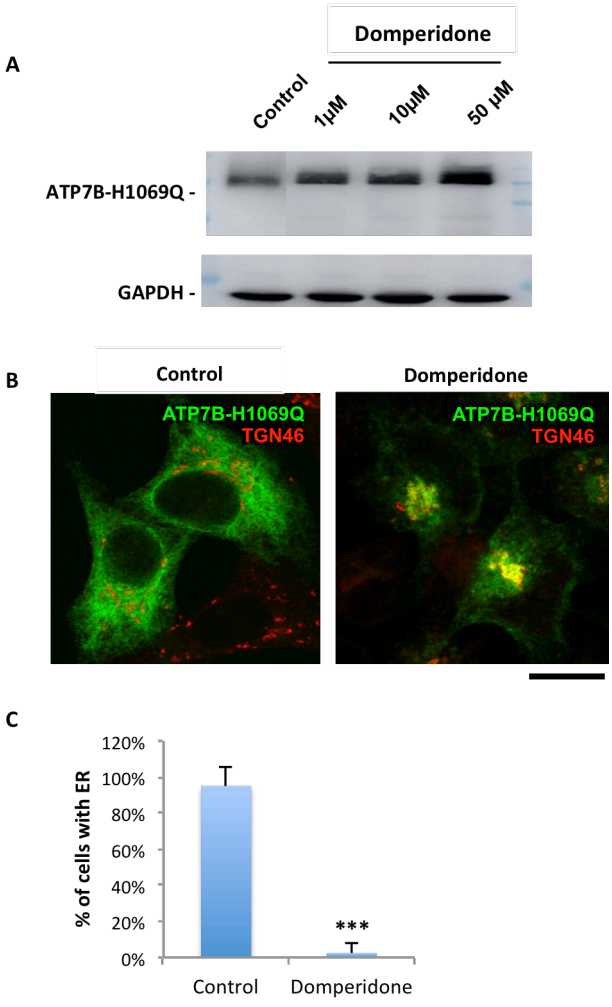

Fig. 22. Domperidone reduces degradation of ATP7B-H1069Q and its retention in the ER.

HepG2 cells expressing GFP-tagged ATP7B-H1069Q were treated with domperidone for 24 h and further processed for western blot (A) or confocal microscopy (B). **(A)** Western blot shows that domperidone treatment increases ATP7B-H1069Q levels in a concentration-dependent manner. **(B)** Confocal microscopy revealed that domperidone treatment (10μM) reduces the amount of ATP7B-H1069Q within the ER and promotes the mutant trafficking to the Golgi.
Scale bars= 4 μm

(C) Morphometric analysis confirms that domperidone decreases the percentage of cells exhibiting ATP7B-H1069Q mutant within the ER (n=10 fields). *** - $p<0.001$ (t-test).

correcting its localization and inhibiting degradation, while others did not make significant impact on mutant function/localization. Domperidone is a peripherally selective antagonist of dopamine D_2 receptor, which is expressed mainly in brain (Champion et al., 1986; Sakano et al., 2016). This drug is normally used as an antiemetic, gastroprokinetic agent, and galactogogue (Leeser and Bateman, 1985; Ortiz et al., 2015; Robbins et al., 2016; Schey et al., 2016).

Western blot revealed that domperidone increases ATP7B-H1069Q levels in a concentration-dependent manner (Fig. 22A) probably protecting the mutant from degradation. In parallel, I treated HepG2 cells expressing the mutant with Domperidone to evaluate the impact of the drug on ATP7B-H1069Q localization. Domperidone-treated cells exhibit less mutant in the ER when compared to untreated cells, while ATP7B-H1069Q colocalization with the Golgi marker TGN46 improved (Fig. 22B). Morphometric analysis supported these observations and indicated very robust reduction in the number of cells retaining the ATP7B mutant in the ER (Fig. 22C). Finally, I tested whether domperidone facilitates delivery of ATP7B-H1069Q mutant to the canalicular domain in polarized hepatic cells upon increase in Cu levels. Even upon stimulation with Cu ATP7B-H1069Q fails to reach MRP2-positive canalicular domains in polarized HepG2 cells as most of the protein remains within the ER (Fig. 23A). In contrast, Domperidone-mediated rescue of ATP7B mutant from the ER allowed ATP7B-H1069Q to be at least partially delivered to canalicular domain of HepG2 cells (Fig. 23B).

In conclusion, our results together suggest that domperidone treatment improves ATP7B-H1069Q localization and significantly attenuates the mutant degradation. Importantly, domperidone is considered to be very safe drug as it is widely used against nausea and vomiting (Leeser and Bateman, 1985; Ortiz et al., 2015; Robbins

et al., 2016; Schey et al., 2016). Considering that large cohort of WD patients develop nausea and vomiting symptoms under standard treatment (Zn salts or Cu chelators), domperidone could be used straightforwardly in such patients and, thus, its beneficial impact on individuals with H1069Q mutation in ATP7B may be easily evaluated in clinical studies. In the case of positive outcome this FDA-approved drug could be rapidly repurposed for WD treatment.

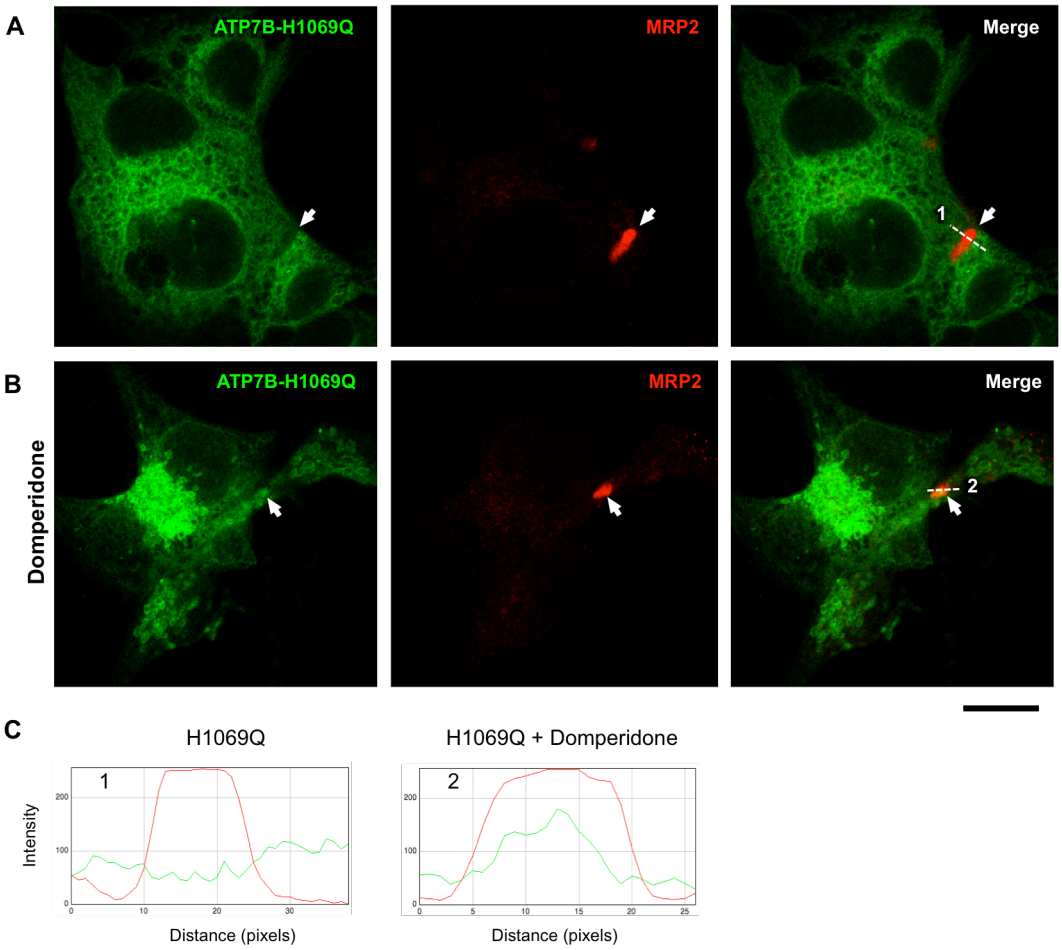

Fig. 23. Domperidone facilitates delivery of ATP7B-H1069Q to canalicular domains of polarized hepatic cells.

Polarized HepG2 expressing H1069Q were exposed to CuSO4 for 4h and stained with canalicular marker MRP2. Domperidone (10μM) was added to the same wells with ATP7B-H1069Q expressing cells before exposure to Cu. Arrows in all images indicate MRP2-positive canalicular vacuole (cyst). Panel A shows that the mutant is absent in the canalicular area and remain diffusively distributed over the ER. Domperidone treatment induced ATP7B-H1069Q trafficking to the canalicular surface (arrows in B). Panel C shows intensities of ATP7B-H1069Q (green) and MRP2 (red) signals along the lines 1 and 2 drawn through the canalicular vacuole in panels A and B, respectively. ATP7B-H1069Q signal did not exhibit any increase in MRP-positive canalicular area of untreated cells (1), while the peaks of ATP7B-H1069Q and MRP signals coincided in the cells exposed to domperidone (2). Scale bars for panels A and B = 5 μm. Experiment was done in triplicate.

3.3.3 Bioinformatics search for FDA-approved drugs that rescue ATP7B mutant

As outlined above, the second strategy for identification of safe ATP7B-H1069Q correctors consisted in bioinformatics screening for FDA-approved compounds that may inhibit HSP70 expression. It is important to note that I tried to select HSP70 supressing compounds without serious impact on other chaperone HSP90. A growing body of evidences suggest that while HSP70 could direct ER-retained proteins (like Δ508F CFTR mutant) to either degradation or folding, HSP90 mainly acts as pro-folding factor to stabilise mutant proteins (Young, 2014). Thus, HSP90 inactivation would be undesirable while attempting ATP7B mutant correction.

Thus, to find FDA-approved drugs with potential for HSP70 suppression (having no impact on HSP90) TIGEM Bioinformatics Core made a search in available transcriptome databases (Lamb et al., 2006)(see also Methods).

This bioinformatics search returned a list of about 200 candidates and I decided first to see whether top hits from the list inhibit HSP70 expression in HepG2 cells. Among top 24 compounds from the list only one, Doxorubicin, substantially (almost 2 fold) reduced HSP70 expression as revealed by western blot (Fig. 24). This compound is known for its antineoplastic activity and frequently used for cancer treatment (Batist et al., 2002; Carvalho et al., 2009; Guo et al., 2011; Keizer et al., 1990; Marina et al., 2002; Meredith and Dass, 2016; Minotti et al., 2004; Ruggiero et al., 2013; Weekes et al., 2002). Doxorubicin intercalates between base pairs in the DNA helix, thereby preventing DNA replication and ultimately inhibiting protein synthesis (Meredith and Dass, 2016). This mechanism suppresses growth of tumor cells, but extended (in terms of time) use of Doxorubicin could induce serious toxicities in tissues and organs with rapid cell turnover. Thus, its use for WD cure is doubtful due to the possibility of

serious side effects. The lack of significant impact on HSP70 expression by majority of top candidates from bioinformatics

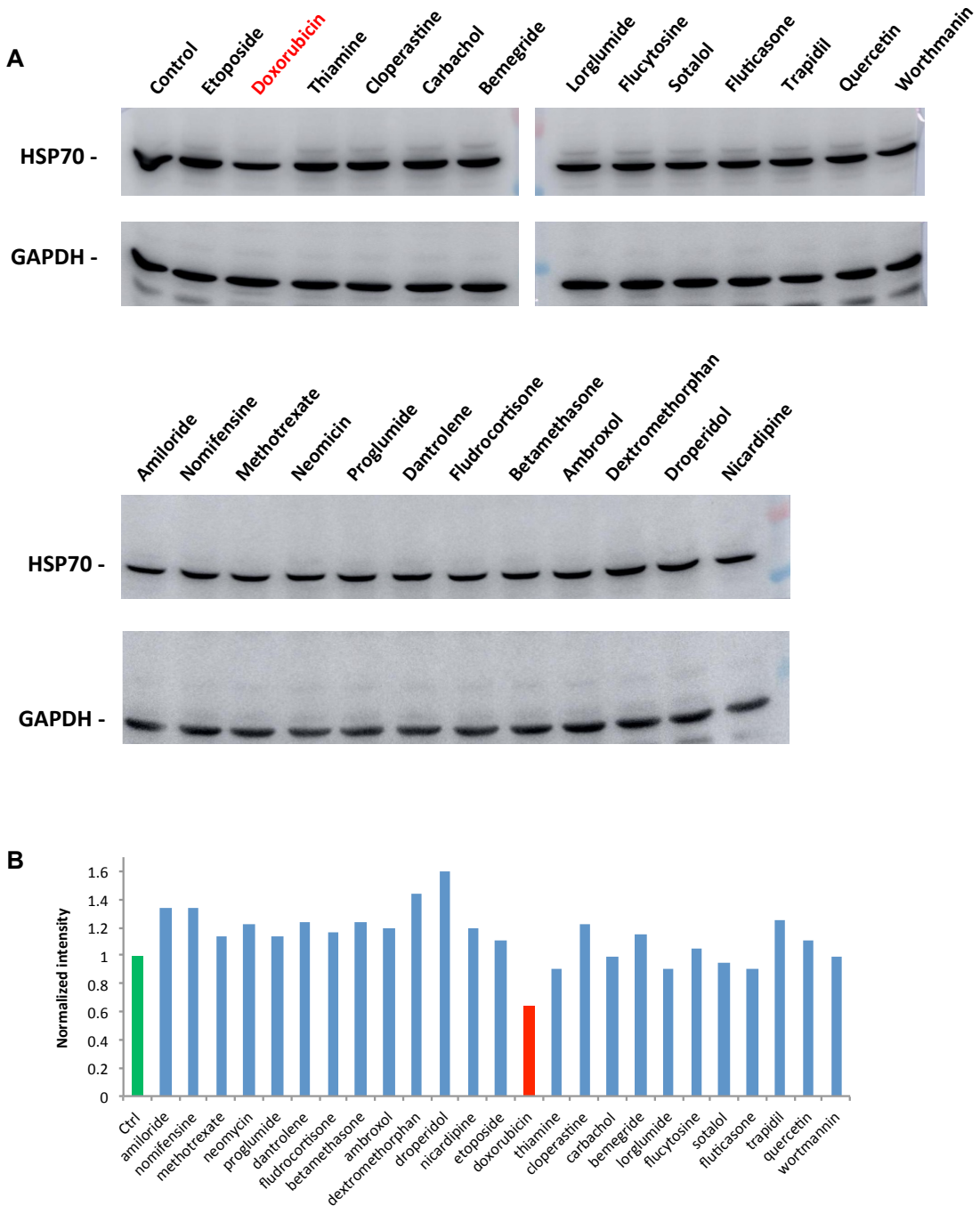

Fig. 24. Impact of FDA approved drugs on HSP70 expression.

Top FDA-approved drugs from bioinformatics study were supplied to HepG2 cells at 10µM concentration for 24 h. Expression of HSP70 in treated cells was analysed using Western blot (**A**) and quantified using normalization to housekeeping protein GAPDH (**B**). Only Doxorubicin (shown in red) was capable of substantially reducing HSP expression. Experiment was done in triplicate.

searches prompted me to look for available literature data that would help to prioritize bioinformatics hits for ATP7B-H1069Q correction. I found that anti-inflammatory corticoids have been reported to correct to some extent stability and function of CFTR mutant (Pesce et al., 2016). Among the hits from bioinformatics search beclometasone belong to this family. Thus, I decided to evaluate potential of this drug as well as similar FDA-approved compounds (Momethasone and Dexamethasone) for ATP7B mutant rescue.

3.3.4. FDA-approved glucocorticoid receptor agonists correct localization of ATP7B-H1069Q and reduce its degradation.

Beclomethasone, Mometasone and Dexamethasone belong to a class of glucocorticoid receptor (GCR) agonists and are widely used as anti-inflammatory agents in skin disorders, allergic rhinitis, asthma, autoimmune diseases, etc. (Amar et al., 2016; Kim et al., 2017; Liu et al., 2017; Manguso et al., 2016; Orellana et al., 2012; Podvigina et al., 2012; Singh et al., 2016; Ushkalova et al., 2016; Virkud et al., 2017). To evaluate whether GCR agonists have any impact on ATP7B-H1069Q localization I treated mutant-expressing HepG2 cells with beclomethasone, mometasone and dexamethasone at different concentration and evaluated the degree of ATP7B re-location from the ER to distal compartments of the biosynthetic pathway. Fig. 25A shows that all three drugs reduced the amount of the mutant detectable in the ER and favoured trafficking of ATP7B-H1069Q to the Golgi and post-Golgi compartments. This observation was supported by morphometric analysis, which indicates significant reduction in the percentage of cells exhibiting ATP7B-

H1069Q in the ER upon beclomethasone, mometasone and dexamethasone treatment (Fig. 25B).

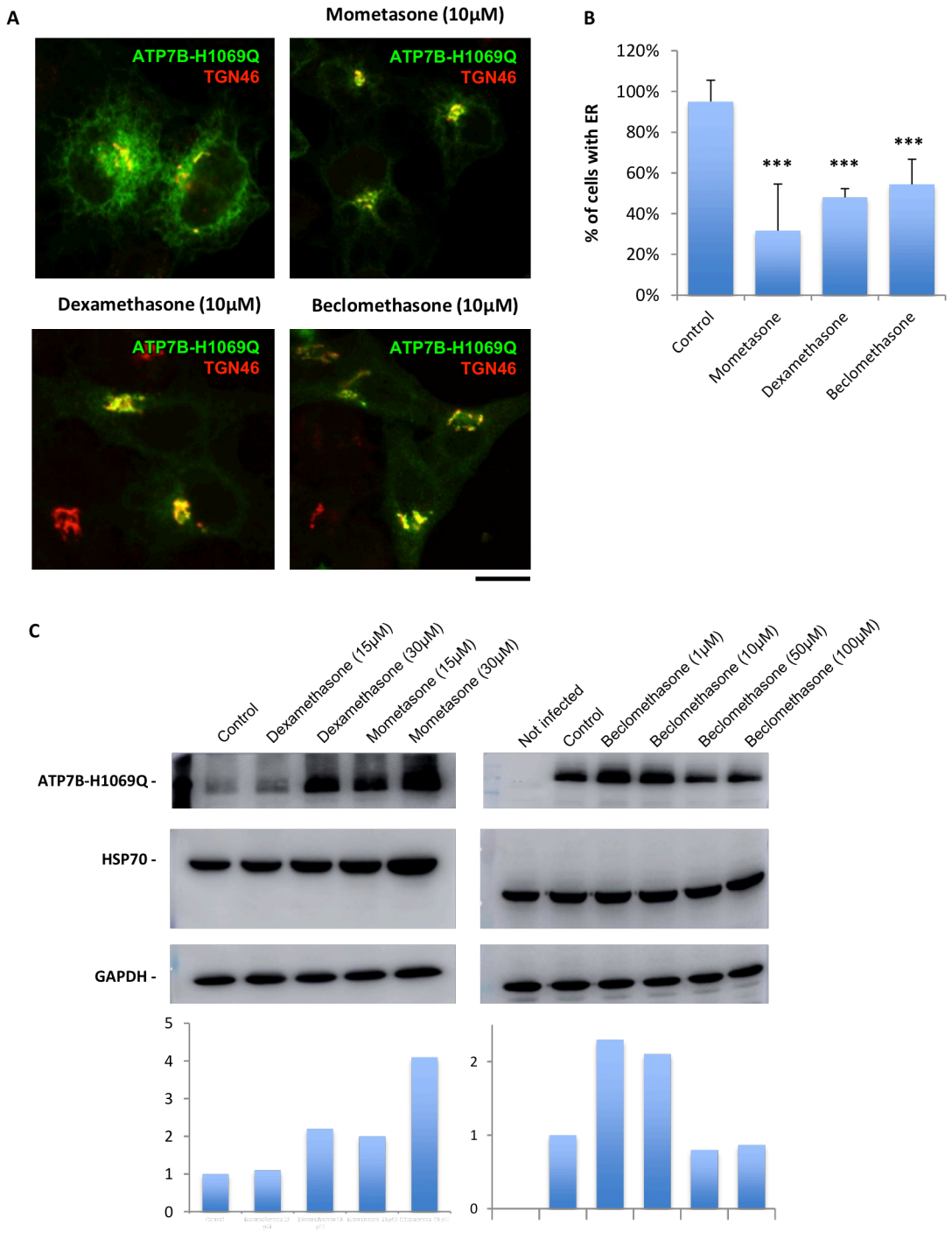

Fig. 25. FDA-approved GCR agonists reduce retention of ATP7B-H1069Q in the ER and its degradation.

HepG2 cells expressing GFP-tagged ATP7B-H1069Q were treated with drugs as indicated in corresponding panels for 24 h and further processed for confocal microscopy **(A)** or Western blot **(B)**. **(A)** Confocal microscopy shows reduced retention of ATP7B-H1069Q within the ER in cells treated with GCR agonists. Scale bar for panel A = 4.5 µm **(B)** Morphometric analysis confirms that FDA-approved drugs reduce the percentage of the cells, which contain ATP7B-H1069Q mutant within the ER (n= 10 fields). *** - $p<0.001$ (t-test). **(C)** Western blots indicates that Dexamethasone (15µM and 30µM), Mometasone (15µM and 30µM) and Beclomethasone (1µM and

10μM) increase the ATP7B-H1069Q levels. The graphs show changes in ATP7B mutant levels. Experiment was done in triplicate.

In parallel, Western blot experiments revealed that GCR agonists increase amount of ATP7B mutant protein product in a concentration-dependent manner (Fig. 25C), indicating that these FDA approved compounds attenuate mutant degradation.

It remains unclear how GCR agonists facilitate export of ATP7B-H1060Q from the ER and reduce degradation of the mutant. Fig. 25C indicates that neither drug caused a decrease in HSP70 levels. Instead, it seems that in the case of mometasone treatment HSP70 expression increases. Therefore, we tried to uncover the mechanisms through which beclomethasone, mometasone and dexamethasone rescue localization and stability of ATP7B-H1069Q.

3.3.5. Impact of GCR agonists on ATP7B-H1069Q interaction with HSP70.

Considering that GCR agonists do not seem to reduce HSP70 expression I hypothesised that the interaction of ATP7B-H1069Q with HSP70 could be altered by these drugs resulting in correction of the ATP7B mutant. In addition, I considered testing whether and to what extent HSP70 partner chaperones HSP90 and DNAJB1 bind ATP7B-H1069Q in the presence of beclomethasone, mometasone and dexamethasone. As mentioned above, coupling of HSP70 with specific chaperones directs the fate of the misfolded transmembrane proteins to either degradation (as in the case of DNAJ proteins) or folding (as in the case of HSP90) (Young, 2014). It is also worth noting that both HSP90 and DNAJB1 were detected in ATP7B-WT and mutant interactomes (although the interaction score was not very high) and, hence, could modulate HSP70 activity on ATP7B-H1069Q.

To evaluate the impact of GCR agonists on ATP7B mutant interaction with chaperones, HepG2 cells were transduced with Ad-ATP7B-H1069Q and treated with Beclomethasone, Mometasone

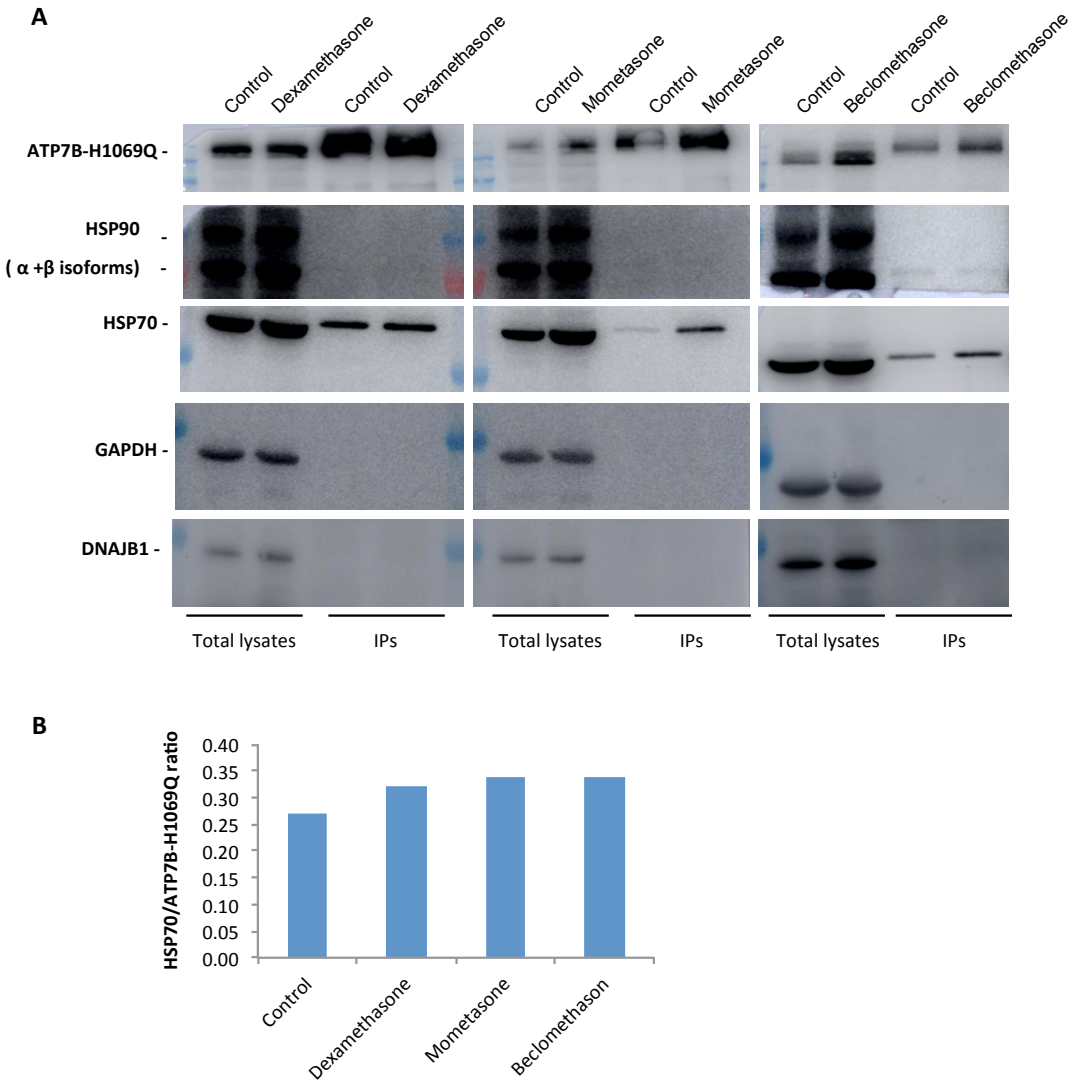

Fig. 26. Interaction of the ATP7B mutant HSP70 in GCR agonist-treated cells

(A) HepG2 cells were infected with adenovirus carrying GFP-tagged ATP7B-H1069Q and treated with Dexamethasone, Mometasone and Beclomethasone. Then ATP7B mutant was immunoprecipated from the cell lysates. 1/10 of µg of total lysates and 10/10 µg of immunoprecipitates (IPs) were separated by SDS-PAGE and labelled with corresponding antibodies to reveal levels of ATP7B-H1069Q, HSP90, HSP70, DNAJB1 and GAPDH. **(B)** Quantification of the bands in IPs does not reveal significant changes in the ration between HSP70 and ATP7B mutant. Experiment was done in triplicate.

and Dexamethasone. Then, ATP7B-H1069Q was immunoprecipitated from HepG2 cell lysates and amounts of HSP70, HSP90 and DNAJB1 were revealed using specific antibodies in Western blots. Analysis of immunoprecipitates suggests that neither drug reduced HSP70 binding to the mutant (Fig. 26A). I noted that mometasone apparently increases HSP70 amounts in ATP7B mutant pull downs. However careful quantification of HSP70/ATP7B mutant ratio did not support this impression (Fig. 26B). Importantly, both HSP90 and DNAJB1 were absent or barely detectable in immunoprecipitates although significant amounts of the proteins were revealed in cell lysates. Thus it seems that both chaperones do not bind to ATP7B mutant at significant levels and do not cooperate with HSP70 in regulation of ATP7B-H1069Q proteostasis. On the other hand, lack of impact on ATP7B-H1069Q/Hsp70 interaction suggests that GCR agonist do not necessarily act through HSP70 in the process of mutant correction. Although impact of these drugs on HSP70 activity cannot be entirely ruled out, it is likely that GRC agonist facilitate ATP7B-H1069Q trafficking through HSP70-independent mechanism.

3.3.6. Drug-set enrichment Analysis (DSEA) suggests a possible molecular pathway of GCR agonist-mediated correction of ATP7B-H1069Q

To understand the mechanisms behind rescue of ATP7B mutant by GCR agonists we employed bioinformatics analysis using DSEA (Drug-set Enrichment Analysis) tool (Napolitano et al., 2016). This computational method is based on drug-induced gene expression profiles and is able to identify the molecular pathways that are targeted by most of the drugs in the set. It has been already applied to identify the mechanisms of action shared by drugs known to be partially effective in rescuing CFTR mutant gene function in Cystic Fibrosis (Pesce et al., 2016). DSEA revealed that Momethasone,

Dexamethasone and Beclomethasone upregulate genes that belong to "Chaperone-mediated protein transport" (GO:0072321) group. This pathway includes several genes: *TIMM8B, TIMM8A, CLIP3, TIMM13, TIMM10, TIMM9, PEX19, TOR1A, HSPA8*. Literature mining indicated that *TIMM8B, TIMM8A, CLIP3, TIMM13, TIMM10, TIMM9* genes mainly operate in mitochondrial function (Lutz et al., 2003;

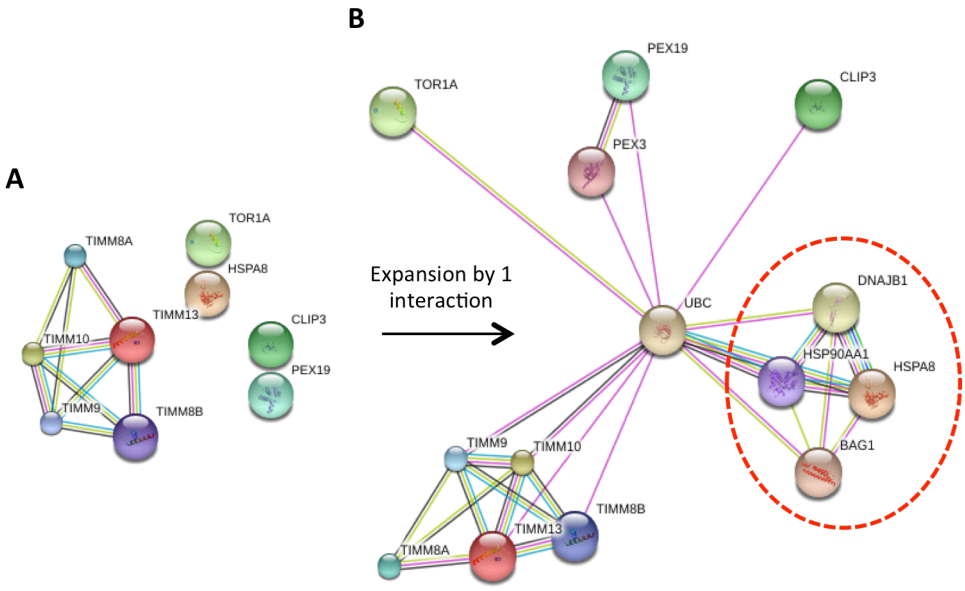

Fig. 27: Interaction network of putative GCR agonist targets.
(A) Interactions between possible targets of GCR agonists were evaluated by STRING, which revealed network containing mainly TIMM proteins. **(B)** Minimal expansion of the network linked all candidates and revealed node (outlined by red oval) containing 4 chaperone proteins.

Roesch et al., 2004) and could be hardly associated with ATP7B proteostasis. Instead HSPA8 is a cytosolic chaperone (member of the HSP70 protein family), which plays a role in ERAD (Matsumura et al., 2013). Therefore, HSPA8 emerges as a possible component of regulation of ATP7B mutant degradation.

In order to evaluate eventual links between hits from DSEA study I used STRING 9.1 database, which indicates potential and documented interaction within the group of genes or their protein products (http://string-db.org/).The first layer of analysis

indicated a strong interaction cluster of TIMM proteins without links to any other DSEA-derived hit (Fig. 27A). However, the minimal expansion of the network by one additional interaction resulted in generation of the chaperone cluster with HSPA8, HSP90AA1, DNAJB1 and BAG1 (Fig. 27B). The latter three proteins were detected as putative interactors of ATP7B-WT and ATP7B-H1069Q in SILAC experiments. Thus, their role in GCR agonist-mediated rescue of ATP7B mutant should be eventually addressed, although IP data did not provide solid confirmation of HSP90AA1 or DNAJB1 with ATP7B-H1069Q.

3.3.7. Correctors of ATP7B-H1069Q mutant protect ATP7B-deficient cells from Cu toxicity

My results outlined in previous sections indicate that several FDA-approved drugs were capable of decreasing the degradation of ATP7B-H1069Q mutant as well as its retention in the endoplasmic reticulum. Such impact of the compounds on the mutant is expected to reduce accumulation of toxic Cu in hepatic cells, which express ATP7B-H1069Q. To test whether this is a case I took advantage of recently developed hepatic cells lines, which exhibit different degree of ATP7B function loss. ATP7B knock out HepG2 cell line was developed using zinc finger nuclease technology (Chandhok et al., 2014). This cell line was used further to develop HepG2 cells stably expressing the 2 most frequent ATP7B mutants H1069Q and R778L (Chandhok et al., 2016). I managed to obtain these cells shortly before the end of my PhD project and used them to validate efficiency of FDA-approved correctors of ATP7B mutant. ATP7B knockout (KO) cells as well as mutant expressing lines (H1069Q and R778L cells) do not resist Cu at low mM concentrations. We took advantage of this property of all 3 ATP7B-deficient HepG2 cell lines and treated them for 24h with 1mM Cu in

the absence or presence of GCR agonists, domperidone and HSP70 inhibitor to evaluate whether any mutant corrector improves viability of the cells in the presence

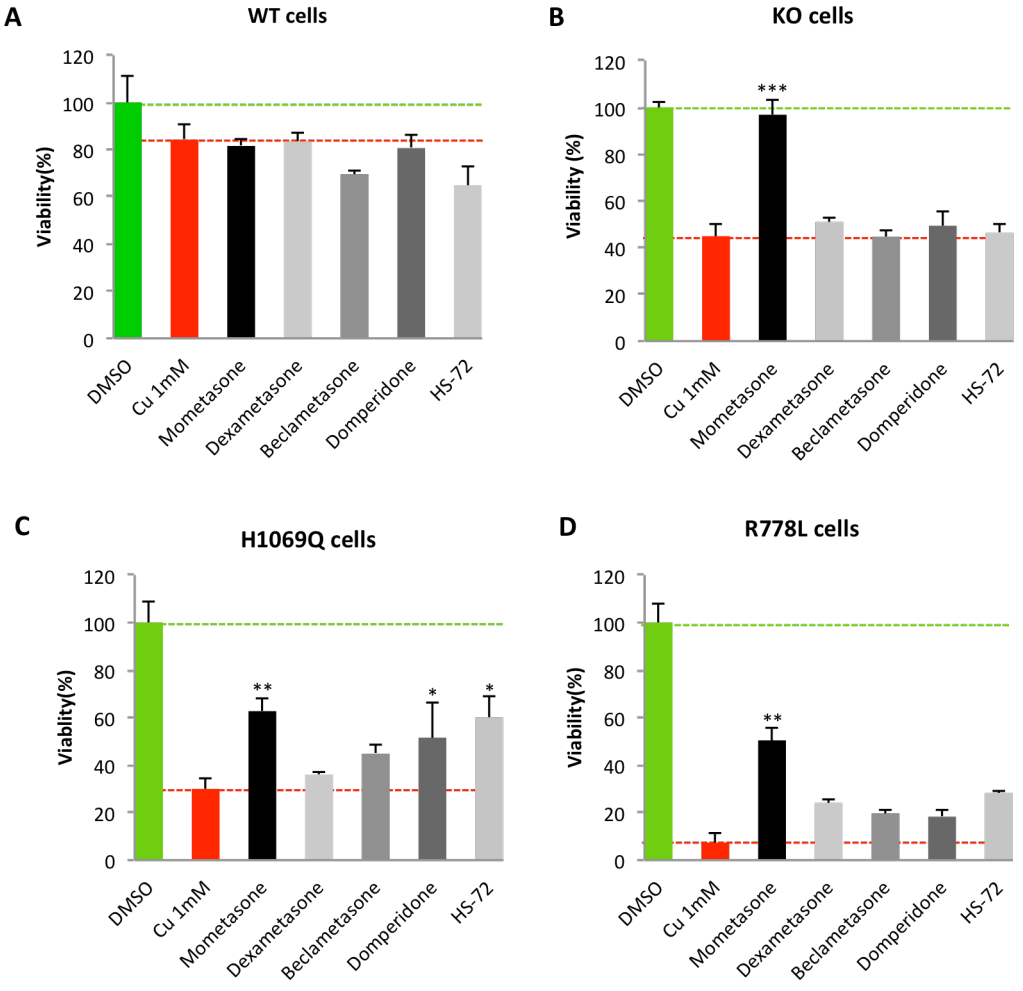

Fig. 28. Impacts of FDA-approved compounds on resistance of ATP7B-deficient cells to toxic Cu.
Survival of *ATP7B-deficient* cell lines after 10 μM Mometasone, Dexamethasone and Beclometasone, 1 μM Domperidone and 100 nM of HS-72 was analysed using MTT assay. Bar graphs indicate cell viability after treatment with drugs following by exposure to 1mM $CuCl_2$ for 24h. Differences in viability between 1mM $CuCl_2$ treated cells and cells treated with drugs and then 1mM $CuCl_2$ were analysed using T-test. A value of $P<0.05$ was considered significant. All data is represented as mean ± SE of at least three independent experiments. *** - $p<0.001$, ** - $p<0.01$, * - $p<0.05$ compared to Cu-treated cells.

of toxic Cu. Cell survival was analyzed using MTT assay and ATP7B KO cells, which stably express WT-ATP7B (WT cells), were utilized as a control in these experiments. Fig. 28B-D show that Cu significantly decreases viability of all 3 ATP7B-deficient cell lines (KO, H1069Q and R778L), while WT cells resist the same Cu levels in the

medium (Fig. 28A). Mometasone significantly rescued viability of cells expressing either H1069Q or R778L mutant (Fig. 28C, D) indicating substantial resistance of treated cells to toxic Cu. However, mometasone unexpectedly increased resistance of KO cells to Cu (Fig. 28B). This indicates that mometasone apparently increases cell tolerance to Cu through ATP7B-mutant-independent mechanism. Nevertheless, it could not be completely ruled out that correction of the mutant in H1069Q and R778L cells contributes to reduction of Cu toxicity. Further studies will be needed to understand the mechanism through which Mometasone counteracts Cu toxicity.

In contrast, HS-72 and structurally similar drug domperidone failed to improve viability of KO cells in toxic Cu but increased survival of H1069Q cells (Fig. 28C). This observation suggests that both drugs require ATP7B mutant protein product to covey resistance to Cu and, hence, rescue function of ATP7B-H1069Q mutant. HSP inhibitor exhibited positive trend in R778L cells as well (Fig. 28D), although the changes in cell viability were not statistically significant. Testing the panel of different Domperidone concentrations could potentially help to achieve R778L rescue with this drug. Indeed, we reduced significantly the concentration of HS-72 (from 50 μM to 100 nM) to avoid its toxicity. Yet the inhibitor was effective in recuing the function of ATP7B mutants. Thus this HSP70 inhibitor emerges as potential candidate for development of new therapeutic approach for WD. In the mean time Domperidone has been already in therapeutic use for epigastric pain, nausea, and vomiting (Robbins et al., 2016). Thus its translation into use for WD patients carrying H1069Q mutation could be really fast. Mometasone represents another FDA-approved compound that deserves consideration for WD cure, although the mechanism of its action in ATP7B-deficient hepatocytes has to be further investigated.

CONCLUDING REMARKS

In this study the new target and drugs for correction of the most frequent H1069Q mutant of ATP7B were revealed. On one side, this opens new opportunities for development of mutant correction-based therapies, while on the other expands the background for the further research on the proteostatic regulation of pathogenic mutants of ATP7B and other disease-associated misfolded proteins.

Analysing the interactome of WT and H1069Q variants of ATP7B, HSP70 was revealed as a potential target for correction of the ATP7B mutant. Despite the exceptional importance of HSP70 for a number of vitally important processes (protein folding, transport, signaling, e.g.) (Bukau et al., 2006; Frydman, 2001; Hartl et al., 2011; Mayer and Bukau, 2005) the search for safe drugs that suppress HSP70 provided me with several candidates for ATP7B mutant correction and then with validated leads, which can be explored in preclinical studies. This underscores the efficiency and potential of the strategy, which combines proteomics and bioinformatics for drug discovery.

The main findings of my project suggest that HSP70 may represent an effective target for correction of ATP7B-H1069Q mutant. It will be important to understand whether this target can be also utilized to rescue other WD-causing ATP7B variants. It turns out that others chemical inhibitors that improve localization and function of ATP7B-H1069Q have the same impact on the group of other ATP7B mutants (Chesi et al., 2016). Thus, the potential of HS-72 and Domperidone for correction of other ER-retained ATP7B variants has to be explored. However, even if only few *ATP7B* isoforms will be corrected by the HSP70-specific drugs, this should also be considered as a positive outcome. Indeed, selectivity of these compounds for

restricted number of mutants would indicate a specific impact on a limited subset of quality control mechanisms, which does not compromise entire cell proteostasis. Such specific impact would be especially valuable in the context of emerging concept of "personalized medicine", which requires tacking in account a particular genetic background of the individual patient to develop appropriate treatment strategy (Spagnolo et al., 2017).

In addition to ATP7B mutants, the potential of HSP70-specific drugs has to be explored for other diseases. HSP70 involvement in ER retention and degradation of cystic fibrosis-causing ΔF508 CFTR mutant is well documented (Young, 2014). A growing body of evidence also supports the role of the HSP70 chaperone system in other disorders caused by misfolding and aberrant trafficking of such ion channels as the CFTR chloride channel in cystic fibrosis and the hERG potassium channel in cardiac long QT syndrome type 2 (Young, 2014). Thus, targeting HSP70 for rescue of these ER-retained ion transporters appears to be a valuable strategy.

Finally, my findings suggest that mutant correction can be considered as an option for development of new therapeutic approach for WD cure. The treatment of WD mainly remains based on two strategies: increasing Cu excretion using chelators and reducing Cu absorption from the diet by treatment with Zn salts (Ala et al., 2007). Both therapies have own limitations and, hence, development of additional and/or alternative therapeutic strategies for WD is highly demanded (Ferenci, 2006; Roberts et al., 2008). This study indicates that some FDA-approved drugs rescue function of the most frequent ATP7B mutant *in vitro*. It is expected that the use of these compounds might be beneficial for a large group of patients with WD. Certainly, the efficiency of the drugs has to be validated in other WD models, namely: in mice with ATP7B mutant knock in and in hepatic cells reprogramed from patient fibroblasts. On

the other hand, such FDA-approved compound as domperidone has really low toxicities and side effects (Leeser and Bateman, 1985 ; Ortiz et al., 2015; Robbins et al., 2016; Schey et al., 2016) and, therefore, can be quite rapidly repurposed for WD cure. Thus, I hope that translation of my cell biology findings into preclinical and clinical studies will pave a way for new therapeutic strategies to combat Wilson disease.

REFERENCES

Ala, A., Walker, A.P., Ashkan, K., Dooley, J.S., and Schilsky, M.L. (2007). Wilson's disease. Lancet *369*, 397-408.

Amar, N.J., Shekar, T., Varnell, T.A., Mehta, A., and Philip, G. (2016). Mometasone furoate (MF) improves lung function in pediatric asthma: A double-blind, randomized controlled dose-ranging trial of MF metered-dose inhaler. Pediatr Pulmonol. 2017 Mar;52(3):310-318

Bandmann, O., Weiss, K.H., and Kaler, S.G. (2015). Wilson's disease and other neurological copper disorders. Lancet Neurol *14*, 103-113.

Baroni, M., Cruciani, G., Sciabola, S., Perruccio, F., and Mason, J.S. (2007). A common reference framework for analyzing/comparing proteins and ligands. Fingerprints for Ligands and Proteins (FLAP): theory and application. J Chem Inf Model *47*, 279-294.

Bartee, M.Y., and Lutsenko, S. (2007). Hepatic copper-transporting ATPase ATP7B: function and inactivation at the molecular and cellular level. Biometals *20*, 627-637.

Batist, G., Barton, J., Chaikin, P., Swenson, C., and Welles, L. (2002). Myocet (liposome-encapsulated doxorubicin citrate): a new approach in breast cancer therapy. Expert Opin Pharmacother *3*, 1739-1751.

Braiterman, L., Nyasae, L., Guo, Y., Bustos, R., Lutsenko, S., and Hubbard, A. (2009). Apical targeting and Golgi retention signals reside within a 9-amino acid sequence in the copper-ATPase, ATP7B. Am J Physiol Gastrointest Liver Physiol *296*, G433-444.

Braiterman, L., Nyasae, L., Leves, F., and Hubbard, A.L. (2011). Critical roles for the COOH terminus of the Cu-ATPase ATP7B in protein stability, trans-Golgi network retention, copper sensing, and retrograde trafficking. Am J Physiol Gastrointest Liver Physiol *301*, G69-81.

Brewer, G.J., Dick, R.D., Yuzbasiyan-Gurkan, V., Johnson, V., and Wang, Y. (1994). Treatment of Wilson's disease with zinc. XIII: Therapy with zinc in presymptomatic patients from the time of diagnosis. J Lab Clin Med *123*, 849-858.

Brewer, G.J., Dick, R.D., Yuzbasiyan-Gurkin, V., Tankanow, R., Young, A.B., and Kluin, K.J. (1991). Initial therapy of patients with Wilson's disease with tetrathiomolybdate. Arch Neurol *48*, 42-47.

Buchanan, B.W., Lloyd, M.E., Engle, S.M., and Rubenstein, E.M. (2016). Cycloheximide Chase Analysis of Protein Degradation in Saccharomyces cerevisiae. J Vis Exp. Apr 18;(110).

Bukau, B., Weissman, J., and Horwich, A. (2006). Molecular chaperones and protein quality control. Cell *125*, 443-451.

Bull, P.C., Thomas, G.R., Rommens, J.M., Forbes, J.R., and Cox, D.W. (1993). The Wilson disease gene is a putative copper transporting P-type ATPase similar to the Menkes gene. Nat Genet *5*, 327-337.

Camakaris, J., Voskoboinik, I., and Mercer, J.F. (1999). Molecular mechanisms of copper homeostasis. Biochem Biophys Res Commun *261*, 225-232.

Carosati, E., Sciabola, S., and Cruciani, G. (2004). Hydrogen bonding interactions of covalently bonded fluorine atoms: from crystallographic data to a new angular function in the GRID force field. J Med Chem *47*, 5114-5125.

Carvalho, C., Santos, R.X., Cardoso, S., Correia, S., Oliveira, P.J., Santos, M.S., and Moreira, P.I. (2009). Doxorubicin: the good, the bad and the ugly effect. Curr Med Chem *16*, 3267-3285.

Cater, M.A., Forbes, J., La Fontaine, S., Cox, D., and Mercer, J.F. (2004). Intracellular trafficking of the human Wilson protein: the role of the six N-terminal metal-binding sites. Biochem J *380*, 805-813.

Cater, M.A., La Fontaine, S., Shield, K., Deal, Y., and Mercer, J.F. (2006). ATP7B mediates vesicular sequestration of copper: insight into biliary copper excretion. Gastroenterology *130*, 493-506.

Chakrabarti, O., Rane, N.S., and Hegde, R.S. (2011). Cytosolic aggregates perturb the degradation of nontranslocated secretory and membrane proteins. Mol Biol Cell *22*, 1625-1637.

Champion, M.C., Hartnett, M., and Yen, M. (1986). Domperidone, a new dopamine antagonist. CMAJ *135*, 457-461.

Chandhok, G., Horvath, J., Aggarwal, A., Bhatt, M., Zibert, A., and Schmidt, H.H. (2016). Functional analysis and drug response to zinc and D-penicillamine in stable ATP7B mutant hepatic cell lines. World journal of gastroenterology *22*, 4109-4119.

Chandhok, G., Schmitt, N., Sauer, V., Aggarwal, A., Bhatt, M., and Schmidt, H.H. (2014). The effect of zinc and D-penicillamine in a stable human hepatoma ATP7B knockout cell line. PloS one *9*, e98809.

Chesi, G., Hegde, R.N., Iacobacci, S., Concilli, M., Parashuraman, S., Festa, B.P., Polishchuk, E.V., Di Tullio, G., Carissimo, A., Montefusco, S.*, et al.* (2016). Identification of p38 MAPK and JNK as new targets for correction of Wilson disease-causing ATP7B mutants. Hepatology *63*, 1842-1859.

Concilli, M., Iacobacci, S., Chesi, G., Carissimo, A., and Polishchuk, R. (2016). A systems biology approach reveals new endoplasmic reticulum-associated targets for the correction of the ATP7B mutant causing Wilson disease. Metallomics *8*, 920-930.

Coppinger, J.A., Hutt, D.M., Razvi, A., Koulov, A.V., Pankow, S., Yates, J.R., 3rd, and Balch, W.E. (2012). A chaperone trap contributes to the onset of cystic fibrosis. PloS one *7*, e37682.

Culotta, V.C., Klomp, L.W., Strain, J., Casareno, R.L., Krems, B., and Gitlin, J.D. (1997). The copper chaperone for superoxide dismutase. J Biol Chem *272*, 23469-23472.

Culotta, V.C., Yang, M., and O'Halloran, T.V. (2006). Activation of superoxide dismutases: putting the metal to the pedal. Biochim Biophys Acta *1763*, 747-758.

D'Agostino, M., Lemma, V., Chesi, G., Stornaiuolo, M., Cannata Serio, M., D'Ambrosio, C., Scaloni, A., Polishchuk, R., and Bonatti, S. (2013). The cytosolic chaperone alpha-crystallin B rescues folding and compartmentalization of misfolded multispan transmembrane proteins. J Cell Sci *126*, 4160-4172.

de Bie, P., Muller, P., Wijmenga, C., and Klomp, L.W. (2007). Molecular pathogenesis of Wilson and Menkes disease: correlation of mutations with molecular defects and disease phenotypes. J Med Genet *44*, 673-688.

Efremov, R.G., Kosinsky, Y.A., Nolde, D.E., Tsivkovskii, R., Arseniev, A.S., and Lutsenko, S. (2004). Molecular modelling of the nucleotide-binding domain of Wilson's disease protein: location of the ATP-binding site, domain dynamics and potential effects of the major disease mutations. Biochem J *382*, 293-305.

Ferenci, P. (2006). Regional distribution of mutations of the ATP7B gene in patients with Wilson disease: impact on genetic testing. Human genetics *120*, 151-159.

Forbes, J.R., and Cox, D.W. (1998). Functional characterization of missense mutations in ATP7B: Wilson disease mutation or normal variant? Am J Hum Genet *63*, 1663-1674.

Franceschini, A., Szklarczyk, D., Frankild, S., Kuhn, M., Simonovic, M., Roth, A., Lin, J., Minguez, P., Bork, P., von Mering, C.*, et al.* (2013). STRING v9.1: protein-protein interaction networks, with increased coverage and integration. Nucleic Acids Res *41*, D808-815.

Frydman, J. (2001). Folding of newly translated proteins in vivo: the role of molecular chaperones. Annu Rev Biochem *70*, 603-647.

Gitlin, J.D. (2003). Wilson disease. Gastroenterology *125*, 1868-1877.

Gomes, A., and Dedoussis, G.V. (2016). Geographic distribution of ATP7B mutations in Wilson disease. Ann Hum Biol *43*, 1-8.

Goodford, P.J. (1985). A computational procedure for determining energetically favorable binding sites on biologically important macromolecules. J Med Chem *28*, 849-857.

Guo, B., Zhu, H.L., Li, S.X., Lu, X.C., and Fan, H. (2011). Individualized liposomal doxorubicin-based treatment in elderly patients with non-Hodgkin's lymphoma. Onkologie *34*, 184-188.

Guo, H., Lee, J.D., Uzui, H., Toyoda, K., Geshi, T., Yue, H., and Ueda, T. (2005). Effects of copper and zinc on the production of homocysteine-induced extracellular matrix metalloproteinase-2 in cultured rat vascular smooth muscle cells. Acta Cardiol *60*, 353-359.

Harada, M., Kawaguchi, T., Kumemura, H., Terada, K., Ninomiya, H., Taniguchi, E., Hanada, S., Baba, S., Maeyama, M., Koga, H.*, et al.* (2005). The Wilson disease protein ATP7B resides in the late endosomes with Rab7 and the Niemann-Pick C1 protein. Am J Pathol *166*, 499-510.

Harada, M., Sakisaka, S., Kawaguchi, T., Kimura, R., Taniguchi, E., Koga, H., Hanada, S., Baba, S., Furuta, K., Kumashiro, R.*, et al.* (2000). Copper does not alter the intracellular distribution of ATP7B, a copper-transporting ATPase. Biochem Biophys Res Commun *275*, 871-876.

Hartl, F.U., Bracher, A., and Hayer-Hartl, M. (2011). Molecular chaperones in protein folding and proteostasis. Nature *475*, 324-332.

Hosp, F., Vossfeldt, H., Heinig, M., Vasiljevic, D., Arumughan, A., Wyler, E., Genetic, Environmental Risk for Alzheimer's Disease, G.C., Landthaler, M.,

Hubner, N., *et al.* (2015). Quantitative interaction proteomics of neurodegenerative disease proteins. Cell Rep *11*, 1134-1146.

Howe, M.K., Bodoor, K., Carlson, D.A., Hughes, P.F., Alwarawrah, Y., Loiselle, D.R., Jaeger, A.M., Darr, D.B., Jordan, J.L., Hunter, L.M., *et al.* (2014). Identification of an allosteric small-molecule inhibitor selective for the inducible form of heat shock protein 70. Chem Biol *21*, 1648-1659.

Hsi, G., Cullen, L.M., Moira Glerum, D., and Cox, D.W. (2004). Functional assessment of the carboxy-terminus of the Wilson disease copper-transporting ATPase, ATP7B. Genomics *83*, 473-481.

Hung, Y.H., Layton, M.J., Voskoboinik, I., Mercer, J.F., and Camakaris, J. (2007). Purification and membrane reconstitution of catalytically active Menkes copper-transporting P-type ATPase (MNK; ATP7A). Biochem J *401*, 569-579.

Huster, D., Kuhne, A., Bhattacharjee, A., Raines, L., Jantsch, V., Noe, J., Schirrmeister, W., Sommerer, I., Sabri, O., Berr, F., *et al.* (2012). Diverse functional properties of Wilson disease ATP7B variants. Gastroenterology *142*, 947-956 e945.

Iida, M., Terada, K., Sambongi, Y., Wakabayashi, T., Miura, N., Koyama, K., Futai, M., and Sugiyama, T. (1998). Analysis of functional domains of Wilson disease protein (ATP7B) in Saccharomyces cerevisiae. FEBS Lett *428*, 281-285.

Inesi, G., Pilankatta, R., and Tadini-Buoninsegni, F. (2014). Biochemical characterization of P-type copper ATPases. Biochem J *463*, 167-176.

Iorio, F., Bosotti, R., Scacheri, E., Belcastro, V., Mithbaokar, P., Ferriero, R., Murino, L., Tagliaferri, R., Brunetti-Pierri, N., Isacchi, A., *et al.* (2010). Discovery of drug mode of action and drug repositioning from transcriptional responses. Proc Natl Acad Sci U S A *107*, 14621-14626.

Kaler, S.G. (2013). Inborn errors of copper metabolism. Handb Clin Neurol *113*, 1745-1754.

Keizer, H.G., Pinedo, H.M., Schuurhuis, G.J., and Joenje, H. (1990). Doxorubicin (adriamycin): a critical review of free radical-dependent mechanisms of cytotoxicity. Pharmacol Ther *47*, 219-231.

Kettern, N., Dreiseidler, M., Tawo, R., and Hohfeld, J. (2010). Chaperone-assisted degradation: multiple paths to destruction. Biol Chem *391*, 481-489.

Kim, B.E., Nevitt, T., and Thiele, D.J. (2008). Mechanisms for copper acquisition, distribution and regulation. Nat Chem Biol *4*, 176-185.

Kim, D.H., Kim, B.Y., Shin, J.H., Kim, S.W., and Kim, S.W. (2017). Intranasal azelastine and mometasone exhibit a synergistic effect on a murine model of allergic rhinitis. Am J Otolaryngol. Mar - Apr;38(2):198-203

Kim, S.H., Kang, J.G., Kim, C.S., Ihm, S.H., Choi, M.G., Yoo, H.J., and Lee, S.J. (2014). The hsp70 inhibitor VER155008 induces paraptosis requiring de novo protein synthesis in anaplastic thyroid carcinoma cells. Biochem Biophys Res Commun *454*, 36-41.

Klomp, L.W., Lin, S.J., Yuan, D.S., Klausner, R.D., Culotta, V.C., and Gitlin, J.D. (1997). Identification and functional expression of HAH1, a novel human gene involved in copper homeostasis. J Biol Chem *272*, 9221-9226.

Kodama, H., Abe, T., Takama, M., Takahashi, I., Kodama, M., and Nishimura, M. (1993). Histochemical localization of copper in the intestine and kidney of macular mice: light and electron microscopic study. J Histochem Cytochem *41*, 1529-1535.

Kuo, Y.M., Gitschier, J., and Packman, S. (1997). Developmental expression of the mouse mottled and toxic milk genes suggests distinct functions for the Menkes and Wilson disease copper transporters. Hum Mol Genet *6*, 1043-1049.

Lamb, J., Crawford, E.D., Peck, D., Modell, J.W., Blat, I.C., Wrobel, M.J., Lerner, J., Brunet, J.P., Subramanian, A., Ross, K.N.*, et al.* (2006). The Connectivity Map: using gene-expression signatures to connect small molecules, genes, and disease. Science *313*, 1929-1935.

Leeser, J., and Bateman, D.N. (1985). Domperidone. Br Med J (Clin Res Ed) *290*, 241-242.

Lim, C.M., Cater, M.A., Mercer, J.F., and La Fontaine, S. (2006). Copper-dependent interaction of dynactin subunit p62 with the N terminus of ATP7B but not ATP7A. J Biol Chem *281*, 14006-14014.

Lin, S.J., Pufahl, R.A., Dancis, A., O'Halloran, T.V., and Culotta, V.C. (1997). A role for the Saccharomyces cerevisiae ATX1 gene in copper trafficking and iron transport. J Biol Chem *272*, 9215-9220.

Linder, M.C., Wooten, L., Cerveza, P., Cotton, S., Shulze, R., and Lomeli, N. (1998). Copper transport. Am J Clin Nutr *67*, 965S-971S.

Liu, W., Zhou, L., Zeng, Q., and Luo, R. (2017). Combination of mometasone furoate and oxymetazoline for the treatment of adenoid hypertrophy concomitant with allergic rhinitis: A randomized controlled trial. Sci Rep *7*, 40425.

Lutsenko, S. (2010). Human copper homeostasis: a network of interconnected pathways. Curr Opin Chem Biol *14*, 211-217.

Lutsenko, S., Barnes, N.L., Bartee, M.Y., and Dmitriev, O.Y. (2007). Function and regulation of human copper-transporting ATPases. Physiol Rev *87*, 1011-1046.

Lutsenko, S., and Petris, M.J. (2003). Function and regulation of the mammalian copper-transporting ATPases: insights from biochemical and cell biological approaches. J Membr Biol *191*, 1-12.

Lutz, T., Neupert, W., and Herrmann, J.M. (2003). Import of small Tim proteins into the mitochondrial intermembrane space. EMBO J *22*, 4400-4408.

Manguso, F., Bennato, R., Lombardi, G., Riccio, E., Costantino, G., and Fries, W. (2016). Efficacy and Safety of Oral Beclomethasone Dipropionate in Ulcerative Colitis: A Systematic Review and Meta-Analysis. PloS one *11*, e0166455.

Marina, N.M., Cochrane, D., Harney, E., Zomorodi, K., Blaney, S., Winick, N., Bernstein, M., and Link, M.P. (2002). Dose escalation and pharmacokinetics of pegylated liposomal doxorubicin (Doxil) in children with solid tumors: a pediatric oncology group study. Clin Cancer Res *8*, 413-418.

Materia, S., Cater, M.A., Klomp, L.W., Mercer, J.F., and La Fontaine, S. (2011). Clusterin (apolipoprotein J), a molecular chaperone that facilitates degradation of the copper-ATPases ATP7A and ATP7B. J Biol Chem *286*, 10073-10083.

Matsumura, Y., Sakai, J., and Skach, W.R. (2013). Endoplasmic reticulum protein quality control is determined by cooperative interactions between Hsp/c70 protein and the CHIP E3 ligase. J Biol Chem *288*, 31069-31079.

Mayer, M.P., and Bukau, B. (2005). Hsp70 chaperones: cellular functions and molecular mechanism. Cellular and molecular life sciences : CMLS *62*, 670-684.

Menkes, J.H., Alter, M., Steigleder, G.K., Weakley, D.R., and Sung, J.H. (1962). A sex-linked recessive disorder with retardation of growth, peculiar hair, and focal cerebral and cerebellar degeneration. Pediatrics *29*, 764-779.

Meredith, A.M., and Dass, C.R. (2016). Increasing role of the cancer chemotherapeutic doxorubicin in cellular metabolism. J Pharm Pharmacol *68*, 729-741.

Michalczyk, A.A., Rieger, J., Allen, K.J., Mercer, J.F., and Ackland, M.L. (2000). Defective localization of the Wilson disease protein (ATP7B) in the mammary gland of the toxic milk mouse and the effects of copper supplementation. Biochem J *352 Pt 2*, 565-571.

Minotti, G., Menna, P., Salvatorelli, E., Cairo, G., and Gianni, L. (2004). Anthracyclines: molecular advances and pharmacologic developments in antitumor activity and cardiotoxicity. Pharmacol Rev *56*, 185-229.

Moller, L.B., Petersen, C., Lund, C., and Horn, N. (2000). Characterization of the hCTR1 gene: genomic organization, functional expression, and identification of a highly homologous processed gene. Gene *257*, 13-22.

Monty, J.F., Llanos, R.M., Mercer, J.F., and Kramer, D.R. (2005). Copper exposure induces trafficking of the menkes protein in intestinal epithelium of ATP7A transgenic mice. J Nutr *135*, 2762-2766.

Morgan, C.T., Tsivkovskii, R., Kosinsky, Y.A., Efremov, R.G., and Lutsenko, S. (2004). The distinct functional properties of the nucleotide-binding domain of ATP7B, the human copper-transporting ATPase: analysis of the Wilson disease mutations E1064A, H1069Q, R1151H, and C1104F. J Biol Chem *279*, 36363-36371.

Muller, T., Muller, W., and Feichtinger, H. (1998). Idiopathic copper toxicosis. Am J Clin Nutr *67*, 1082S-1086S.

Nagasaka, H., Inoue, I., Inui, A., Komatsu, H., Sogo, T., Murayama, K., Murakami, T., Yorifuji, T., Asayama, K., Katayama, S.*, et al.* (2006). Relationship between oxidative stress and antioxidant systems in the liver of patients with Wilson disease: hepatic manifestation in Wilson disease as a consequence of augmented oxidative stress. Pediatr Res *60*, 472-477.

Napolitano, F., Sirci, F., Carrella, D., and di Bernardo, D. (2016). Drug-set enrichment analysis: a novel tool to investigate drug mode of action. Bioinformatics *32*, 235-241.

Nevitt, T., Ohrvik, H., and Thiele, D.J. (2012). Charting the travels of copper in eukaryotes from yeast to mammals. Biochim Biophys Acta *1823*, 1580-1593.

Nyasae, L.K., Schell, M.J., and Hubbard, A.L. (2014). Copper directs ATP7B to the apical domain of hepatic cells via basolateral endosomes. Traffic *15*, 1344-1365.

Ong, S.E., Blagoev, B., Kratchmarova, I., Kristensen, D.B., Steen, H., Pandey, A., and Mann, M. (2002). Stable isotope labeling by amino acids in cell culture, SILAC, as a simple and accurate approach to expression proteomics. Mol Cell Proteomics *1*, 376-386.

Orellana, M., Buttinghausen, V., Aspillaga, M.A., and Chandia, C.M. (2012). [Hodgkin lymphoma with hepatic involvement treated with dexametasone,

gemcitabine and cisplatin as a bridge to standard therapy: report of one case]. Rev Med Chil *140*, 902-905.

Ortiz, A., Cooper, C.J., Alvarez, A., Gomez, Y., Sarosiek, I., and McCallum, R.W. (2015). Cardiovascular safety profile and clinical experience with high-dose domperidone therapy for nausea and vomiting. Am J Med Sci *349*, 421-424.

Palmer, D., and Ng, P. (2003). Improved system for helper-dependent adenoviral vector production. Mol Ther *8*, 846-852.

Pankow, S., Bamberger, C., Calzolari, D., Martinez-Bartolome, S., Lavallee-Adam, M., Balch, W.E., and Yates, J.R., 3rd (2015). F508 CFTR interactome remodelling promotes rescue of cystic fibrosis. Nature *528*, 510-516.

Payne, A.S., Kelly, E.J., and Gitlin, J.D. (1998). Functional expression of the Wilson disease protein reveals mislocalization and impaired copper-dependent trafficking of the common H1069Q mutation. Proc Natl Acad Sci U S A *95*, 10854-10859.

Pesce, E., Gorrieri, G., Sirci, F., Napolitano, F., Carrella, D., Caci, E., Tomati, V., Zegarra-Moran, O., di Bernardo, D., and Galietta, L.J. (2016). Evaluation of a systems biology approach to identify pharmacological correctors of the mutant CFTR chloride channel. J Cyst Fibros *15*, 425-435.

Petris, M.J., Strausak, D., and Mercer, J.F. (2000). The Menkes copper transporter is required for the activation of tyrosinase. Hum Mol Genet *9*, 2845-2851.

Petris, M.J., Voskoboinik, I., Cater, M., Smith, K., Kim, B.E., Llanos, R.M., Strausak, D., Camakaris, J., and Mercer, J.F. (2002). Copper-regulated trafficking of the Menkes disease copper ATPase is associated with formation of a phosphorylated catalytic intermediate. J Biol Chem *277*, 46736-46742.

Podvigina, T.T., Bagaeva, T.P., Morozova, O., and Filaretova, L.P. (2012). [A comparative analysis of corticosterone, cortisol and dexametasone effects on gastric erosion in rats]. Ross Fiziol Zh Im I M Sechenova *98*, 879-889.

Polishchuk, E.V., Concilli, M., Iacobacci, S., Chesi, G., Pastore, N., Piccolo, P., Paladino, S., Baldantoni, D., van, I.S.C., Chan, J.*, et al.* (2014). Wilson disease protein ATP7B utilizes lysosomal exocytosis to maintain copper homeostasis. Dev Cell *29*, 686-700.

Polishchuk, R., and Lutsenko, S. (2013). Golgi in copper homeostasis: a view from the membrane trafficking field. Histochem Cell Biol *140*, 285-295.

Pratt, W.B., and Toft, D.O. (2003). Regulation of signaling protein function and trafficking by the hsp90/hsp70-based chaperone machinery. Exp Biol Med (Maywood) *228*, 111-133.

Prota, L.F., Cebotaru, L., Cheng, J., Wright, J., Vij, N., Morales, M.M., and Guggino, W.B. (2012). Dexamethasone regulates CFTR expression in Calu-3 cells with the involvement of chaperones HSP70 and HSP90. PloS one *7*, e47405.

Puig, S., and Thiele, D.J. (2002). Molecular mechanisms of copper uptake and distribution. Curr Opin Chem Biol *6*, 171-180.

Rayman, M.P. (2012). Selenium and human health. Lancet *379*, 1256-1268.

Riordan, S.M., and Williams, R. (2001). The Wilson's disease gene and phenotypic diversity. J Hepatol *34*, 165-171.

Robbins, N.M., Ito, H., Scheinman, M.M., and Goadsby, P.J. (2016). Safety of domperidone in treating nausea associated with dihydroergotamine infusion and headache. Neurology *87*, 2522-2526.

Roberts, E.A., Schilsky, M.L., and American Association for Study of Liver, D. (2008). Diagnosis and treatment of Wilson disease: an update. Hepatology *47*, 2089-2111.

Rodriguez-Granillo, A., Sedlak, E., and Wittung-Stafshede, P. (2008). Stability and ATP binding of the nucleotide-binding domain of the Wilson disease protein: effect of the common H1069Q mutation. J Mol Biol *383*, 1097-1111.

Roesch, K., Hynds, P.J., Varga, R., Tranebjaerg, L., and Koehler, C.M. (2004). The calcium-binding aspartate/glutamate carriers, citrin and aralar1, are new substrates for the DDP1/TIMM8a-TIMM13 complex. Hum Mol Genet *13*, 2101-2111.

Royce, P.M., Camakaris, J., and Danks, D.M. (1980). Reduced lysyl oxidase activity in skin fibroblasts from patients with Menkes' syndrome. Biochem J *192*, 579-586.

Ruggiero, A., De Rosa, G., Rizzo, D., Leo, A., Maurizi, P., De Nisco, A., Vendittelli, F., Zuppi, C., Mordente, A., and Riccardi, R. (2013). Myocardial performance index and biochemical markers for early detection of doxorubicin-induced cardiotoxicity in children with acute lymphoblastic leukaemia. Int J Clin Oncol *18*, 927-933.

Sakano, D., Choi, S., Kataoka, M., Shiraki, N., Uesugi, M., Kume, K., and Kume, S. (2016). Dopamine D2 Receptor-Mediated Regulation of Pancreatic beta Cell Mass. Stem Cell Reports *7*, 95-109.

Scheinberg, I.H., and Gitlin, D. (1952). Deficiency of ceruloplasmin in patients with hepatolenticular degeneration (Wilson's disease). Science *116*, 484-485.

Schey, R., Saadi, M., Midani, D., Roberts, A.C., Parupalli, R., and Parkman, H.P. (2016). Domperidone to Treat Symptoms of Gastroparesis: Benefits and Side Effects from a Large Single-Center Cohort. Dig Dis Sci *61*, 3545-3551.

Schilsky, M.L., Scheinberg, I.H., and Sternlieb, I. (1994). Liver transplantation for Wilson's disease: indications and outcome. Hepatology *19*, 583-587.

Singh, A., Nandan, D., Dewan, V., and Sankar, J. (2016). Comparison of clinical effects of beclomethasone dipropionate & budesonide in treatment of children with mild persistent asthma: A double-blind, randomized, controlled study. Indian J Med Res *144*, 250-257.

Sirci, F., Goracci, L., Rodriguez, D., van Muijlwijk-Koezen, J., Gutierrez-de-Teran, H., and Mannhold, R. (2012a). Ligand-, structure- and pharmacophore-based molecular fingerprints: a case study on adenosine A(1), A (2A), A (2B), and A (3) receptor antagonists. J Comput Aided Mol Des *26*, 1247-1266.

Sirci, F., Istyastono, E.P., Vischer, H.F., Kooistra, A.J., Nijmeijer, S., Kuijer, M., Wijtmans, M., Mannhold, R., Leurs, R., de Esch, I.J.*, et al.* (2012b). Virtual fragment screening: discovery of histamine H3 receptor ligands using ligand-based and protein-based molecular fingerprints. J Chem Inf Model *52*, 3308-3324.

Soderberg, O., Gullberg, M., Jarvius, M., Ridderstrale, K., Leuchowius, K.J., Jarvius, J., Wester, K., Hydbring, P., Bahram, F., Larsson, L.G.*, et al.* (2006). Direct observation of individual endogenous protein complexes in situ by proximity ligation. Nat Methods *3*, 995-1000.

Spagnolo, P., Oldham, J.M., Jones, M.G., and Lee, J.S. (2017). Personalized medicine in interstitial lung diseases. Current opinion in pulmonary medicine.

Stohs, S.J., and Bagchi, D. (1995). Oxidative mechanisms in the toxicity of metal ions. Free Radic Biol Med *18*, 321-336.

Strausak, D., La Fontaine, S., Hill, J., Firth, S.D., Lockhart, P.J., and Mercer, J.F. (1999). The role of GMXCXXC metal binding sites in the copper-induced redistribution of the Menkes protein. J Biol Chem *274*, 11170-11177.

Suzuki, M., Cela, R., Clarke, C., Bertin, T.K., Mourino, S., and Lee, B. (2010). Large-scale production of high-quality helper-dependent adenoviral vectors using adherent cells in cell factories. Hum Gene Ther *21*, 120-126.

Tanner, M.S. (1998). Role of copper in Indian childhood cirrhosis. Am J Clin Nutr *67*, 1074S-1081S.

Tapiero, H., and Tew, K.D. (2003). Trace elements in human physiology and pathology: zinc and metallothioneins. Biomed Pharmacother *57*, 399-411.

Traub, L.M., and Bonifacino, J.S. (2013). Cargo recognition in clathrin-mediated endocytosis. Cold Spring Harb Perspect Biol *5*, a016790.

Treyer, A., and Musch, A. (2013). Hepatocyte polarity. Compr Physiol *3*, 243-287.

Trinkle-Mulcahy, L., Boulon, S., Lam, Y.W., Urcia, R., Boisvert, F.M., Vandermoere, F., Morrice, N.A., Swift, S., Rothbauer, U., Leonhardt, H.*, et al.* (2008). Identifying specific protein interaction partners using quantitative mass spectrometry and bead proteomes. J Cell Biol *183*, 223-239.

Tsivkovskii, R., Efremov, R.G., and Lutsenko, S. (2003). The role of the invariant His-1069 in folding and function of the Wilson's disease protein, the human copper-transporting ATPase ATP7B. J Biol Chem *278*, 13302-13308.

Tsivkovskii, R., Eisses, J.F., Kaplan, J.H., and Lutsenko, S. (2002). Functional properties of the copper-transporting ATPase ATP7B (the Wilson's disease protein) expressed in insect cells. J Biol Chem *277*, 976-983.

Tyedmers, J., Mogk, A., and Bukau, B. (2010). Cellular strategies for controlling protein aggregation. Nat Rev Mol Cell Biol *11*, 777-788.

Ushkalova, E.A., Zyryanov, S.K., and Shvarts, G.Y. (2016). The use of intranasal glucocorticosteroids in the treatment of rhinosinusitis: Focus on mometasone furoate. Vestn Otorinolaringol *81*, 59-66.

van den Berghe, P.V., Folmer, D.E., Malingre, H.E., van Beurden, E., Klomp, A.E., van de Sluis, B., Merkx, M., Berger, R., and Klomp, L.W. (2007). Human copper transporter 2 is localized in late endosomes and lysosomes and facilitates cellular copper uptake. Biochem J *407*, 49-59.

van den Berghe, P.V., Stapelbroek, J.M., Krieger, E., de Bie, P., van de Graaf, S.F., de Groot, R.E., van Beurden, E., Spijker, E., Houwen, R.H., Berger, R.*, et al.* (2009). Reduced expression of ATP7B affected by Wilson disease-causing mutations is rescued by pharmacological folding chaperones 4-phenylbutyrate and curcumin. Hepatology *50*, 1783-1795.

Vanderwerf, S.M., and Lutsenko, S. (2002). The Wilson's disease protein expressed in Sf9 cells is phosphorylated. Biochem Soc Trans *30*, 739-741.

Virkud, Y.V., Hornik, C.P., Benjamin, D.K., Laughon, M.M., Clark, R.H., Greenberg, R.G., and Smith, P.B. (2017). Respiratory Support for Very Low Birth Weight Infants Receiving Dexamethasone. J Pediatr.

Voskoboinik, I., Brooks, H., Smith, S., Shen, P., and Camakaris, J. (1998). ATP-dependent copper transport by the Menkes protein in membrane vesicles isolated from cultured Chinese hamster ovary cells. FEBS Lett *435*, 178-182.

Voskoboinik, I., Mar, J., Strausak, D., and Camakaris, J. (2001). The regulation of catalytic activity of the menkes copper-translocating P-type ATPase. Role of high affinity copper-binding sites. J Biol Chem *276*, 28620-28627.

Walshe, J.M. (1956a). Penicillamine, a new oral therapy for Wilson's disease. Am J Med *21*, 487-495.

Walshe, J.M. (1956b). Wilson's disease; new oral therapy. Lancet *270*, 25-26.

Weekes, C.D., Vose, J.M., Lynch, J.C., Weisenburger, D.D., Bierman, P.J., Greiner, T., Bociek, G., Enke, C., Bast, M., Chan, W.C.*, et al.* (2002). Hodgkin's disease in the elderly: improved treatment outcome with a doxorubicin-containing regimen. J Clin Oncol *20*, 1087-1093.

Wessling-Resnick, M. (2002). Understanding copper uptake at the molecular level. Nutr Rev *60*, 177-179.

Xu, Z., and Zhou, J. (2013). Zinc and myocardial ischemia/reperfusion injury. Biometals *26*, 863-878.

Young, J.C. (2014). The role of the cytosolic HSP70 chaperone system in diseases caused by misfolding and aberrant trafficking of ion channels. Dis Model Mech *7*, 319-329.

Yu, J., Roh, S., Lee, J.S., Yang, B.H., Choi, M.R., Chai, Y.G., and Kim, S.H. (2010). The Effects of Venlafaxine and Dexamethasone on the Expression of HSP70 in Rat C6 Glioma Cells. Psychiatry Investig *7*, 43-48.

Yuan, D.S., Dancis, A., and Klausner, R.D. (1997). Restriction of copper export in Saccharomyces cerevisiae to a late Golgi or post-Golgi compartment in the secretory pathway. J Biol Chem *272*, 25787-25793.

Yuan, D.S., Stearman, R., Dancis, A., Dunn, T., Beeler, T., and Klausner, R.D. (1995). The Menkes/Wilson disease gene homologue in yeast provides copper to

a ceruloplasmin-like oxidase required for iron uptake. Proc Natl Acad Sci U S A *92*, 2632-2636.

Zhou, B., and Gitschier, J. (1997). hCTR1: a human gene for copper uptake identified by complementation in yeast. Proc Natl Acad Sci U S A *94*, 7481-7486.